Low Complexity DPD for Multi-Band Radio over Fiber Transmission Systems

Zijian Cheng

A Thesis

In

The Department

Of

Electrical and Computer Engineering

Presented in Partial Fulfillment of the Requirements

For the Degree of Master of Applied Science
(Electrical and Computer Engineering) at

Concordia University

Montreal, Quebec, Canada
June 2023

CONCORDIA UNIVERSITY
School of Graduate Studies

This is to certify that the thesis prepared

By: Zijian Cheng

Entitled: Low Complexity DPD for Multi-Band Radio over Fiber

and submitted in partial fulfillment of the requirements for the degree of

Master of Applied Science (Electrical and Computer Engineering)

complies with the regulations of the University and meets the accepted standards with respect to originality and quality.

Signed by the final examining committee:

Dr. G. Cowan _____ Chair

Dr. G. Cowan _____ Examiner

Dr. Y. Zhang _____ Examiner

Dr. J. X. Zhang _____ Thesis Supervisor(s)

Approved by Dr. Z. Kabir _____
Chair of Department or Graduate Program Director

Dr. M. Debbabi,

Dean of **Faculty**

ABSTRACT

Low Complexity DPD for Multi-Band Radio over Fiber Transmission Systems

Zijian Cheng

The increasing demand for broadband wireless transmission in the modern internet has led to the proposal and standardization of the fifth-generation (5G) mobile communication system, which offers massive device connectivity, high bit rates, low latency, and cost sustainability. However, maintaining a high transmission rate as well as low latency is difficult to achieve simultaneously, which requires some state-of-art fronthaul transmission techniques. Therefore, radio over fiber (RoF) with different approaches like digital RoF (D-RoF), analog RoF (A-RoF), and delta-sigma modulation based RoF (DSM-RoF) for 5G fronthaul transmission has been introduced. Those RoF techniques may significantly reduce complexity and power consumption at base stations, but the extra electric to optic (E/O), optic to electric (O/E) converters and power amplifiers could introduce extra nonlinearity into the system. Moreover, ultra-broadband or multi-band ultra-broadband signal is introduced in 5G to further increase the transmission rate, which further increases the impact of the nonlinearity. Therefore, broadband linearization techniques are necessary for RoF fronthaul transmission systems due to the fragile of the signal and the inherent nonlinear distortions introduced by RoF link. To reduce the degradation of nonlinearity for RoF link, digital predistortion (DPD) techniques have been extensively researched to address these challenges.

In a multi-band or multi-dimensional RoF system, multi-band DPD is required. Multi-dimensional DPD should be able to suppress the internal distortion within each band/dimension but also inter-distortion between different bands/dimensions. Unfortunately, the dimension higher than 3 causes a high calculation complexity to get the DPD function coefficients. There have been lots of efforts that have been made to obtain less-complexity

DPD with better accuracy for multi-band or multidimensional signals. However, very limited DPD techniques have been proposed in simplifying the fundamental linearization function for bands exceeding four. Thus, the multi-band/multidimensional DPD has not been really got in used in commercial products because of the high complexity, high cost and high-power consumption. Thus, a simplified linearization approach for multi-band DPD is still needed.

In this thesis, a new low-complexity multidimensional DPD is introduced. This proposed DPD introduces a simplified DPD function, which evolves from the conventional memory polynomial function. Compared with the conventional multi-dimensional DPD, this proposed approach has lower complexity increased with the increase of signal bands or dimensions, nonlinearity orders, and memory effect depth. For example, the conventional DPD function needs a total of 40040 coefficients for the 6-band signals with a nonlinearity order of 10 and a memory depth of 5. However, this proposed low-complexity DPD function needs 640 coefficients. A substantial reduction in complexity is clearly observed.

The performance of the proposed DPD is evaluated by both simulation and experiments. An up to 6-band 64-QAM orthogonal frequency division multiplexing (OFDM) signal with each band of 200 MHz in simulations and an up to 5-band 20 MHz 64-QAM OFDM signal in experiments are used. The performance is evaluated in the means of error vector magnitude (EVM) of the received signal. The average improvement of EVM in simulation for 3-band, 4-band, 5-band and 6-band signals is 19.97 dB, 18.65 dB, 16.64 dB and 15.44 dB, respectively. The average improvement of EVM in experiments for 4-band and 5-band signals is 5.67 dB and 8.1 dB, respectively. The above results prove that the proposed DPD can significantly reduce the complexity and provide good linearization.

ACKNOWLEDGEMENTS

I extend my heartfelt gratitude to Professor John Xiupu Zhang for his invaluable guidance, assistance, and unwavering support throughout the completion of my thesis.

I would also like to express my sincere appreciation to my colleague Xiaoran Xie for his patience, assistance, and advice during the experimental verification phase.

Furthermore, I am deeply thankful to my parents for their boundless love, understanding, and unwavering support.

Table of Contents

List of Figures

List of Tables

List of Acronyms

A-RoF	Analog radio over fiber
ACPR	Adjacent channel power ratio
AWG	Arbitrary waveform generator
BBU	Baseband unit
C-RAN	Cloud radio access network
CPU	Central processing unit
D-RoF	Digital radio over fiber
DL	Downlink
DPD	Digital predistortion
DSM	Delta-sigma modulation
DSP	Digital signal processing
E/O	Electric to optic
EVM	Error vector magnitude
FDMA	Frequency division multiple access
IDM	Intermodulation distortion
IFFT	Inverse fast Fourier transform
LUT	Look up table
MIMO	Multiple input multiple output
NR	New radio
O/E	Optic to electric
OFDM	Orthogonal frequency division multiplexing
PA	Power amplifier

QAM	Quadrature amplitude modulation
RAU	Remote antenna unit
RF	Radio frequency
RoF	Radio over fiber
RRH	Remote radio head
SDR	Software-defined Radio
TDMA	Time division multiple access
UL	Uplink

Chapter 1 Introduction

1.1 Wireless access networks

For the wireless communication technology, the fifth generation has been developed and in used nowadays. It's important to look back at past developments. In early mobile networks (1G and 2G), base stations were all-in-one devices that integrated complex functions into large cabinets. They required dedicated rooms with ancillary facilities and were often expensive to install and maintain.

In 3G and 4G networks, the base station is divided into two parts: the remote radio head (RRH) and the baseband unit (BBU). They are connected by optical fiber, which reduces transmission loss and allows for more flexible layouts.

Cloud Radio Access Network (C-RAN) takes the distributed architecture a step further by migrating all BBUs into a centralized BBU pool. Each BBU can serve multiple RRHs, enabling dynamic frequency resource allocation and reducing installation and maintenance costs.

RoF technology is the same as the C-RAN architecture but uses fiber optics to transmit radio frequency (RF) signals between the Central Processing Unit (CPU) and the Remote Radio Unit (RRU). This simplifies the RRH architecture by allowing functions such as up-conversion, down-conversion, modulation and demodulation to be performed in the BBU instead of the RRH.

Fiber optics have low attenuation loss and high bandwidth compared to traditional transmission lines such as coaxial cable. Simplified RRH structure and reuse of baseband components reduces the cost of the entire transmission system. Resistant to electromagnetic interference, thereby reducing noise levels and increasing signal bandwidth. Communication

protocol transparency, allowing the RRU to serve any new protocol in its operating band.

However, there are still some challenges for the RoF technology. First, RoF is an analog system and defects such as nonlinearities and memory effects can lead to signal distortion. Secondly, Linearization techniques are required to mitigate signal distortion and deploy RoF transmission systems effectively.

RoF technology offers significant advantages for future mobile networks, especially in the context of 5G and deployment of small cells. By simplifying the RRH architecture and reducing costs, RoF can be an important solution to improve the efficiency and performance of cellular networks.

1.2 5G and RoF

The 5G access network comprises the backhaul and fronthaul networks. The backhaul is also evolved in 5G but not the focus of this thesis. In terms of fronthaul, the existing fronthaul transmission technologies used in 3G and 4G may not be suitable for 5G [3]. Therefore, alternative options such as frequency division multiple access (FDMA) and time-division multiple access (TDMA) based radio over fiber (RoF) have been considered more appropriate for 5G fronthaul networks [3].

The RoF systems can be categorized into three types: digital RoF (D-RoF), analog RoF(A-RoF), and 1-bit delta-sigma modulation based RoF (DSM-RoF). Digital RoF involves converting baseband digital signals into optical signals for transmission over fiber. These systems support high data rates and are compatible with various digital communication standards. They are commonly used in applications like fiber-to-the-home, cellular backhaul, and high-speed data transmission. Analog RoF is designed for transmitting analog signals, such as RF signals, over fiber. The analog signal is directly modulated onto an optical carrier, enabling efficient transmission of analog signals over long distances. Analog RoF can be deployed into cellular networks, satellite communication, and distributed antenna systems.

1-bit DSM-RoF utilizes DSM to convert analog signals into a single-bit digital format for transmission over a fiber. In DSM-RoF, the analog signal is oversampled and quantized into a series of 1-bit data, which is then modulated onto an optical carrier for transmission. While D-RoF offers digital optical transmission, it requires a complex and costly remote antenna unit (RAU), leading to high power consumption. Additionally, the RF power amplifier in the RAU necessitates complex broadband linearization [3-20]. A-RoF, on the other hand, employs a simpler RAU, but its analog fiber transmission introduces nonlinear distortions, requiring even more complex broadband linearization [21-34]. DSM-RoF combines digital optical transmission with a purely analog and simple RAU, it still requires straightforward broadband linearization [35]. Consequently, broadband linearization is necessary for all three fronthaul transmission technologies.

Besides, in 5G fronthaul [2], the bandwidth of signal is significantly increased, which leads to higher nonlinear effect. In detail, the bandwidth of component carrier varies depending on the frequency range. For the frequency range of 24250-52600 MHz, the component carrier bandwidth ranges from 50 MHz to 400 MHz, as shown in Table 1-1. In the frequency range of 450 MHz to 6000 MHz, the component carrier bandwidth ranges from 5 MHz to 100 MHz, as shown in Table 1-2. These tables provide detailed information about the specific bandwidth allocations for different frequency ranges in 5G NR.

NR ***operating band***	**Uplink (UL) and Downlink (DL)** ***operating band*** **BS transmit/receive** **UE transmit/receive** F_{UL_low} – F_{UL_high} F_{DL_low} – F_{DL_high}	**Duplex Mode**
n257	26500 MHz – 29500 MHz	TDD
n258	24250 MHz – 27500 MHz	TDD
n260	37000 MHz – 40000 MHz	TDD
n261	27500 MHz – 28350 MHz	TDD

Table 1-1 5G NR frequency bands supported for 24250-52600 MHz [2]

With the increase of the bandwidth, the linearity of the PA and RoF link became a major challenge. It is a challenge of balancing the PAs efficiency while keeping the distortion low [1]. Thus, the digital predistortion (DPD) has been deployed. DPD has been proposed to increase the PA efficiency and RoF linearity in 4G communications and could be a part of

the component of the 5G architectures.

NR *operating band*	Uplink (UL) *operating band* BS receive / UE transmit F_{UL_low} – F_{UL_high}	Downlink (DL) *operating band* BS transmit / UE receive F_{DL_low} – F_{DL_high}	Duplex Mode
n1	1920 MHz – 1980 MHz	2110 MHz – 2170 MHz	FDD
n2	1850 MHz – 1910 MHz	1930 MHz – 1990 MHz	FDD
n3	1710 MHz – 1785 MHz	1805 MHz – 1880 MHz	FDD
n5	824 MHz – 849 MHz	869 MHz – 894 MHz	FDD
n7	2500 MHz – 2570 MHz	2620 MHz – 2690 MHz	FDD
n8	880 MHz – 915 MHz	925 MHz – 960 MHz	FDD
n12	699 MHz – 716 MHz	729 MHz – 746 MHz	FDD
n20	832 MHz – 862 MHz	791 MHz – 821 MHz	FDD
n25	1850 MHz – 1915 MHz	1930 MHz – 1995 MHz	FDD
n28	703 MHz – 748 MHz	758 MHz – 803 MHz	FDD
n34	2010 MHz – 2025 MHz	2010 MHz – 2025 MHz	TDD
n38	2570 MHz – 2620 MHz	2570 MHz – 2620 MHz	TDD
n39	1880 MHz – 1920 MHz	1880 MHz – 1920 MHz	TDD
n40	2300 MHz – 2400 MHz	2300 MHz – 2400 MHz	TDD
n41	2496 MHz – 2690 MHz	2496 MHz – 2690 MHz	TDD
n50	1432 MHz – 1517 MHz	1432 MHz – 1517 MHz	TDD
n51	1427 MHz – 1432 MHz	1427 MHz – 1432 MHz	TDD
n66	1710 MHz – 1780 MHz	2110 MHz – 2200 MHz	FDD
n70	1695 MHz – 1710 MHz	1995 MHz – 2020 MHz	FDD
n71	663 MHz – 698 MHz	617 MHz – 652 MHz	FDD
n74	1427 MHz – 1470 MHz	1475 MHz – 1518 MHz	FDD
n75	N/A	1432 MHz – 1517 MHz	SDL
n76	N/A	1427 MHz – 1432 MHz	SDL
n77	3300 MHz – 4200 MHz	3300 MHz – 4200 MHz	TDD
n78	3300 MHz – 3800 MHz	3300 MHz – 3800 MHz	TDD
n79	4400 MHz – 5000 MHz	4400 MHz – 5000 MHz	TDD
n80	1710 MHz – 1785 MHz	N/A	SUL
n81	880 MHz – 915 MHz	N/A	SUL
n82	832 MHz – 862 MHz	N/A	SUL
n83	703 MHz – 748 MHz	N/A	SUL
n84	1920 MHz – 1980 MHz	N/A	SUL
n86	1710 MHz – 1780 MHz	N/A	SUL

Table 1-2 5G NR frequency bands supported for 450-6000 MHz [2]

1.3 Linearization techniques and Digital predistortion (DPD)

In a 5G concurrent RF/millimeter-wave multi-band system, the bandwidth of the signal and the number of the bands are both increased, which significantly increases the complexity of linearization and consequently the power consumption. This is because the multi-band OFDM signal will introduce even higher peak-to-average ratio, which is more affected by the nonlinearity in the system. Moreover, the increased number of signal bands also raises the sampling rate during digital to analog conversion, which increases the effect

of memory effect. Therefore, DPD has been extensively investigated as one of the key linearization techniques. Specifically, DPD techniques for linearizing multi-band signals are being developed with a focus on reducing complexity without compromising linearization performance. However, there are still some challenges in broadband linearization.

The first challenge in linearizing broadband or multi-band signals is the limited bandwidth of linearization. A pre-distorted signal for a broadband/multi-band signal requires a wider bandwidth to include possible nonlinear distortion components that interfere with the signal. Under-sampling DPD [6][13] and high-precision joint in-band/out-of-band DPD [4] are two methods that alleviate this problem. Alternatively, designing an RoF or power amplifier capable of supporting broadband or multi-band signals [36-37] is another approach.

The second challenge is the memory effect, which increases with signal bandwidth. Lagging and leading memory effect are two types of memory nonlinearities that may arise, extending the output signal's memory to previous time instances. One technique involves connecting several quasi-Wiener-Hammerstein processes in parallel, capturing different aspects of the system's memory effect and providing a better overall approximation of its behavior [38].

The third challenge relates to power consumption. DPD complexity results in considerable power consumption, making less-complex DPD techniques desirable. Reduction of DPD complexity has been investigated [11-12][16-20]. For instance, one method involves a combination of cross-term switching and coefficient switching [5], focusing only on significant terms with a large impact on nonlinear distortion. To address the complexity induced by strong memory effect, a moving average nested general memory polynomial function was proposed [39], improving the accuracy of envelope memory polynomial by connecting several memory branches of the envelope memory polynomial in parallel. Furthermore, a frequency shift technique was introduced to reduce complexity, where pre-calculated 3rd and 5th order intermodulation distortion (IMD3) (IMD5) influence on memory effect terms and nonlinearity terms are utilized to evaluate an error until the desired performance is achieved [18]. Another approach is the pre-training assisted DPD,

which reduces complexity under known nonlinearity [20]. Additionally, dynamic model sizing for broadband DPD demonstrated the resizing of unnecessary coefficients to reduce complexity [40].

In addition to reducing DPD complexity, splitting a broadband signal into two or multiple bands has been proposed [41-42]. To improve linearization accuracy, machine learning [14,15,23,28] and look-up table [9] methods have been suggested. To reduce sampling rates in DPD, a technique adjusts the group delay of signal samples and sums them up to cancel out aliasing distortion [13, 43].

Due to its high complexity, multidimensional DPD has limited adoption in commercial products. The computational complexity significantly increases for dimensions higher than three for obtaining the DPD function coefficients. As a result, the practical implementation of multidimensional DPD becomes challenging. A low complexity multi-band DPD is needed.

1.4 Motivation and Contribution

There were lots of efforts that have been made to obtain less-complexity DPD with better accuracy for multi-band or multidimensional signals. However, there has been limited exploration in simplifying the fundamental linearization function for bands exceeding four. Therefore, a simplified linearization function of multi-band DPD is needed.

In this work, a low-complexity multi-band DPD is proposed with an evolved linearization function from the conventional memorial polynomial function. Unlike the conventional DPD/memory polynomial, the proposed approach has limited increases of the DPD complexity with the increase of signal bands, nonlinearity orders and the long-term memory effect. For example, the conventional DPD requires a total of 40040 coefficients, while the proposed low-complexity DPD only requires 640 coefficients for the 6-band signals with a nonlinearity order of 10 and a memory depth of 5.

For the performance of the proposed DPD, the tests are conducted on both simulation and experiments. An up to 6-band 64-QAM OFDM signal with each band of 200 MHz in simulations is used and an up to 5-band 20 MHz 64-QAM OFDM signal in experiments is used. The performance is verified in the means of error vector magnitude (EVM) of the received signal. The average improvement of EVM in simulation for 3-band, 4-band, 5-band and 6-band signals is 19.97 dB, 18.65 dB, 16.64 dB and 15.44 dB, respectively. The average improvement of EVM in experiment for 4-band and 5-band signals is 5.67 dB and 8.1 dB, respectively.

1.5 Thesis Outline

This thesis is organized as follows:

Chapter 2 provides an overview of distortion and linearization, starting with an introduction to harmonic and intermodulation distortion. This is followed by an explanation of four linearization methods: feedback, feedforward linearization, memoryless polynomial predistortion, and look-up table. This chapter also covers the concept of memory effect and its mitigation using memory polynomial predistortion linearization.

Chapter 3 presents the theoretical framework of the proposed low-complexity multi-band DPD and its basic functionality of low-complexity DPD is outlined.

In Chapter 4, the simulation methodology and results are presented. Simulations were performed in MATLAB to validate the proposed DPD, categorized based on the number of input signal bands. A fronthaul transmission system was simulated, involving data generation, digital predistortion, nonlinear transmission, and data analysis. Performance analysis was carried out through spectrum and constellation diagrams, focusing on EVM. The simulations included 3-band, 4-band, 5-band, and 6-band signals to validate the proposed multi-band DPD.

Chapter 5 focuses on the experimental validation. A 64-QAM OFDM signal

generated in MATLAB is fed into a Tektronix AWG7122B arbitrary waveform generator (AWG). The optical signal is transmitted through an 8-kilometer standard single mode optical fiber using a MITEQ SCM fiber optic link. The optical receiver of the link demodulates the optical signal back into an RF signal, which is amplified by an SHF810 broadband amplifier. The RF signal is then captured by an DSO81204B oscilloscope and saved for further processing in MATLAB. Two sets of experiments were conducted, one with a four-band DPD and the other with a five-band DPD, both utilizing a signal bandwidth of 20 MHz. These experiments were carried out to validate the feasibility of the proposed DPD.

The final chapter concludes the contributions and discusses future directions for the development of a dynamic multi-band DPD.

Chapter 2 Nonlinear Distortion and Linearization

2.1 Nonlinear Distortion

Analog RoF and RF power amplifiers (PA) play a significant role in modern communication systems but are prone to introducing nonlinear distortion at the transmitter and receiver side. One prominent characteristic of nonlinearity is the presence of harmonic distortion (HD). The other is intermodulation distortion (IMD). In order to compensate for the distortion, linearization is needed.

Harmonic distortion is characterized by the production of unwanted harmonic frequencies that are integer multiples of the original signal frequency. These harmonics manifest as additional frequency components in the output signal, introducing distortion and potentially causing interference with nearby frequency bands. This type of distortion can significantly impact the integrity of the signal [1].

Intermodulation distortion arises when multiple input signals interact within a nonlinear system, giving rise to new frequencies or combinations of frequencies that are not present in the original signals. These additional frequencies can cause interference and spectral spreading, resulting in a degradation of the signal quality. IMD can have a detrimental effect on the fidelity and integrity of the signal being transmitted or processed.

2.1.1 Harmonic Distortion

A nonlinear device, such as power amplifier, its nonlinearity can be expressed by using the Taylor series [1]

$$f(v_i) = a_0 + a_1 v_i + a_2 v_i^2 + a_3 v_i^3 + \cdots + a_N v_i^N + \cdots \quad (2\text{-}1)$$

where v_i is the input voltage and $a_0, \ldots, a_N$ are the coefficients. When the v_i is expanded as

$$v_i(t) = V_i \cos(\omega_1 t) \tag{2-2}$$

where V_i is the amplitude of the input voltage and $\omega_1$is the frequency. The Taylor series can be rewritten as

$$\begin{aligned} f(v_i(t)) &= a_0 + a_1 V_i \cos(\omega_1 t) + a_2 (V_i \cos(\omega_1 t))^2 \\ &\quad + a_3 (V_i \cos(\omega_1 t))^3 + \cdots \\ &\quad + a_N (V_i \cos(\omega_1 t))^{\mathrm{N}} + \cdots \end{aligned}$$

$$\begin{aligned} &= \left(a_0 + \frac{a_2 V_i^2}{2}\right) + \left(a_1 V_i + \frac{3}{4} a_3 V_i^3\right) \cos(\omega_1 t) \\ &\quad + \frac{1}{2} a_2 V_i^2 \cos(2\omega_1 t) + \frac{1}{4} a_3 V_i^3 \cos(3\omega_1 t) \\ &\quad + \cdots \end{aligned} \tag{2-3}$$

When a sinusoidal signal is passed through a nonlinear device, the output signal contains not only the fundamental component at frequency ω_1, but also additional components, including the DC component and harmonics with frequencies that are integer multiples of ω. This effect is known as harmonic distortion.

Furthermore, it is observed that the amplitude of the Nth harmonic term is directly proportional to the coefficient a_N and V_i^N. But a_N is inversely proportional to N. So, when the input signal V_i is relatively small, the higher order of harmonic term a_N and V_i^N will be very small and can usually be ignored.

2.1.2 Intermodulation Distortion

Intermodulation distortion is the other significant characteristic of nonlinearity. When multiple signals of various frequencies are simultaneously applied to the input of an amplifier

or an analog system, the nonlinear behavior of the amplifier/analog systems results in the generation of new frequencies. These newly generated frequencies are combination of the original frequencies and known as intermodulation [1].

Intermodulation distortion occurs when these intermodulation components coincide with or are close to the frequencies of the input signals. Filtering out these interfering signals becomes challenging. The presence of intermodulation distortion can be described as follows.

Assume that the input $v_i(t)$ contains two signals as

$$v_i(t) = V_i \cos(\omega_1 t) + V_i \cos(\omega_2 t) \tag{2-4}$$

where V_i is the amplitude of the input voltage and ω_1 and ω_2 are the frequencies. Substituting $v_i(t)$ into the Taylor series, the output of these two-tone input will be

$$\begin{aligned} f(v_i(t)) = {} & (a_0 + a_2 V_i^2) \\ & + \left(a_1 V_i + \frac{9}{4} a_3 V_i^3\right)\left(\cos(\omega_1 t)\right. \\ & \left. + \cos(\omega_2 t)\right) \\ & + \frac{1}{2} a_2 V_i^2 \left(\cos(2\omega_1 t) + \cos(2\omega_2 t)\right) \\ & + a_2 V_i^2 \cos(\omega_1 \pm \omega_2) t \\ & + \frac{3}{4} a_3 V_i^3 (\cos(2\omega_1 \pm \omega_2) t \\ & + \cos(2\omega_2 \pm \omega_1) t) \\ & + \frac{1}{4} a_3 V_i^3 (\cos 3\omega_1 t + \cos 3\omega_2 t) + \cdots \end{aligned} \tag{2-5}$$

The system output contains the fundamental frequencies ω_1 and ω_2, the second order harmonic $2\omega_1$ and $2\omega_2$, the third order harmonic $3\omega_1$ and $3\omega_2$, etc. And it also produces the second-order intermodulation with frequency $\omega_1 \pm \omega_2$, the third-order intermodulation with frequencies $2\omega_1 \pm \omega_2$ and $2\omega_2 \pm \omega_1$, etc. The input signal spectrum and output signal spectrum are shown in Figure 2-1 and Figure 2-2, respectively.

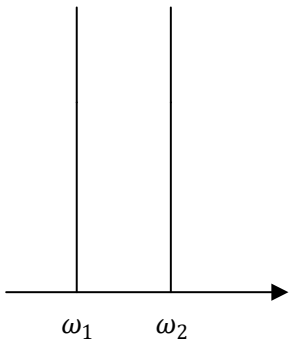

Figure 2-1 Input signal spectrum

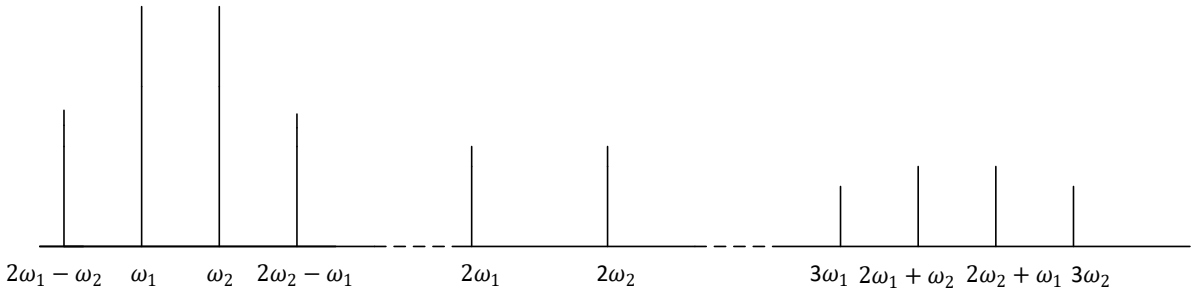

Figure 2-2 Output signal spectrum

As the even-order intermodulation and harmonics are far from the fundamental frequency, they can be simply filtered out by a filter. But the odd-order intermodulation is usually difficult to filter out as it is very close to the fundamental frequencies, especially the third-order intermodulation $2\omega_1 - \omega_2$ and $2\omega_2 - \omega_1$, which have the greatest impact on fundamental signals.

2.2 Linearization for a Memoryless System

Various techniques have been employed for achieving RoF or power amplifier linearization. Among them, three commonly utilized methods are feedforward, feedback, and predistortion methods [1]. Each of these methods encompasses different methods with specific implementations. However, the underlying principle of all these techniques remains the same: utilizing the input signal of the amplifier/analog system as a reference and

comparing it with the output signal. The correction, which is the difference of the reference and output signal, is then applied to the output signal using the mentioned methods.

2.2.1 Feedback Linearization

In the past, the feedback method was widely used as a linearization technique. However, in RF applications, ensuring system stability becomes challenging, leading to the limited use of RF feedback directly. Instead, modulated feedback systems are commonly employed to operate the system at lower frequencies. Two commonly used modulated feedback methods are indirect feedback and Cartesian feedback methodologies [1]. These methods differ in how they obtain feedback signals.

Among the various feedback techniques, Cartesian feedback methodologies have shown the most maturity. The fundamental concept of Cartesian feedback is to decompose the nonlinear distortion signal from the amplifier/analog system's output into its phase and quadrature components. These components are then compared with the original input signal to obtain an error signal. After filtering, the signal is quadrature modulated and passed through the power amplifier for signal feedback [1]. Figure 2-3 illustrates the schematic of a Cartesian feedback system.

The advantage of the feedback method lies in its simple structure, while effective suppression of intermodulation interference is provided. However, a drawback is the narrow bandwidth due to the delay introduced by the circuit components [1].

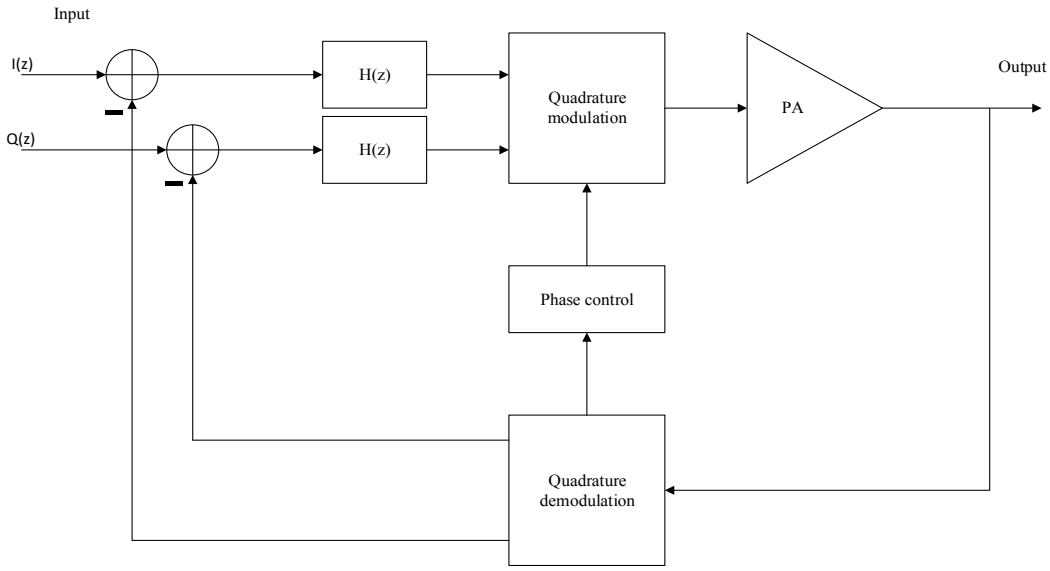

Figure 2-3 Schematic of the Cartesian feedback system

2.2.2 Feedforward Linearization

The feedforward method is a unique approach that incorporates a feedback signal into the output. Its principle involves splitting the input signal into two branches by splitter. One branch drives the main amplifier, while the other serves as a reference signal. The output signal of the main amplifier contains amplifier distortion, which is then compared to the reference signal to obtain an error signal. Finally, the error signal, amplified by the auxiliary amplifier, is subtracted from the main amplifier's output signal. This results in an amplified signal that is free from distortion, effectively improving the amplifier/analog system's linearity.

Feedforward technology offers several advantages, including significant linearity improvement and a wide, stable working bandwidth. However, it comes with drawbacks such as high system complexity and lower efficiency. Figure 2-4 illustrates the schematic of a linearization system employing the feedforward method [1].

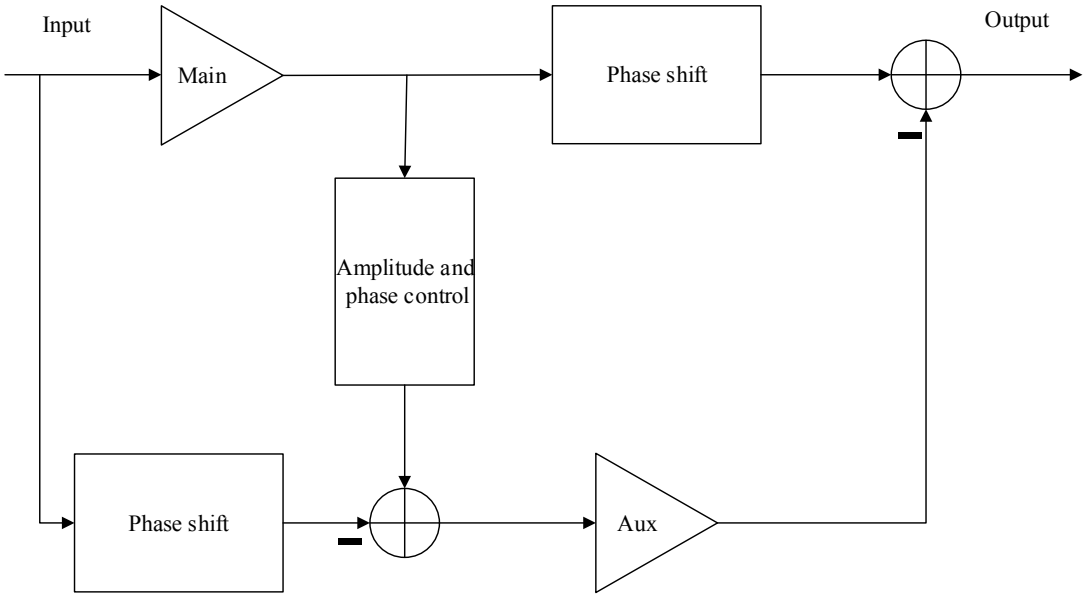

Figure 2-4 Schematic of the Feedforward system

2.2.3 Memoryless Polynomial Predistortion

Due to the rapid development of digital signal processing (DSP) technology and the increasing maturity of software-defined radio (SDR), the digital predistortion method has gained significant popularity in recent years [1]. This method offers numerous advantages, including high flexibility, good consistency, strong applicability, and the ability to easily implement adaptive processing. As a result, DPD holds great potential for effectively mitigating nonlinearity while superior performance and manageable complexity are maintained.

Currently, two prominent digital predistortion methods are widely utilized. The first method involves constructing a predistortion device based on polynomials, while the second method employs a look-up table (LUT) for performing predistortion. Both approaches share the concept of creating a predistortion element with characteristics opposite to those of a power amplifier/analog system. This predistortion component is then connected to the power amplifier/analog system to achieve the desired linearization effect. Figure 2-5 provides an illustration of the principle behind predistortion [1].

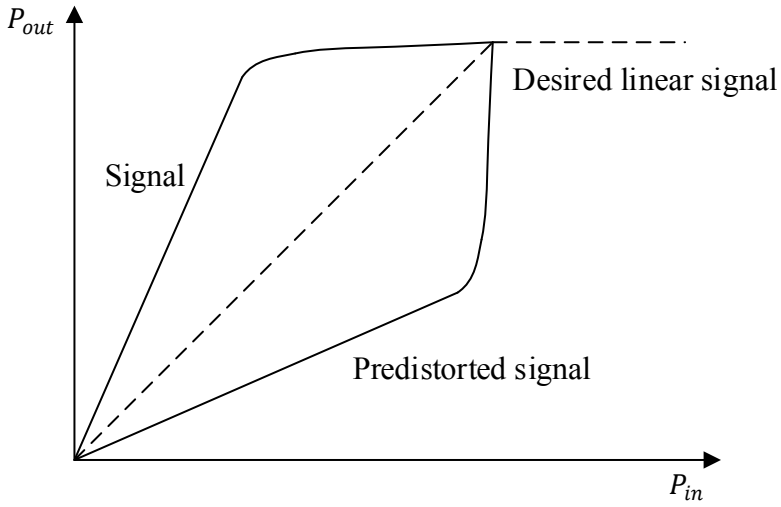

Figure 2-5 Predistortion principle

For the memoryless nonlinear system or the memory effect that is negligible, the system can be expressed by nonlinear instantaneous function as

$$y(n) = \sum_{k=0}^{K} a_k |x(n)|^k \, x(n) \tag{2-6}$$

where $y(n)$ is the output, $x(n)$ is the input, K is the polynomial order and $a_0, \ldots, a_N$ are the coefficients of the polynomial. The polynomial order indicates the nonlinearity order of the system. This polynomial function is relatively simple for single band signal or two-band signals, and it is easy to find the coefficients. Moreover, it is more suitable for computer simulation. Thus, it is currently one of the most popular linearization methods for any nonlinear systems [1].

2.2.4 Look-up Table

Different from the polynomial predistortion method, the look-up table uses a table to store the amplitude and phase nonlinearity of the power amplifier/analog system to address the predistortion. The main idea of the look-up table is by adjusting the input to get a linear

output signal, as Figure 2-6 shown. The LUT gain and the gain of a power amplifier/RoF system work together to make the total gain of the whole circuit constant, so the linearization of power amplifier/ RoF system is realized. LUT is the simplest method of DPD, however it does not consider the temperature and ageing effect of the system [9].

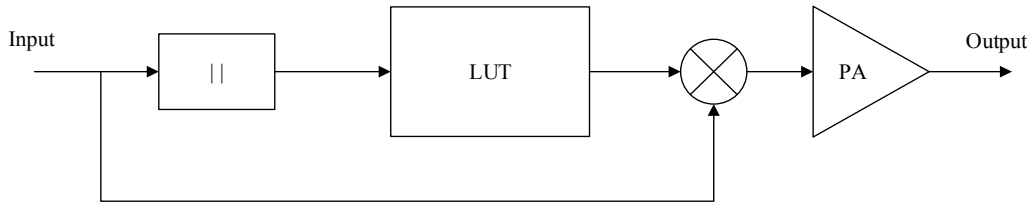

Figure 2-6 Schematic of the Look-up table

2.3 Linearization with Memory Effect

2.3.1 Memory Effect

As digital signal processing systems have developed, non-constant envelope modulations with ultra-wide bandwidth have been widely used. Within these modulations, memory effect has emerged as a significant source of system distortion. Consequently, the memory effect in an analog system, especially PA, need to be addressed. Thus, the digital predistortion device must possess a memory structure to accurately compensate for the memory effect within the power amplifier/RoF. The term "memory effect" denotes the phenomenon wherein the output signal of a power amplifier/RoF is not only dependent on the current input signal but also influenced by past input signals [1].

2.3.2 Volterra Series and Memory Polynomial

The Volterra series is a typical expression of the nonlinear memory effect of a power amplifier, which could also be considered as a Taylor series with memory effect. Assume that the bandpass system input and output are $x(t)$ and $y(t)$. The nonlinear relationship is given by the following Volterra series [1].

$$y(t) = \sum_{l=1}^{L} \int \dots \int h_l(\tau_1, \dots, \tau_l) \prod_{i=1}^{l} x(t-\tau_i) d\tau_1 \dots d\tau_l \tag{2-7}$$

where $h_l(\tau_1, \dots, \tau_l)$ is the lth order kernel of Volterra series. In fact, the data that are used will always be discrete time data. Therefore, for the discrete time, the Volterra series could be rewritten as

$$y(n) = \sum_{n=1}^{N} \sum_{m_1=1}^{M} \dots \sum_{m_n=1}^{M} h_n(m_1, \dots, m_n) \prod_{j=1}^{n} x(n-m_j) \tag{2-8}$$

where N is the nonlinearity order and M is the memory depth.

The Volterra series offers a significant advantage as it allows separated characterization of each order of nonlinear components within a system. Moreover, Volterra series also captures the nonlinear memory effect in different orders. Thus, Volterra series enables an accurate approximation of a wide range of nonlinear systems in any analog system including PA or RoF. However, as the polynomial order and memory depth of the Volterra series increase, the number of coefficients to be calculated or found grows exponentially, which leads to extremely high computational complexity, inducing a limitation on the practical application of the Volterra series.

In response to this limitation, extensive efforts have been dedicated to simplifying the complexity of the Volterra series. One commonly used simplified function is the memory polynomial. By considering only the diagonal terms of the Volterra series, a simplified function can be derived as follows

$$y(n) = \sum_{k=1}^{K} \sum_{m=0}^{M-1} b_{km} x(n-m) |x(n-m)|^{k-1} \tag{2-9}$$

where K represents the nonlinearity order and M is memory depth. This function is composed of the several time delays and the nonlinear static functions. The structure is simple and straightforward.

Chapter 3 Theory of Low-Complexity Multi-band DPD

3.1 Memory Polynomial for Multi-band Signals

In terms of the one-band discrete time input signal, the linearization function using the memory polynomial is the same as (2-9). However, as the number of input signal bands is increased, the expansion of the memory polynomial should contain terms to compensate cross-bands distortion. For example, three-band signal reads

$$x = x_1 e^{-j\omega_1 t} + x_2 e^{-j\omega_2 t} + x_3 e^{-j\omega_3 t} \tag{3-1}$$

where ω_1, ω_2 and ω_3 are the frequencies of three bands. According to [44], the DPD function is given by

$$\begin{aligned} y_1(n) = \sum_{m=0}^{M-1}\sum_{k=0}^{N}\sum_{j=0}^{k}\sum_{i=0}^{s} c_{k,j,i,m}^{(1)} x_1(n \\ - m) \\ \times |x_1(n-m)|^{k-j} \left|x_2(n-m)^{j-i}\right| x_3(n \\ - m)\Big|^{i} e^{-j\omega_1 t} \end{aligned} \tag{3-2}$$

$$\begin{aligned} y_2(n) = \sum_{m=0}^{M-1}\sum_{k=0}^{N}\sum_{j=0}^{k}\sum_{i=0}^{s} c_{k,j,i,m}^{(2)} x_2(n \\ - m) \\ \times |x_1(n-m)|^{k-j} |x_2(n-m)|^{j-i} |x_3(n \\ - m)|^{i} e^{-j\omega_2 t} \end{aligned} \tag{3-3}$$

$$\begin{aligned} y_3(n) = \sum_{m=0}^{M-1}\sum_{k=0}^{N}\sum_{j=0}^{k}\sum_{i=0}^{s} c_{k,j,i,m}^{(3)} x_3(n \\ - m) \\ \times |x_1(n-m)|^{k-j} |x_2(n-m)|^{j-i} |x_3(n \\ - m)|^{i} e^{-j\omega_3 t} \end{aligned} \tag{3-4}$$

where both the in-band distortion and the cross-band distortion are included.

3.2 The Function of Proposed DPD

To illustrate the proposed function, a memoryless nonlinearity function is used first

$$y = \sum_{k=0}^{N} a_k x^k \tag{3-5}$$

where k is the nonlinearity order and note that even orders (k) are not located in band. So, for simplicity, only odd orders will be taken. And to make the expression look more concise, the total nonlinearity orders of five will be taken as an example. Therefore, the new function will be

$$y = \sum_{k=0}^{2} a_{2k} x|x|^{2k} \tag{3-6}$$

Now consider the three-band input signal as an example, i.e. x is given by equation (3-1). Thus, based on equation (3-1) and (3-6), the output signal allocated at $\omega_1$will be

$$\begin{gathered} y(\omega_1) = (a_0 x_1 + a_2 x_1(|x_1|^2 + |x_2|^2 + |x_3|^2) + \\ a_4 x_1(|x_1|^4 + |x_2|^4 + |x_3|^4 + |x_2|^2|x_3|^2 + |x_1|^2|x_2|^2 + \\ |x_1|^2|x_3|^2))e^{-j\omega_1 t} \end{gathered} \tag{3-7}$$

Equation (3-7) can be simplified by using

$$\begin{gathered} s_0 = |x_1| + |x_2| + |x_3| \\ s_1 = |\,(|x_1| - |x_2| - |x_3|)| \\ s_2 = |\,(|x_2| - |x_1| - |x_3|)| \\ s_3 = |\,(|x_3| - |x_2| - |x_1|)| \end{gathered} \tag{3-8}$$

where s_0 is the summation of three signal and s_1 , $s_2$and s_3 are the difference of the three band signals. By combining equation (3-7) and (3-8), the new proposed DPD for the ω_1 is given as

$$y_1(n) = \sum_{k=0}^{K}\sum_{i=0}^{3} c_{m,k,i} x_1(n)|s_i(n)|^k + \sum_{k=0}^{K} c_{m,k,4} x_1(n)|x_1(n)|^k \tag{3-9}$$

Similarly, we can obtain the proposed DPD for ω_2 and ω_3 as

$$y_2(n) = \sum_{k=0}^{K}\sum_{i=0}^{3} c_{m,k,i} x_2(n)|s_i(n)|^k + \sum_{k=0}^{K} c_{m,k,4} x_2(n)|x_2(n)|^k \tag{3-10}$$

and

$$y_3(n) = \sum_{k=0}^{K}\sum_{i=0}^{3} c_{m,k,i} x_3(n)|s_i(n)|^k + \sum_{k=0}^{K} c_{m,k,4} x_3(n)|x_3(n)|^k \tag{3-11}$$

Thus, by considering memory effect, the function of the proposed DPD for multi-band signals is given below. For the multi-band input $x(n)$, the output for the lth band is $y_l(n)$. $l = 1,2,\dots,L$. L denotes the total band number of input signal.

$$y_l(n) = \sum_{m=0}^{M}\sum_{k=0}^{K}\sum_{i=0}^{L} c_{l,m,k,i} x_l(n-m) s_{l,i}^k(n-m) + \sum_{m=0}^{M}\sum_{k=0}^{K} c_{l,m,k,L+1} x_l(n-m)|x_l(n-m)|^k \tag{3-12}$$

where $s_{l,i}$ are the sum and difference of all the input signals, M and K are the memory depth and the nonlinearity order, respectively. s_i is given by

$$
\begin{aligned}
s_0 &= (|x_1| + |x_2| + \cdots + |x_L|) \\
s_1 &= (|x_1| - |x_2| - \cdots - |x_L|) \\
s_2 &= (|x_2| - |x_1| - \cdots - |x_L|) \\
&\cdots \\
s_L &= (|x_L| - |x_1| - \cdots - |x_{L-1}|)
\end{aligned}
\tag{3-13}
$$

Equation (3-12) is the *newly proposed low-complexity multi-band DPD function*. This new function aims to address the challenges of exponentially increased coefficient number in a system that has high nonlinearity order and more frequency bands. Remarkably, this proposed function aims to achieve a significant reduction in complexity while the cross-band modulation effects originating from all other bands are still contained.

By utilizing equation (3-12), the proposed multi-band DPD function can effectively compensate for nonlinear distortions in a system with multiple frequency bands. This is achieved by considering both the in-band modulation and the cross-band modulation. The proposed low-complexity multi-band DPD offers the advantages of improved computational efficiency, lower data requirements, ease of implementation, interpretability, reduced risk of overfitting, stability, and robustness.

3.3 Comparison of Complexity

This low-complexity multiband DPD approach aims to minimize the number of DPD function coefficients required. The complexity of the proposed DPD is compared to a conventional DPD with a fixed memory depth of six. The details are shown in Table 3-1 and Figure 3-1. The black line represents the conventional DPD function, and the red line represents the proposed DPD function. The results demonstrate that as the number of bands and nonlinearity orders increase, the complexity of the conventional DPD significantly rises, while the proposed DPD shows significantly lower complexity. For example, considering the 6-band signals with a nonlinearity order of 10 and a memory depth of 5, the conventional DPD requires a total of 40040 coefficients. However, in the proposed low-complexity DPD

only requires the coefficients of 640. This reduction in complexity offers several advantages, including improved computational efficiency, lower data requirements, ease of implementation, interpretability, reduced risk of overfitting, stability, and robustness.

Nonlinearity order	Conventional 3D-MP	Proposed 3D-DPD	Conventional 4D-MP	Proposed 4D-DPD	Conventional 5D-MP	Proposed 5D-DPD	Conventional 6D-MP	Proposed 6D-DPD
3	80	72	120	144	168	168	224	192
4	160	96	280	192	448	224	672	256
5	280	120	560	240	1008	280	1680	320
6	448	144	1008	288	2016	336	3696	384
7	672	168	1680	336	3696	392	7392	448
8	960	192	2640	384	6336	448	13728	512
9	1320	216	3960	432	10296	504	24024	576
10	1760	240	5720	480	16016	560	40040	640

Table 3-1 Complexity of the proposed DPD and conventional memory polynomial DPD for memory depth of six

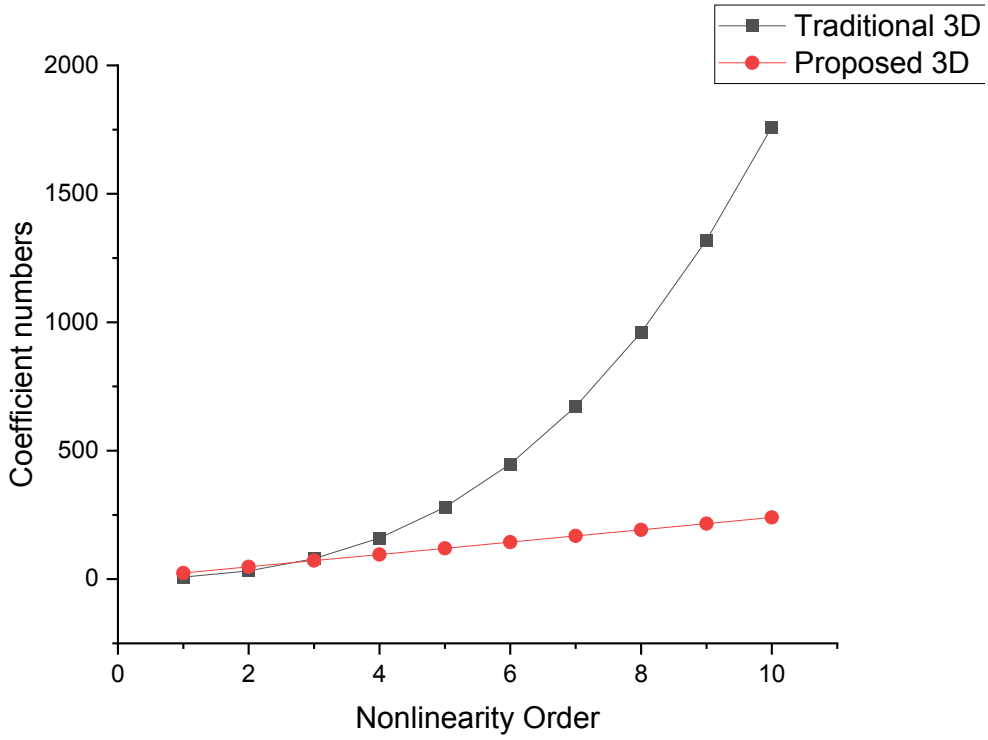

Figure 3-1 (a) Number of coefficients vs nonlinearity orders for three bands DPD

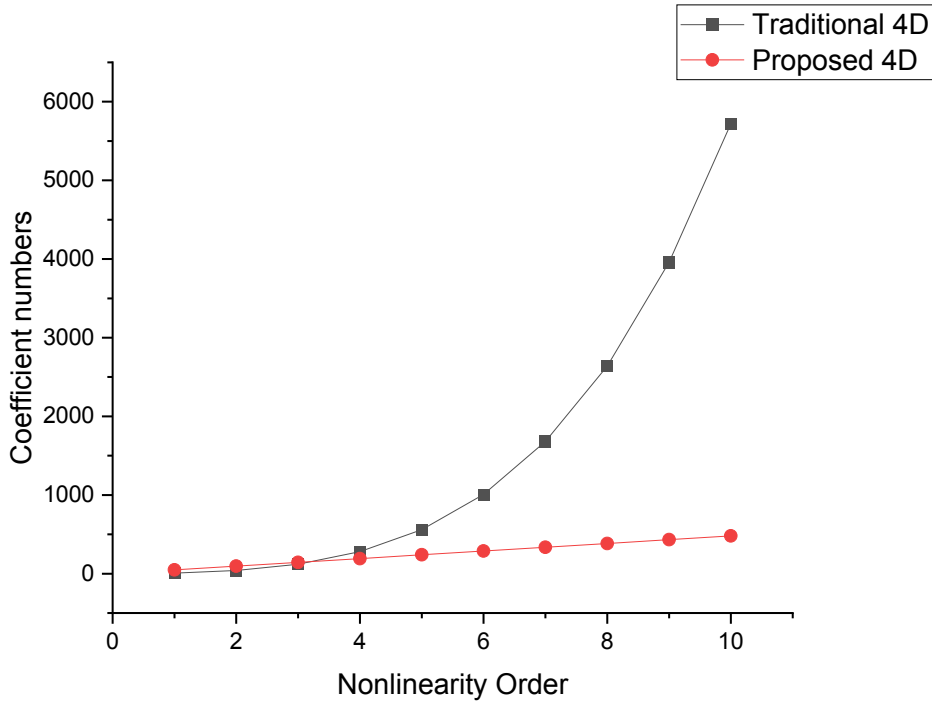

Figure 3-1(b) Number of coefficients vs nonlinearity orders for four bands DPD

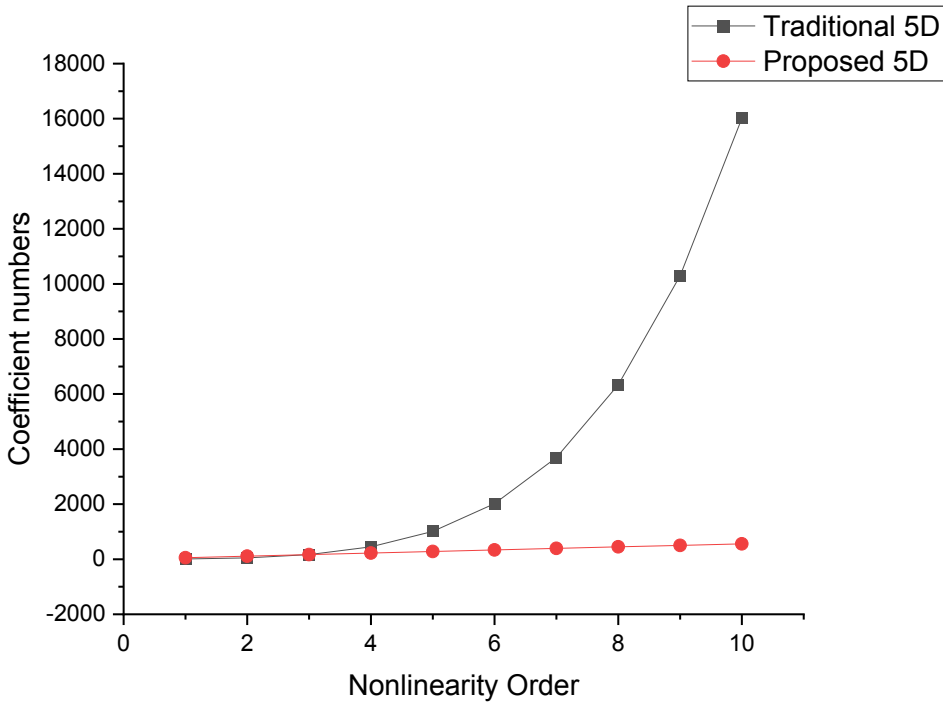

Figure 3-1 (c) Number of coefficients vs nonlinearity orders for five bands DPD

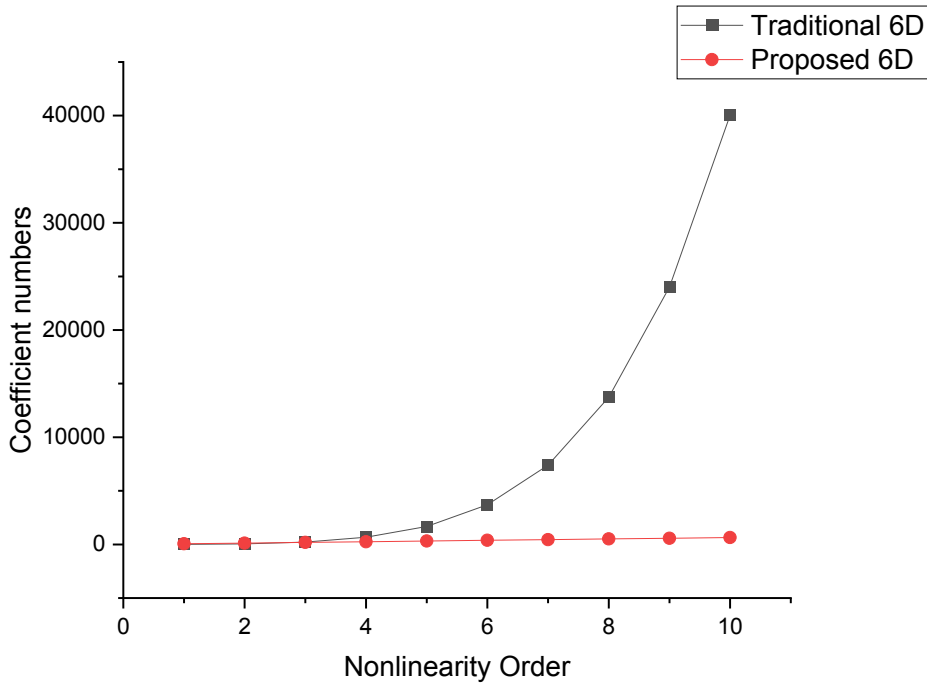

Figure 3-1 (d) Number of coefficients vs nonlinearity orders for six bands DPD

Fig. 3-1 shows the number of DPD function coefficients versus nonlinearity order for 3, 4, 5 and 6 bands of signals. It is seen that the coefficient number of the conventional DPD function increases exponentially, but the counterpart of the proposed DPD only increases linearly, with the increase of nonlinearity order.

Chapter 4 Performance Analysis using Simulations for Low-Complexity Multi-band DPD

4.1 Overview of the Simulation System

In the simulation, MATLAB is used to simulate a front-haul transmission system including data generating module, digital predistortion module, nonlinear transmission module and data analyzing module. The simulations are categorized into four groups based on the number of bands presented in the input signal: three-band, four-band, five-band, and six-band. In each category, the results were visualized and analyzed to assess the performance in terms of spectrum and constellation, considering the EVM as a metric. This analysis provides a comprehensive understanding of how the proposed DPD impacts the spectral characteristics and signal constellation, allowing for an evaluation of the system's overall performance and the effectiveness in mitigating distortions and improving signal quality.

The signal we used in this simulation is a 200 MHz 64-QAM OFDM signal, which has subcarriers bandwidth of 30 kHz. The signal is initially generated in the frequency domain and then undergoes an inverse fast Fourier transform to convert it into the time-domain signal. Subsequently, the transformed signals are transmitted into the DPD module for further processing and distortion mitigation.

In simulation, the rows and columns of the matrix can only start from one. Therefore, when calculating nonlinearity and memory depth, the k and m start from one. Thus, the DPD function will be adjusted as

$$y_l(n) = \sum_{m=1}^{M}\sum_{k=1}^{K}\sum_{i=0}^{L} c_{l,m,k,i}\, x_l(n-(m-1))\, s_{l,i}^{k-1}(n-(m-1)) + \sum_{m=1}^{M}\sum_{k=1}^{K} c_{l,m,k,L+1}\, x_l(n-(m-1))\,|x_l(n-(m-1))|^{k-1} \tag{4-1}$$

The pre-distorted signals then pass through the nonlinear transmission function, i.e. a Wiener-Hammerstein model, which was built by two linear filter with a static nonlinearity polynomial block in the middle in Figure 4-1 [1].

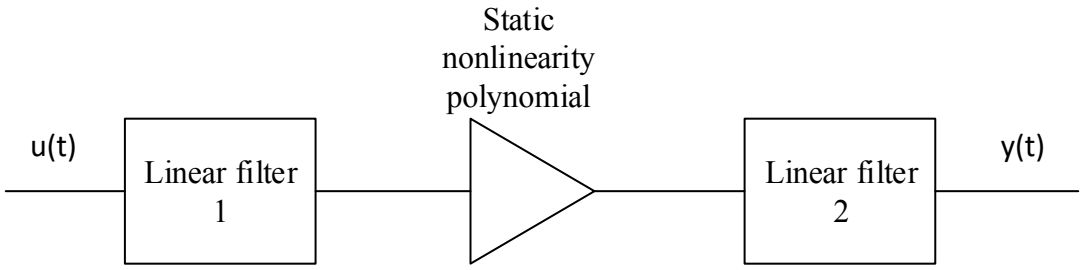

Figure 4-1 Wiener-Hammerstein model

Two linear filters are implemented by finite impulse response filters, which were generated via Matlab. The magnitude and phase response is shown in figure 4-2 and the impulse response is shown in figure 4-3. The transfer function of the filter is given by:

$$H(z) = \frac{-0.07 + 0.60z^{-1} + 0.27z^{-2} - 0.22z^{-3} + 0.18z^{-4} - 0.02z^{-5}}{0.5 - 0.32z^{-2}} \quad (4\text{-}2)$$

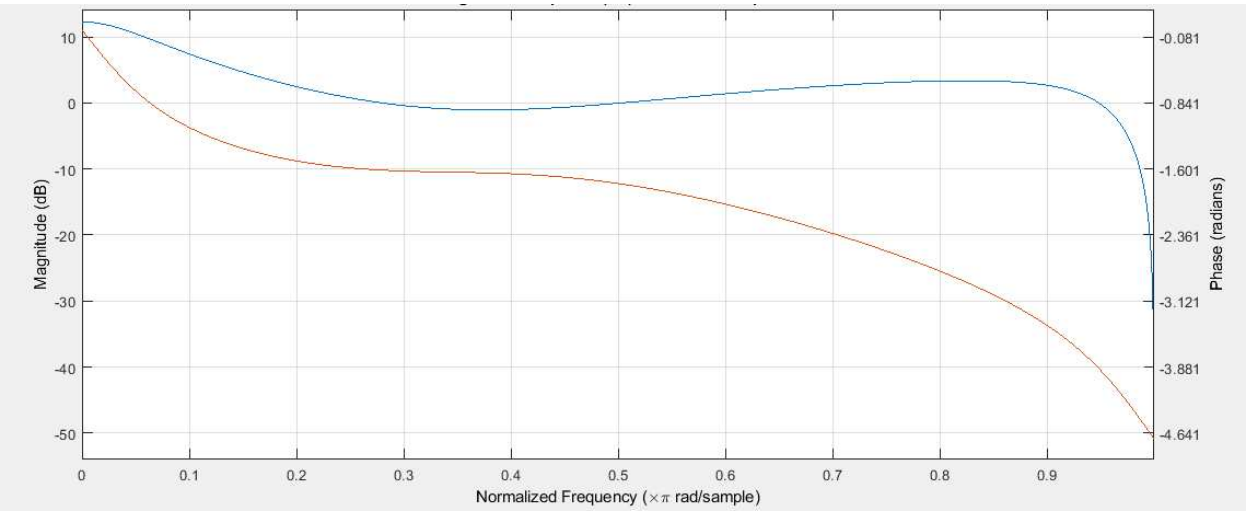

Figure 4-2 Magnitude response (dB) and phase response

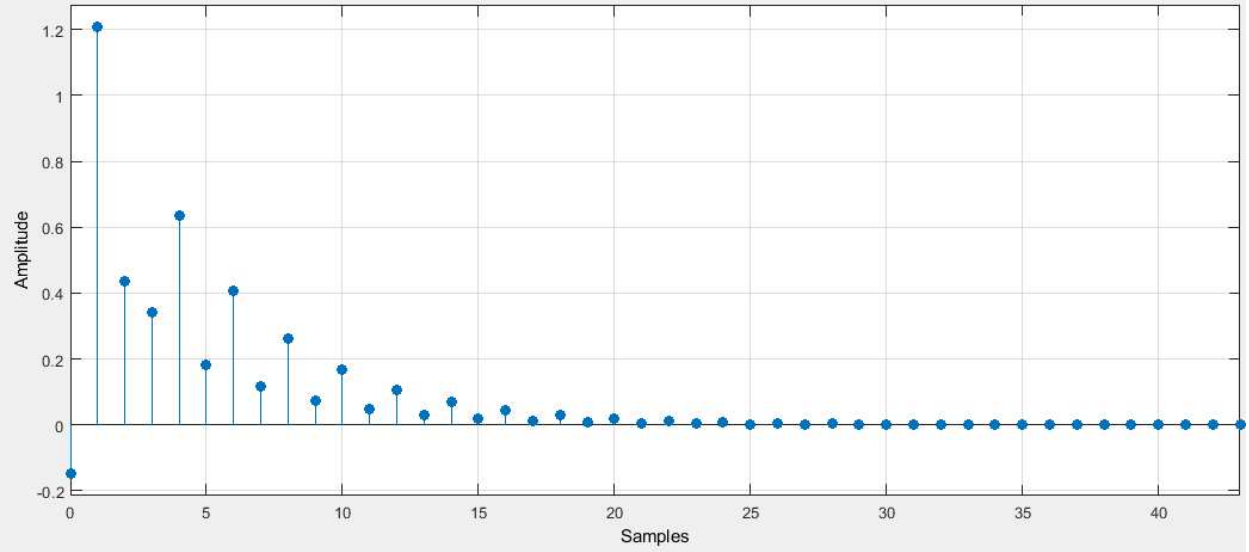

Figure 4-3 Impulse response

Regarding the static nonlinearity model, the exponential equation has been used to simulate the nonlinearity behavior. The exponential equation is a commonly used model for static nonlinearities, and it can be expressed by

$$y = b\left(1 - e^{-x/a}\right) \tag{4-3}$$

where x represents the input signal, a and b are parameters that control the nonlinearity characteristics, and y represents the output signal after passing through the static nonlinearity. In this thesis, b is a sign function of the input signal and a is set to 3 for the desired nonlinearity. Finally, the signals will be analyzed and visualized to determine the DPD performance.

4.2 Determination of Optimal Nonlinearity Order and Memory Depth

The nonlinearity order and memory depth of a transmission system vary depending on its characteristics. Therefore, before evaluating the performance of the proposed DPD, it

is crucial to set the appropriate nonlinearity order and memory depth for the system. To assess in-band distortion, the EVM is a significant parameter. This thesis utilizes EVM to determine the optimal nonlinearity order and memory depth for the DPD.

To determine the optimal nonlinearity order and memory depth of the DPD function, a simulation is conducted using a three-band input. The input signal consists of three 200 MHz bands located at 1.05 GHz, 1.53 GHz, and 2.1 GHz respectively.

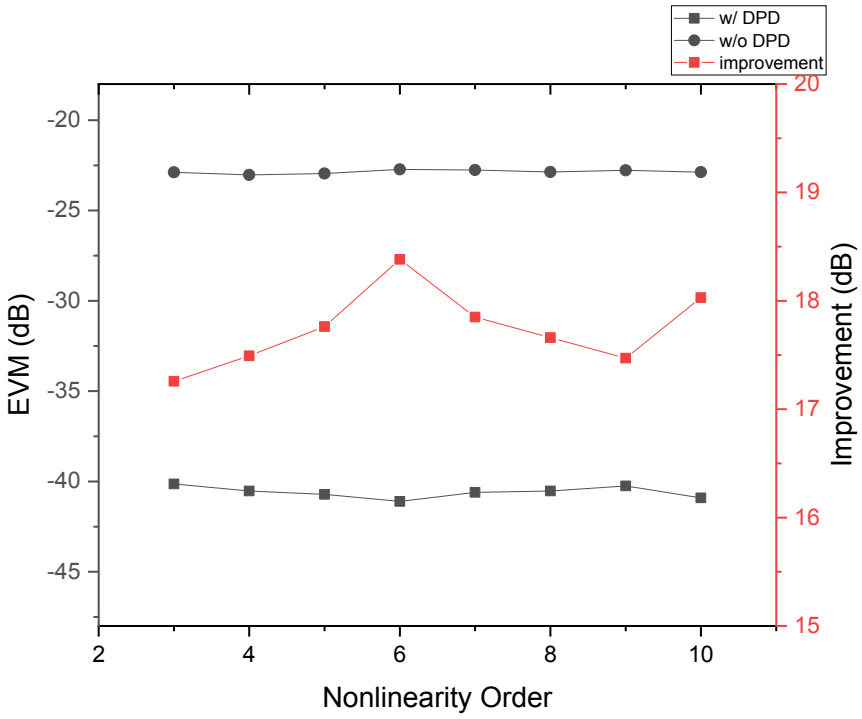

Figure 4-4 (a) EVM vs nonlinearity order K for first band

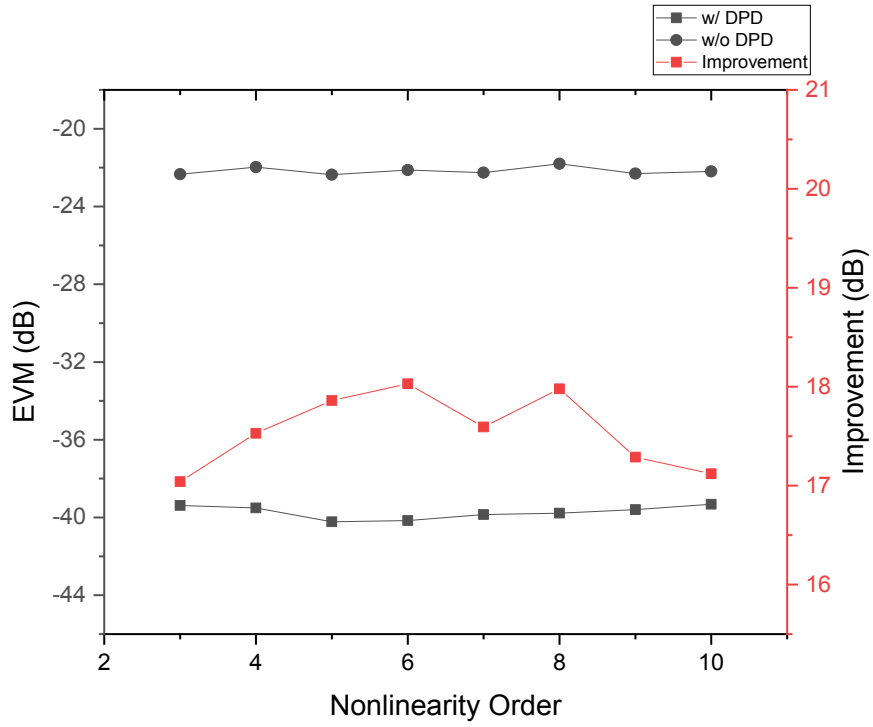

Figure 4-4 (b) EVM vs nonlinearity order K for second band

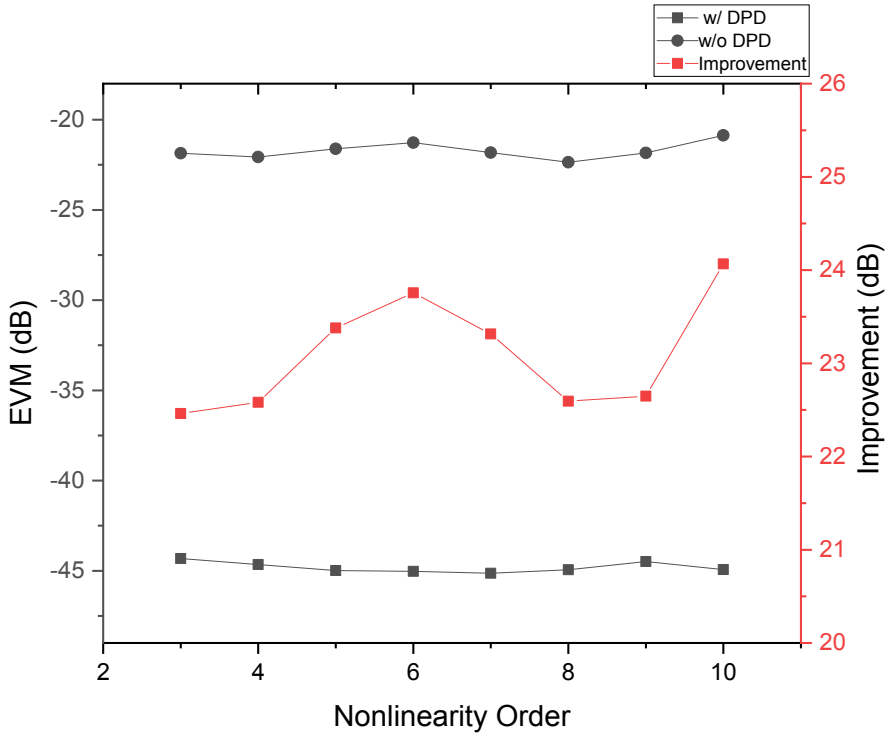

Figure 4-4 (c) EVM vs nonlinearity order K for third band

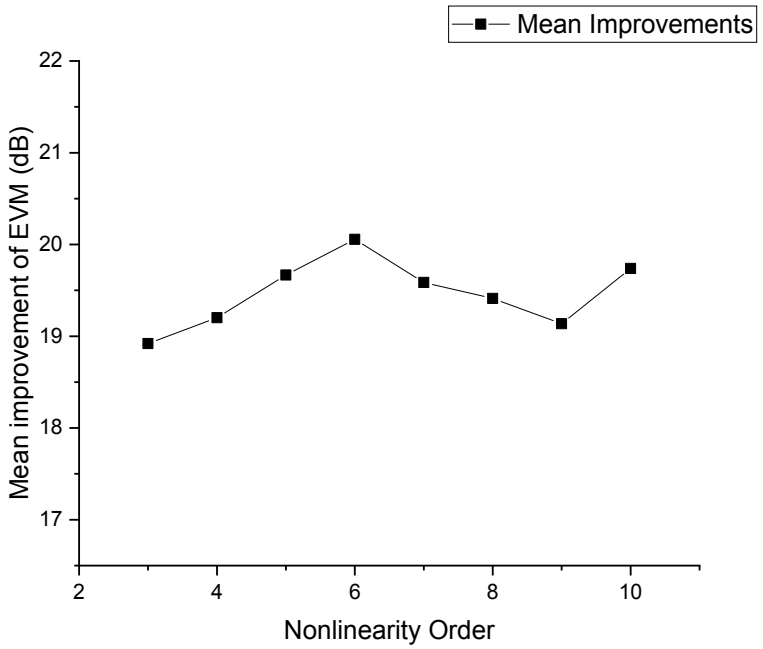

Figure 4-4 (d) Mean improvement of three bands in total

Figure 4-4 illustrates the correlation between EVM and nonlinearity order, for a given memory depth of seven. Figure 4-4 (a), (b) and (c) represent the results for each individual band, while 4-4 (d) represents the mean improvement for all the three bands. Figure 4-4 demonstrates that the performance improves for each band as the nonlinear order K increases. Notably, there is a peak at a nonlinear order of six and another peak at ten for the first and third band. When the nonlinear order for the DPD is chosen, it is important to consider not only the performance (EVM) but also the complexity of the DPD. Consequently, a nonlinear order of six should be good due to its optimal performance, and a further larger nonlinearity order does not continue to improve the performance.

In terms of memory depth, the performances of different memory depth are shown in Figure 4-5.

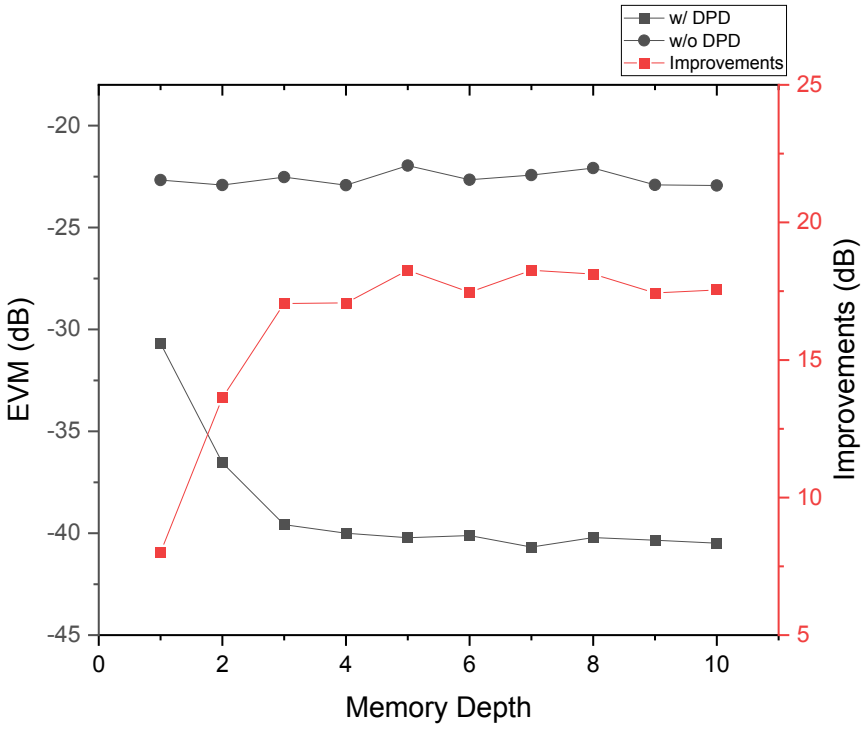

Figure 4-5 (a) EVM vs memory depth for first band

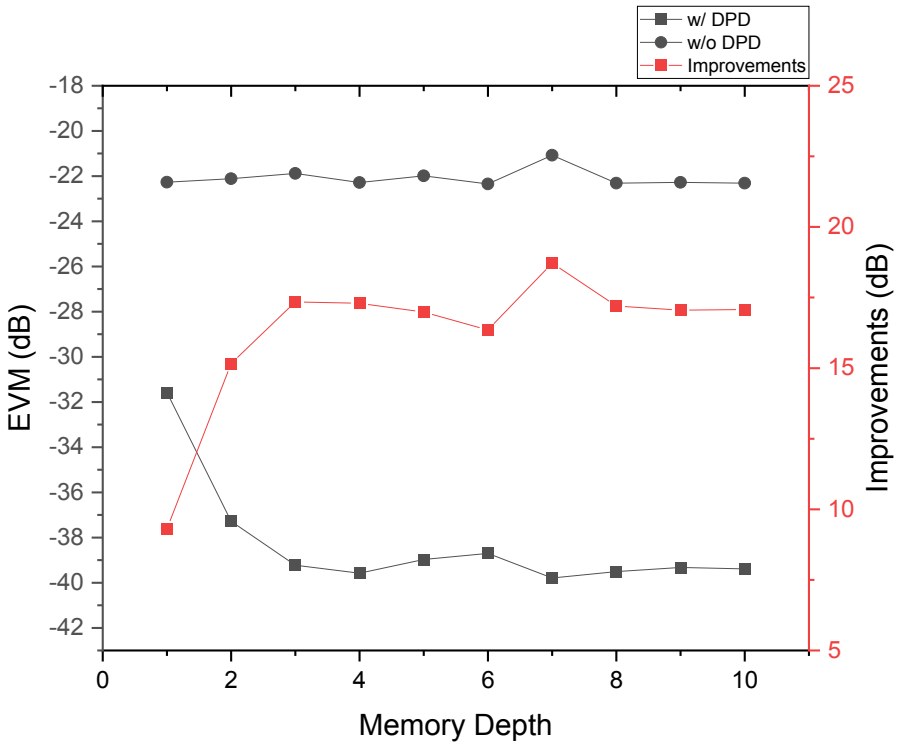

Figure 4-5 (b) EVM vs memory depth for second band

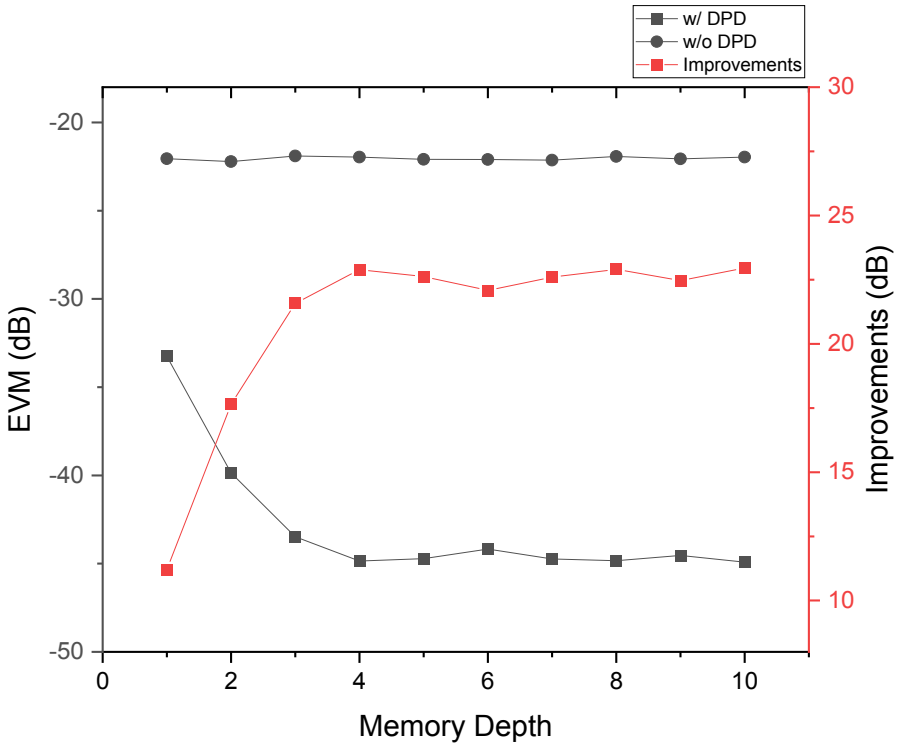

Figure 4-5 (c) EVM vs memory depth for third band

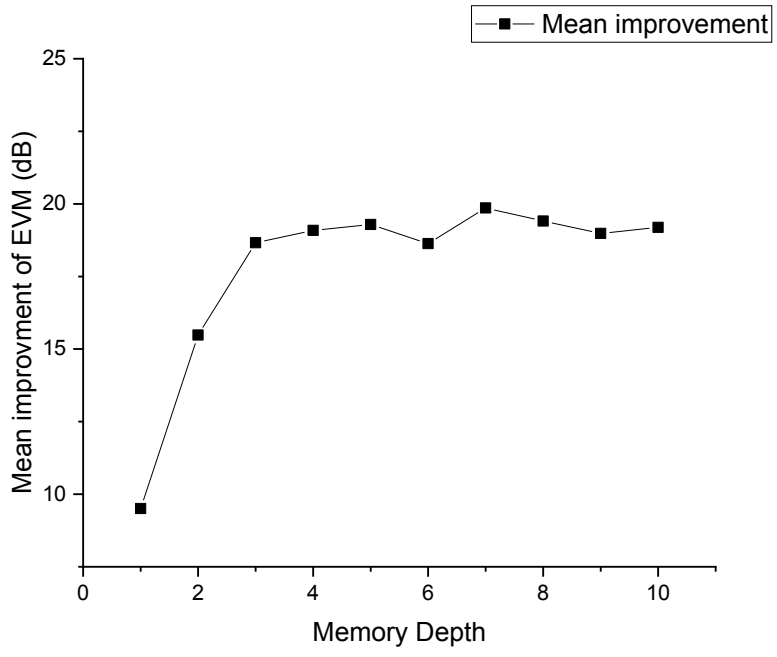

Figure 4-5 (d) Mean improvement of three bands

For the memory depth analysis, the same three-band simulation was conducted for the nonlinearity order fixed at six. The memory depth was varied from one to ten. Figure 4-5 illustrates the relationship between performance and memory depth. Figure 4-5 (a), (b), and (c) represent the results for each individual band, while Figure 4-5 (d) represents the mean improvement across all three bands. It is evident that the performance of each band improves as the memory depth increases, reaching a relatively saturated level after a memory depth of five.

Consequently, a memory depth of five is selected as it offers good performance. Therefore, the optimal DPD it was found for the above system has a memory depth of five and a nonlinearity order of six.

4.3 Simulation for Three-Band DPD

In this simulation, three frequency bands centered around 2.1 GHz, 3.1 GHz, and 4.2 GHz were considered. Each band has a bandwidth of 200 MHz. The memory depth was set to five, and the nonlinearity order was set to six for the proposed DPD. The simulation was implemented using Matlab.

To generate the input data, random signals were generated and organized into a 64-QAM format. The 64-QAM signal was then used as a fundamental component to construct an OFDM waveform. This was achieved by applying the IFFT algorithm, which converts the frequency domain data into a time domain analog OFDM symbol waveform.

The simulated spectrums are presented in Figure 4-6 for the two cases: with and without proposed DPD.

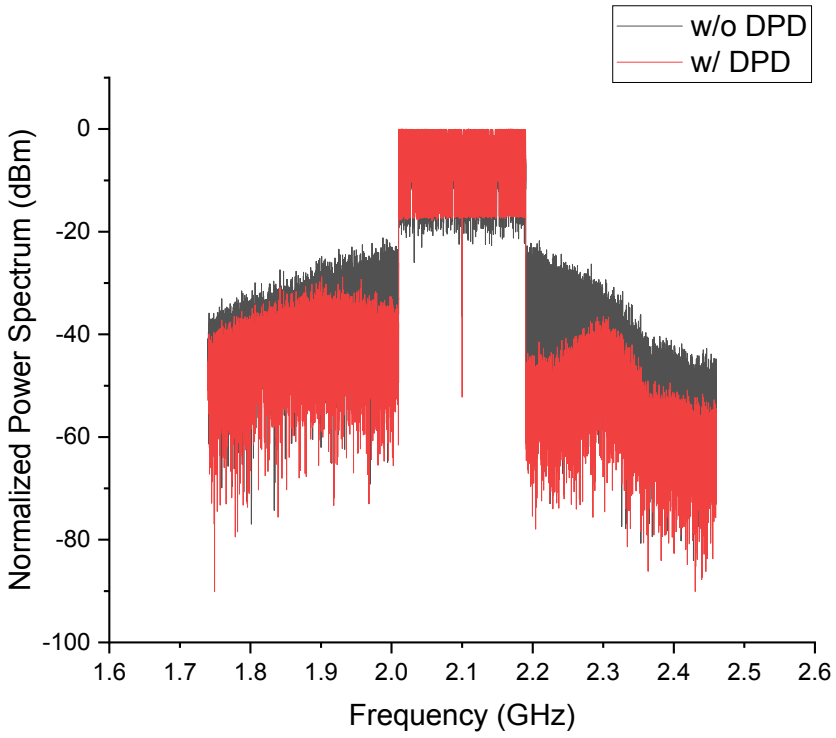

Figure 4-6 (a) Normalized power spectrum for the first band

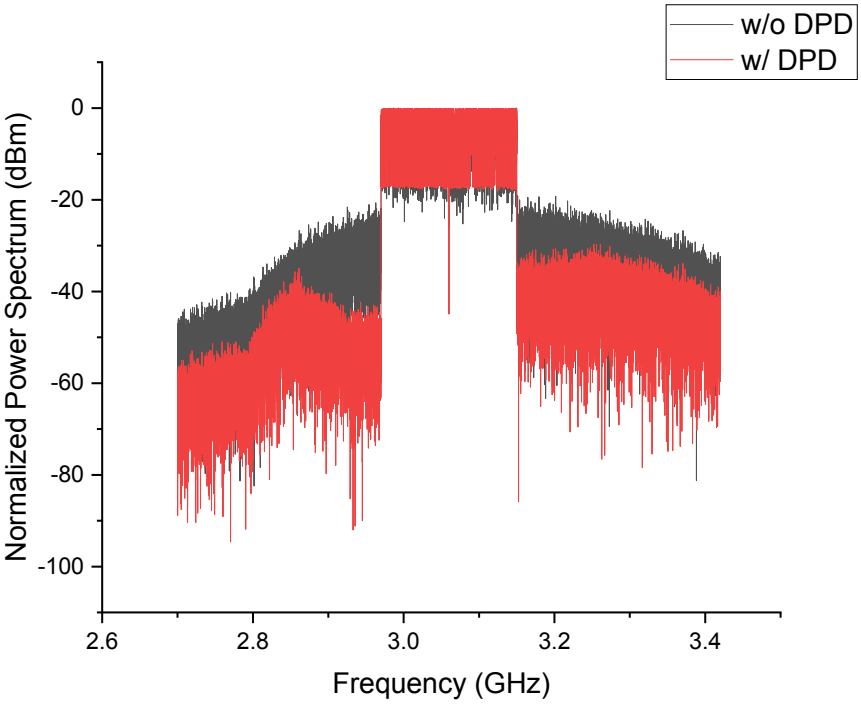

Figure 4-6 (b) Normalized power spectrum for the second band

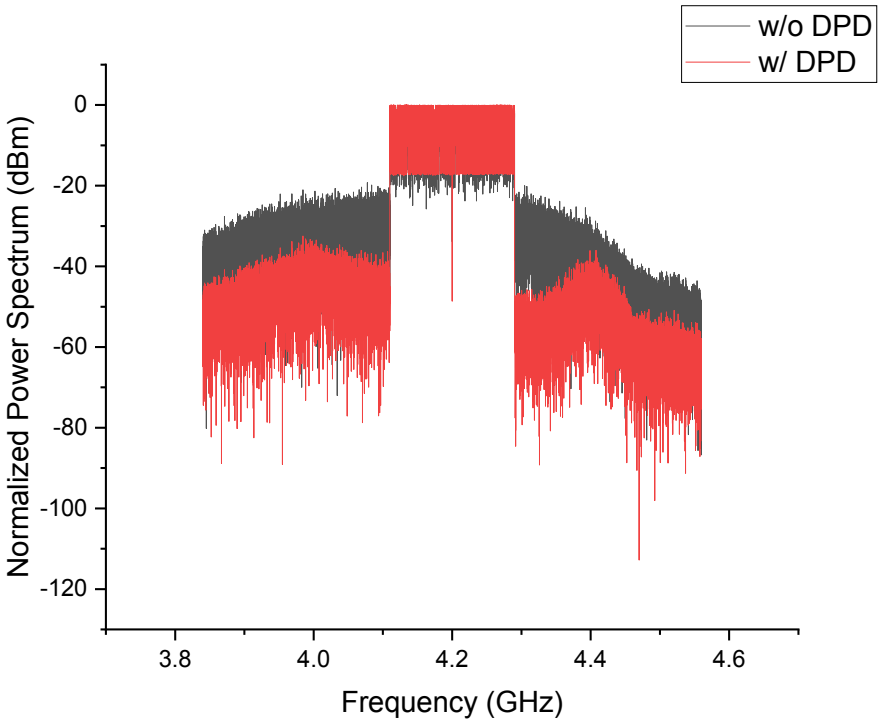

Figure 4-6 (c) Normalized power spectrum for the third band

Figure 4-6 shows the power spectrum of each band with and without the DPD. The black line represents the signal without the DPD, and the red line represents the signal with the proposed DPD. It is clearly demonstrated that the presence of spectrum expansion and power leak in adjacent channels exist when the proposed DPD technique is not applied. This distortion is a result of nonlinearity in the system. The parameters such as error vector magnitude and adjacent channel power ratio (ACPR) are adversely affected. Moreover, the nonlinearity in the system also has a detrimental effect on distant channels. It introduces interference to signals in the neighboring and distant channels, causing further degradation. However, when the proposed DPD is implemented, the out-of-band nonlinearity is effectively suppressed. This suppression reduces the degradation on adjacent channels, resulting in improved overall performance. The average improvement of ACPR is around 20 dB.

In terms of the EVM and the signal constellation, the simulation results are shown in Fig. 4-7. The constellation of signal without DPD is adjusted by the phase adjustment.

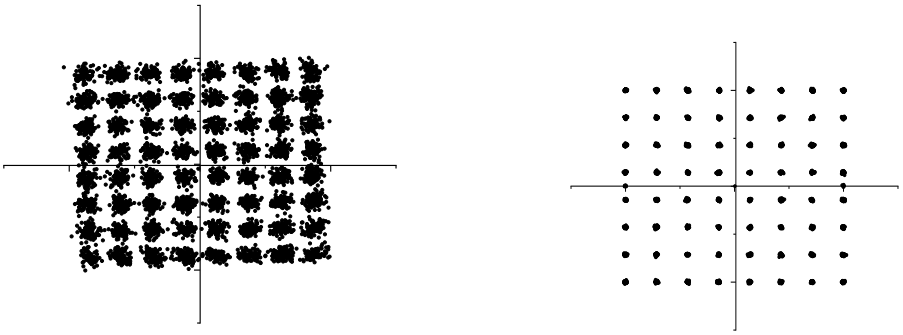

Figure 4-7 (a) Constellation of signal in first band. Left side is the signal without DPD. Right side is the signal with the DPD

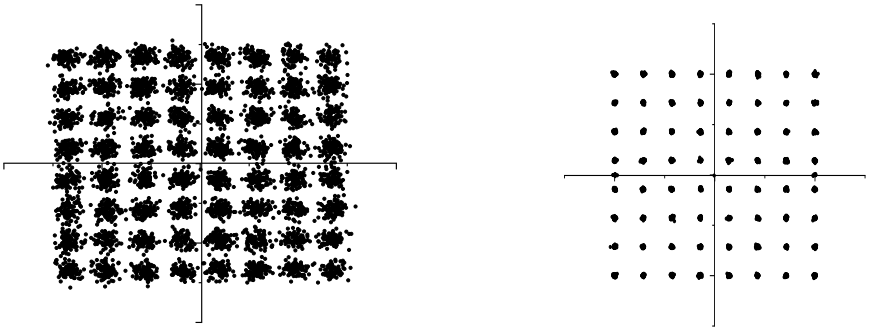

Figure 4-7 (b) Constellation of signal in second band. Left side is the signal without DPD. Right side is the signal with the DPD

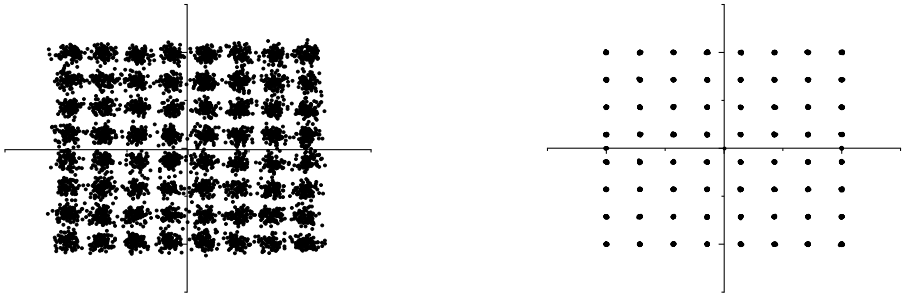

Figure 4-7 (c) Constellation of signal in third band. Left side is the signal without DPD. Right side is the signal with the DPD

Figure 4-7 shows the signal constellation of each band with and without DPD. The left side of Fig.4-7 is the signal without DPD, and the right side is the signal with the proposed DPD. It clearly illustrates the spreading of constellation points in the signal when the proposed DPD technique is not applied. This spreading indicates severe distortion in the signal, resulting in a degradation of the EVM. Additionally, the absence of DPD increases the challenges in signal demodulation and leads to higher bit error rates. Specifically, in the simulations without DPD, the EVM values are -22.84 dB, -22.47 dB, and -22.19 dB for the three bands. These EVM values reflect the extentence of distortion and the difficulties for maintaining signal quality and accuracy.

However, the application of the proposed DPD results in a noticeable concentration of the signal constellation points, leading to a significant improvement in the EVM. The simulations with the proposed DPD give EVM values of -41.18 dB, -40.47 dB, and -45.56 dB for the three bands. This corresponds to improvement in EVM of 18.53 dB, 17.99 dB, and 23.36 dB for each band, with an average improvement of approximate 20 dB across all three bands. These results demonstrate the effectiveness of the DPD in enhancing signal quality and reducing distortion.

In terms of the AM-AM and AM-PM distortions. The simulation results are shown in Figure 4-8. The left side is for AM-AM conversion and the right side is for AM-PM conversion. The black points present the signal without DPD and the red points present the signal with the proposed DPD. The AM-AM graph illustrates the amplitude distortion characteristics of a system or device both with and without the DPD. It depicts the relationship between the input and output amplitudes, highlighting the nonlinear behavior of the system in the absence of DPD. Without DPD, the output power shows nonlinearity, indicating gain compression and expansion caused by system nonlinearities. However, with the application of the DPD, the output power becomes more linear, resulting in a substantial reduction in gain compression and expansion.

The AM-PM graph illustrates the phase distortion introduced by a system or device. It demonstrates the phase shift or modulation of the output signal relative to the input signal

amplitude. In the absence of DPD, the phase distortion is observed. However, with the application of the DPD, the phase distortion is reduced, resulting in a reduction of the observed phase shift.

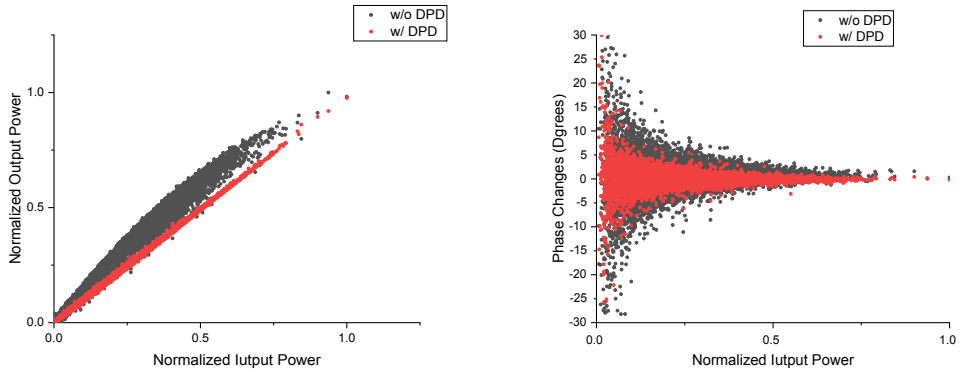

Figure 4-8 (a) AM-AM and AM-PM distortion for the first band with and without the DPD

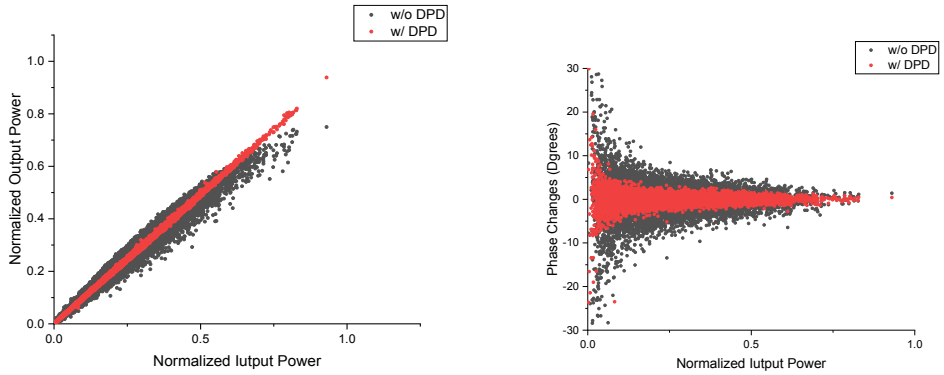

Figure 4-8 (b) AM-AM and AM-PM distortion for the second band with and without the DPD

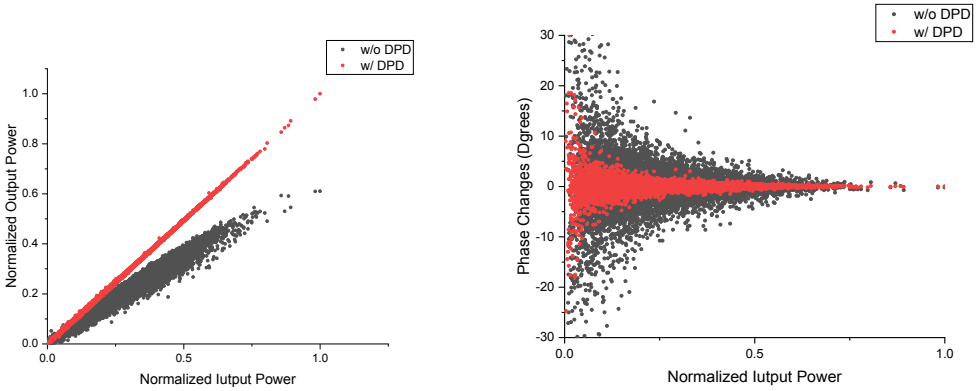

Figure 4-8 (c) AM-AM and AM-PM distortion for the third band with and without the DPD

4.4 Simulation for Four-Band DPD

For this simulation, four bands have been positioned at frequencies of 1.05 GHz, 1.53 GHz, 2.1 GHz, and 2.83 GHz, with each band having a bandwidth of 200 MHz. The memory depth is set to five, and the nonlinearity order is set to six for the calculation of the DPD function. The input data is generated randomly and organized into 64-QAM format. Subsequently, the organized signals are utilized to construct an OFDM waveform by applying the IFFT. The simulation results are presented below.

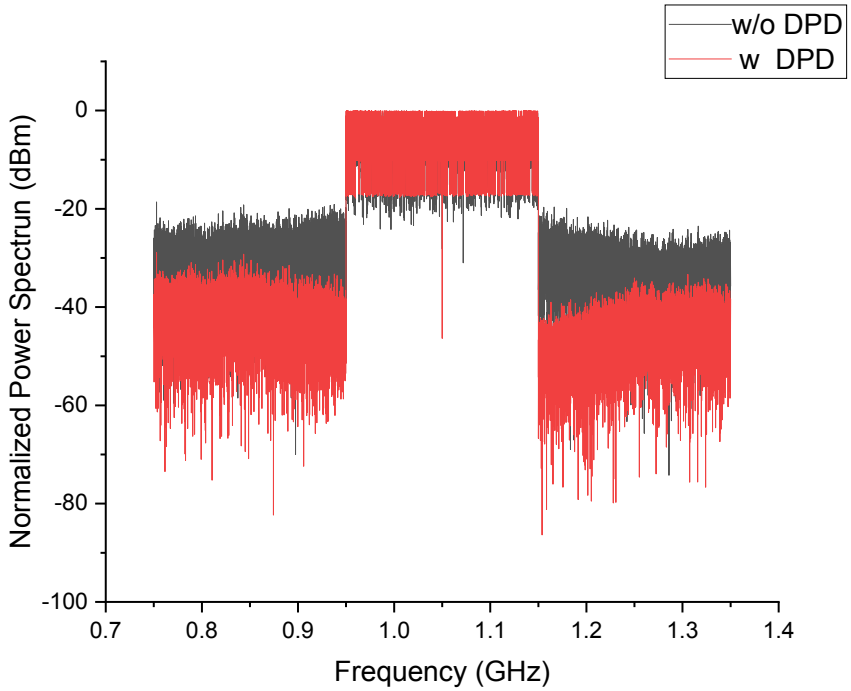

Figure 4-9 (a) Normalized power spectrum for the first band

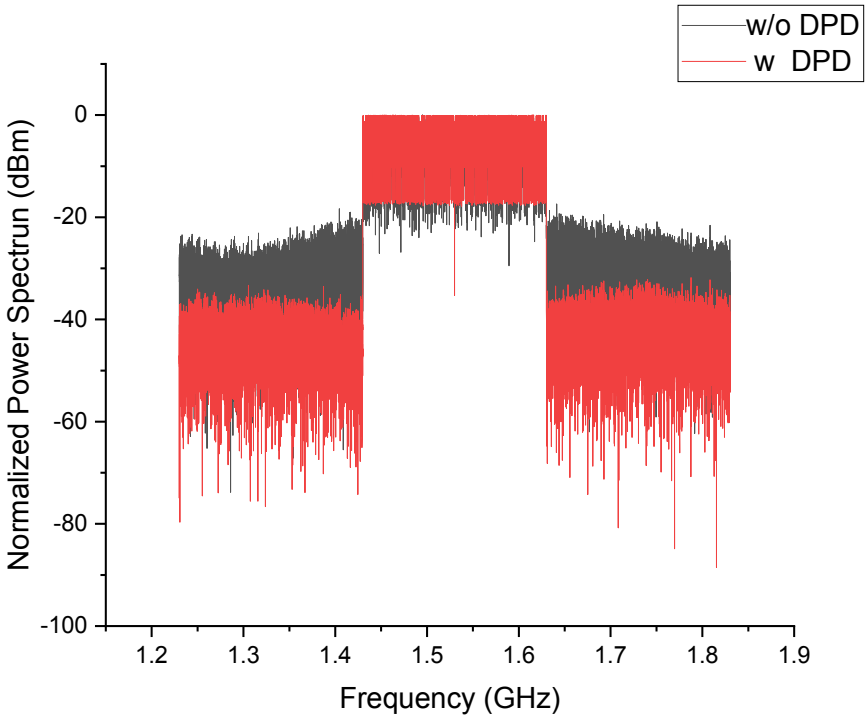

Figure 4-9 (b) Normalized power spectrum for the second band

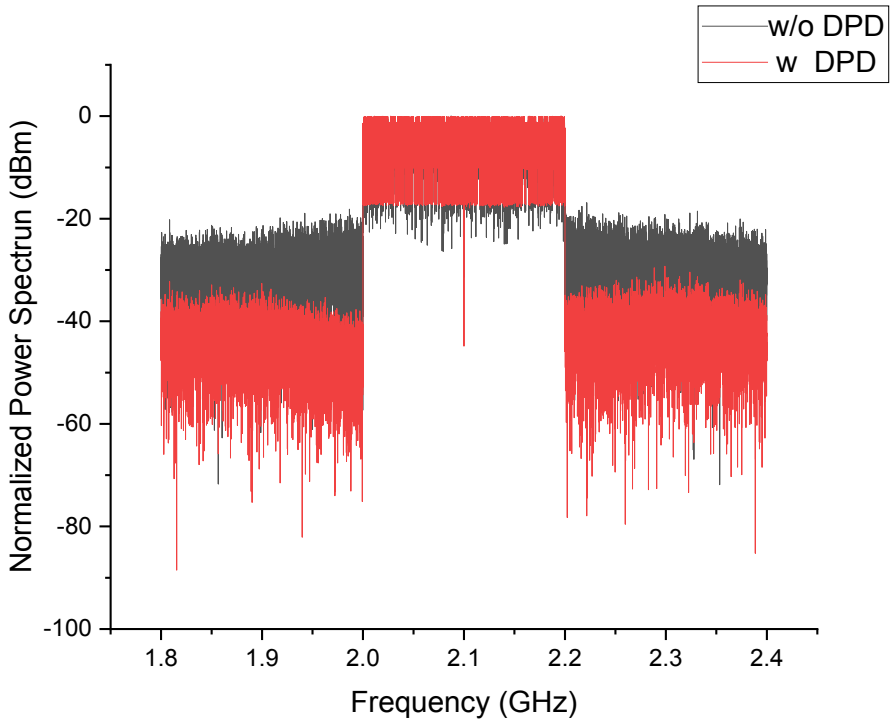

Figure 4-9 (c) Normalized power spectrum for the third band

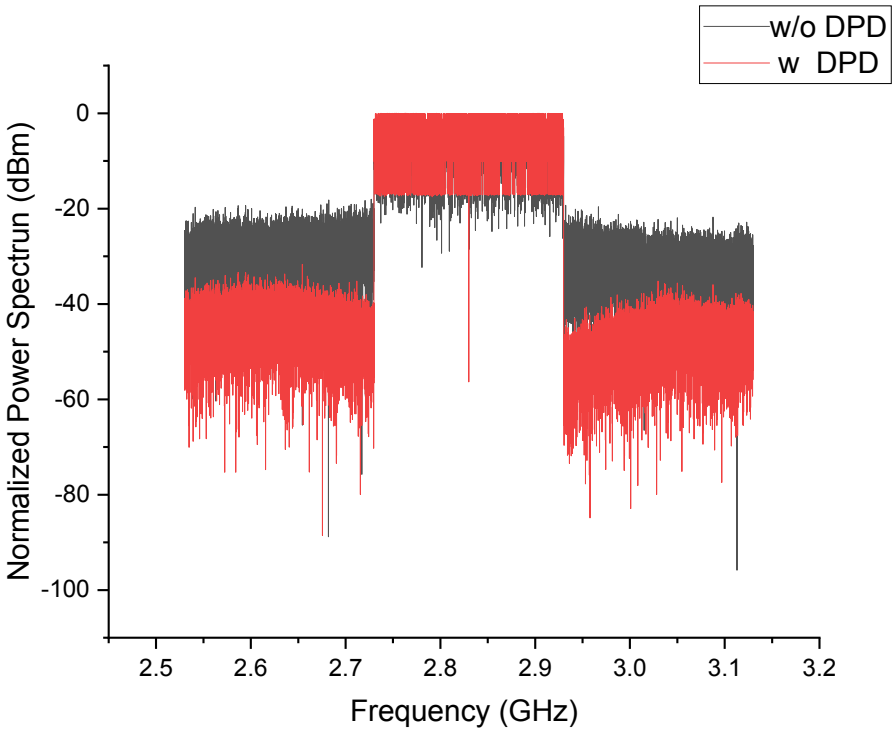

Figure 4-9 (d) Normalized power spectrum for the fourth band

Figure 4-9 shows the power spectrum of each band with and without the DPD. The black line represents the signal without the DPD, and the red line represents the signal with the proposed DPD. It clearly demonstrates that, in the absence of the proposed DPD, the signals centered around 1.05 GHz, 1.53 GHz, 2.1 GHz, and 2.83 GHz show spectrum distortion due to nonlinearity. This distortion affects important parameters such as EVM and ACPR, resulting in signal degradation. Additionally, the out-of-band nonlinearity has a detrimental effect on adjacent and non-adjacent bands, causing interference and potential disruptions. However, with the implementation of the proposed DPD, it is evident that the out-of-band nonlinearity is effectively suppressed, minimizing the degradation on neighbor and non-adjacent bands. The average improvement of ACPR is around 18 dB.

In terms of the signal constellation map and EVM, the simulation results are shown in Fig. 4-8. The constellation of the signal without DPD is adjusted by the phase adjustment.

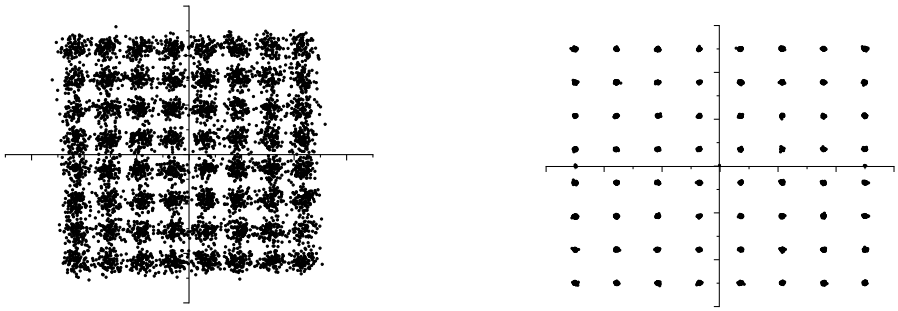

Figure 4-10 (a) Constellation of signal in first band. Left side is the signal without DPD. Right side is the signal with the DPD

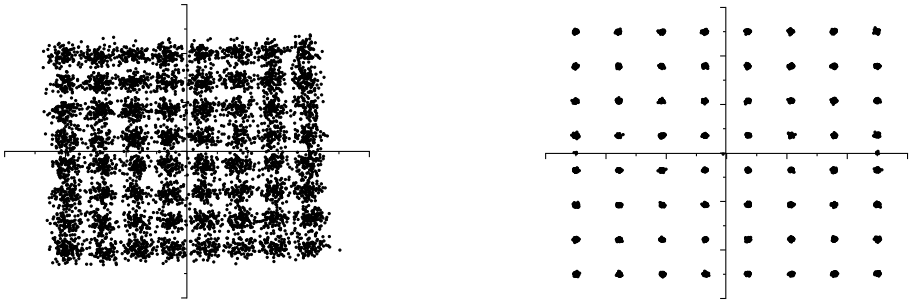

Figure 4-10 (b) Constellation of signal in second band. Left side is the signal without DPD. Right side is the signal with the DPD

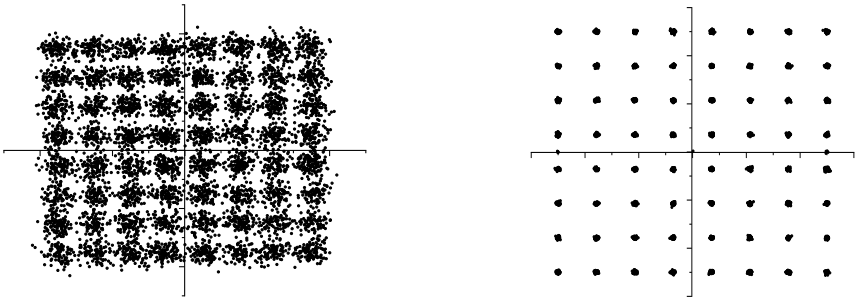

Figure 4-10 (c) Constellation of signal in third band. Left side is the signal without DPD. Right side is the signal with the DPD

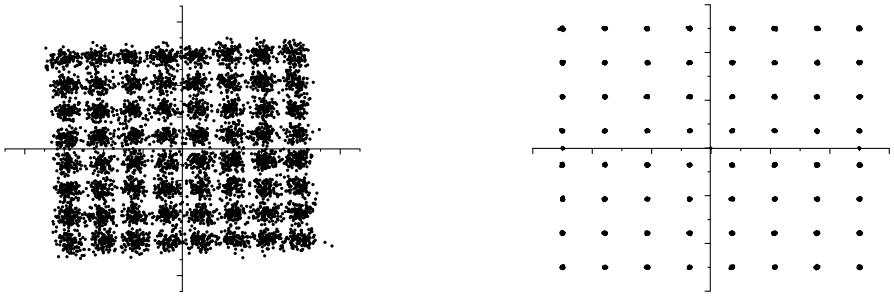

Figure 4-10 (d) Constellation of signal in fourth band. Left side is the signal without DPD. Right side is the signal with the DPD

Figure 4-10 shows the constellation of each band with and without the DPD. The left side of Fig. 4-10 is the signal without DPD, and the right side is the signal with the proposed DPD. It reveals that, in the absence of the proposed DPD, the signal's constellation points are widely dispersed, indicating severe distortion. This directly contributes to the degradation of the EVM. Moreover, the demodulation of the signal and the bit error rate become more challenging, leading to degraded performance. Specifically, the EVM values for the simulations without DPD are -21.06 dB, -20.27 dB, -19.68 dB, and -20.35 dB for the four bands.

However, with the application of the proposed DPD, it becomes evident that the constellation points are tightly concentrated, resulting in improved EVM performance. The simulations with the proposed DPD show EVM values of -40.71 dB, -38.62 dB, -39.65 dB, and -44.08 dB for the four bands. This translates to an improvement in EVM of 19.65 dB, 18.35 dB, 19.96 dB, and 23.72 dB. On average, an improvement of approximate 18.65 dB in the EVM across all the four bands is obtained.

Regarding the AM-AM and AM-PM distortions, the simulation results are presented in Fig. 4-9. The findings align with the discussions in the section on the three-band DPD. Without the DPD, there are gain compression and phase distortion. With the implementation of the proposed DPD, both phase and amplitude distortion are reduced.

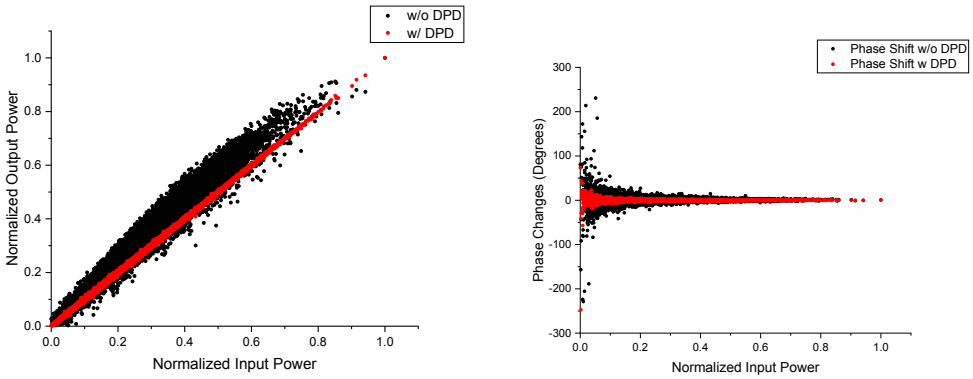

Figure 4-11 (a) AM-AM and AM-PM distortion for the first band with and without the DPD

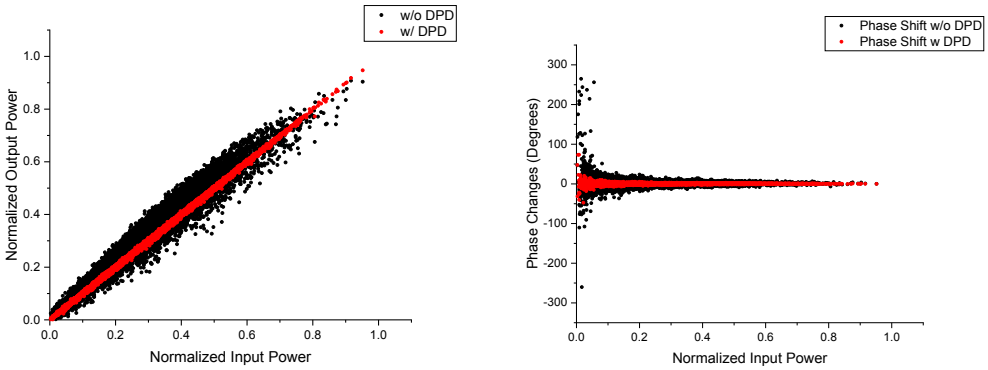

Figure 4-11 (b) AM-AM and AM-PM distortion for the second band with and without the DPD

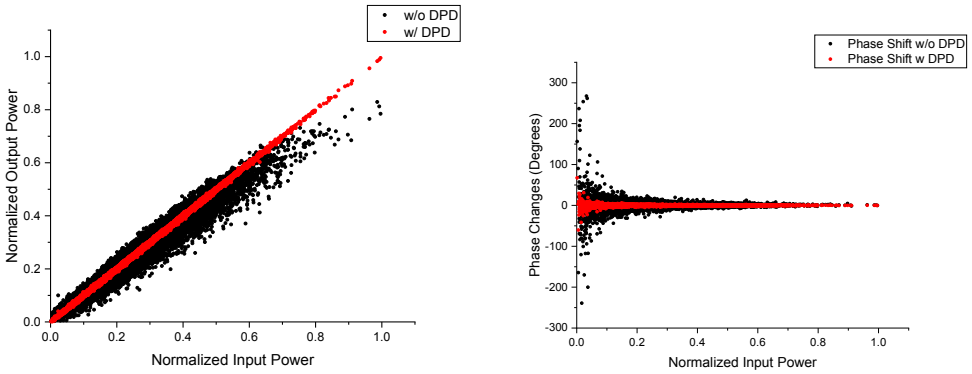

Figure 4-11 (c) AM-AM and AM-PM distortion for the third band with and without the DPD

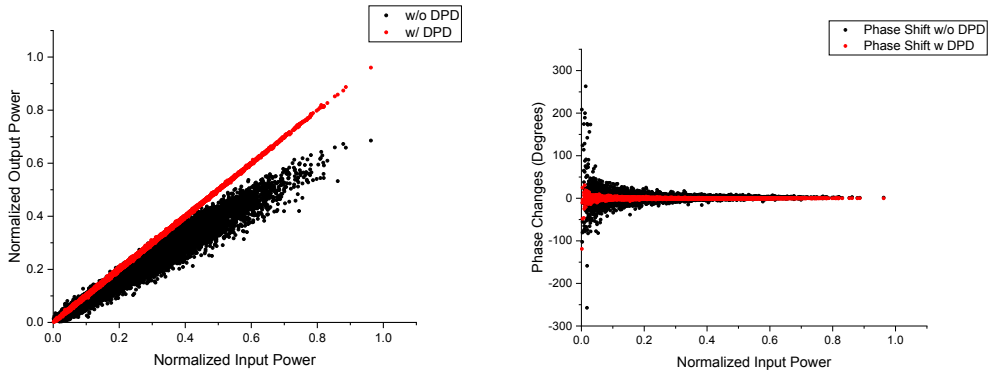

Figure 4-11 (d) AM-AM and AM-PM distortion for the fourth band with and without the DPD

4.5 Simulation for Five-Band DPD

In this section, the simulation focuses on five bands centered around 1.05 GHz, 1.53 GHz, 2.1 GHz, 2.83 GHz, and 3.52 GHz. Each band has a bandwidth of 200 MHz. The memory depth is set to five and the nonlinearity order is set to six for the DPD function, the same as above. Randomly generated input data is organized into 64-QAM, and the resulting signals are used to construct an OFDM waveform using the IFFT. The simulation results are presented below.

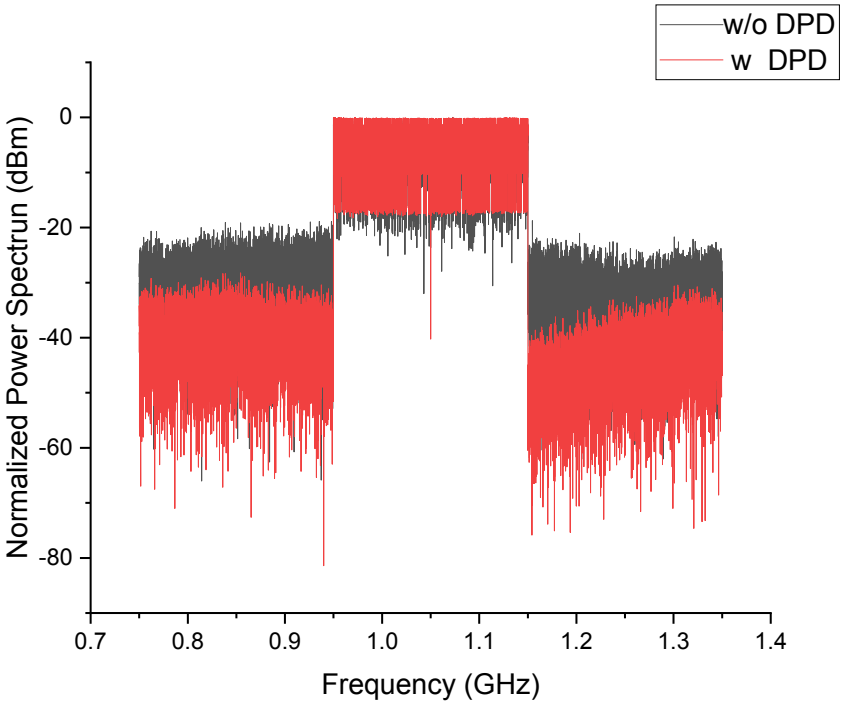

Figure 4-12 (a) Normalized power spectrum for the first band

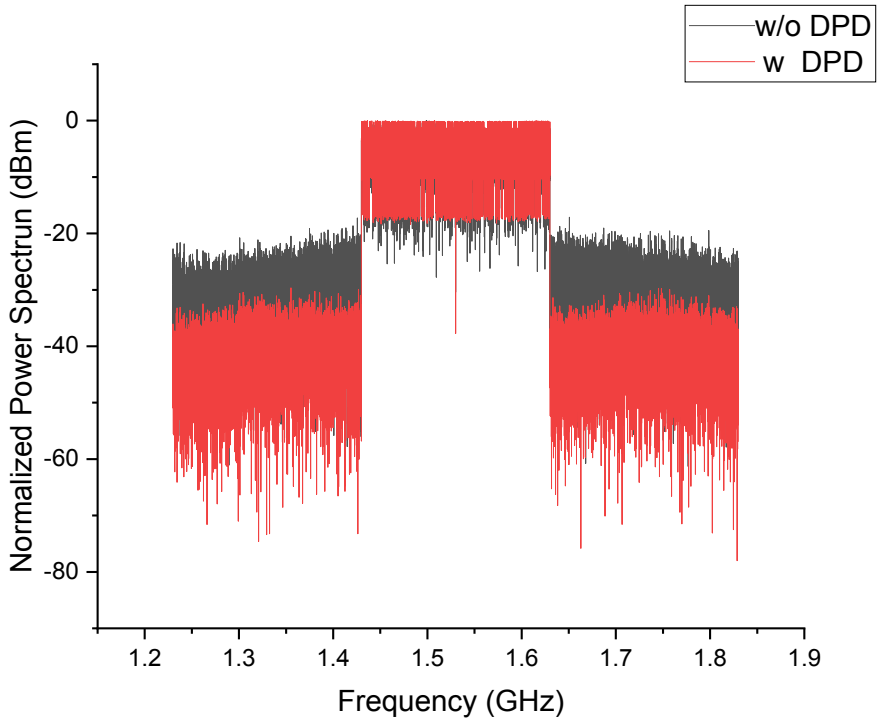

Figure 4-12 (b) Normalized power spectrum for the second band

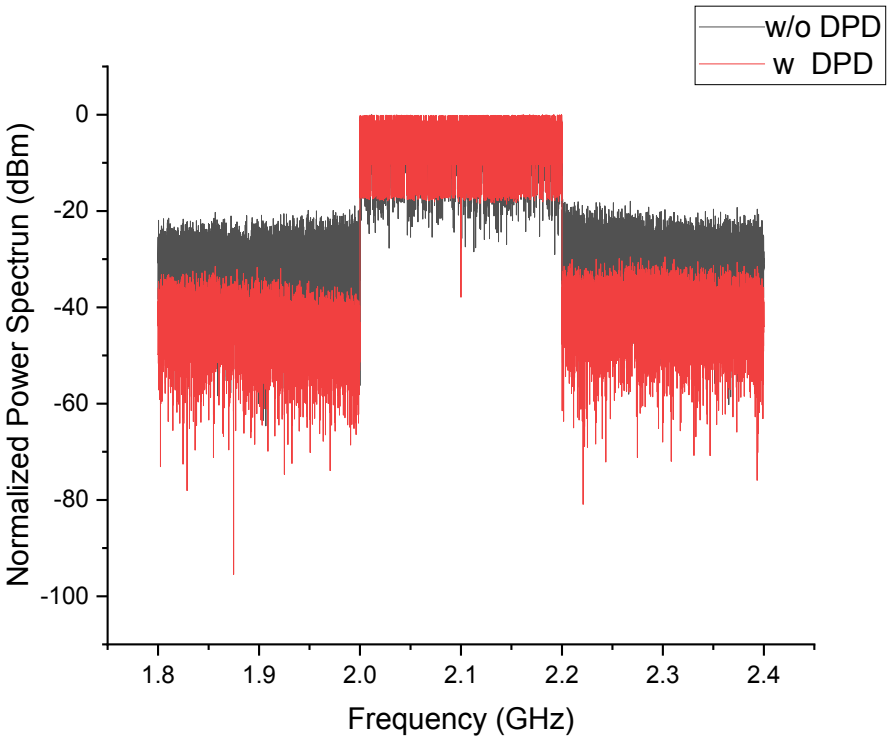

Figure 4-12 (c) Normalized power spectrum for the third band

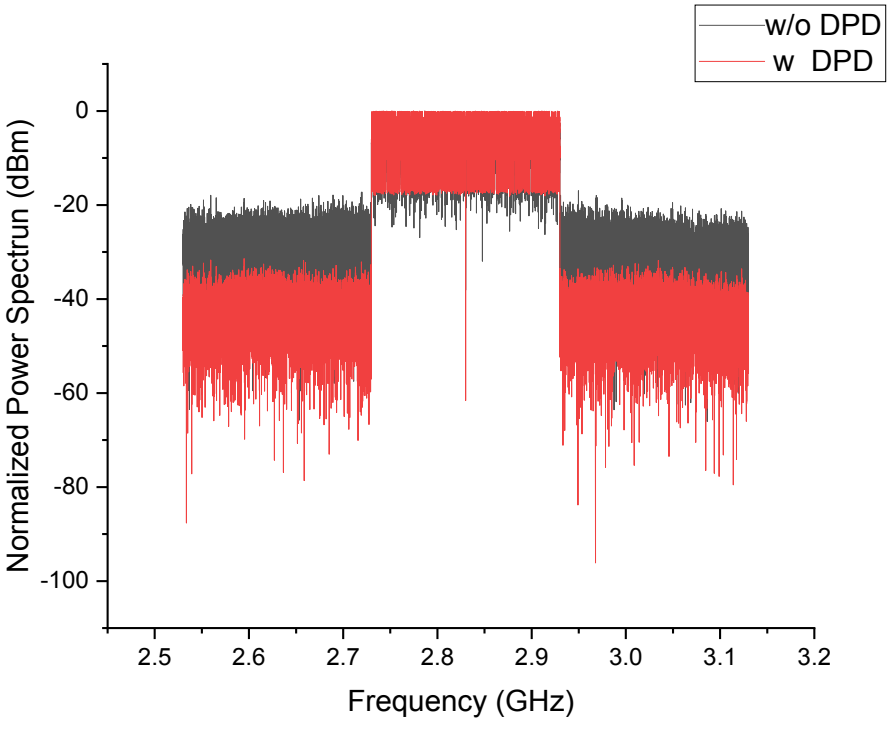

Figure 4-12 (d) Normalized power spectrum for the fourth band

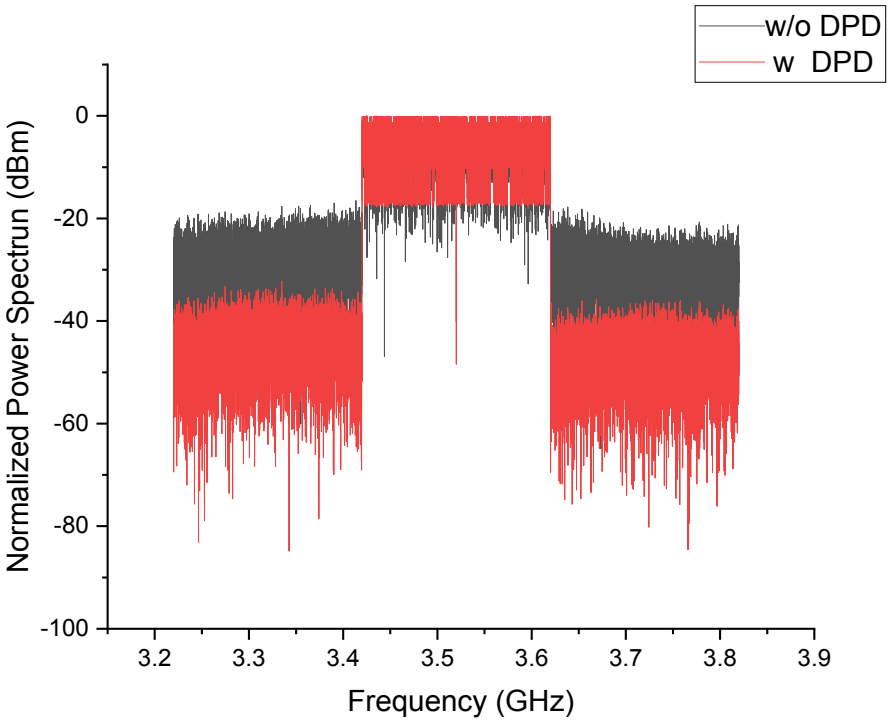

Figure 4-12 (e) Normalized power spectrum for the fifth band

Figure 4-12 shows the power spectrum of each band with and without the DPD. The black line represents the signal without the DPD, and the red line represents the signal with the proposed DPD. It is evident that the signals centered around 1.05 GHz, 1.53 GHz, 2.1 GHz, 2.83 GHz, and 3.52 GHz experience spectrum expansion distortion without the proposed DPD. This distortion is caused by nonlinearity and results in deteriorated parameters such as EVM and ACPR, leading to poor performance. However, with the proposed DPD, the out-of-band nonlinearity is effectively suppressed, reducing the degradation on adjacent and distant channels. The average improvement of ACPR is around 16 dB.

Regarding the constellation map and EVM, the simulation results are presented in Fig. 4-13. The constellation of signal without DPD is adjusted by the phase adjustment.

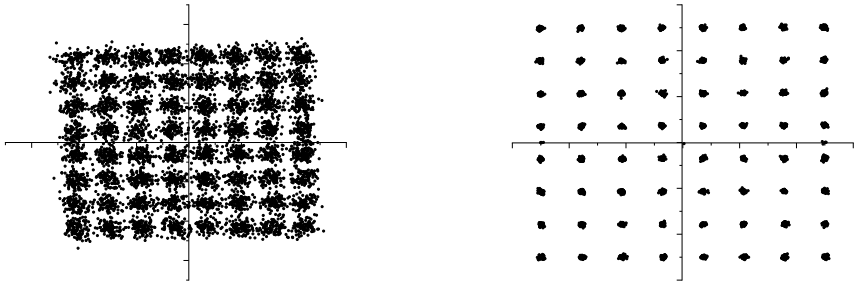

Figure 4-13 (a) Constellation of signal in first band. Left side is the signal without DPD. Right side is the signal with the DPD

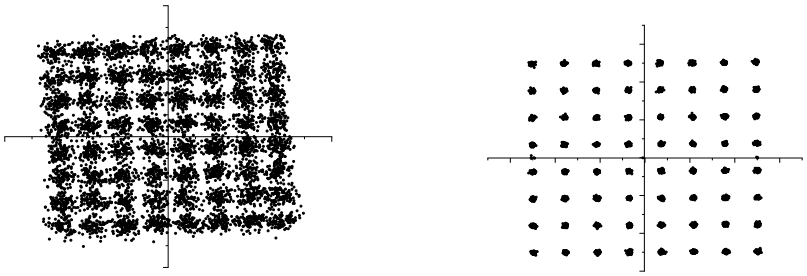

Figure 4-13 (b) Constellation of signal in second band. Left side is the signal without DPD. Right side is the signal with the DPD

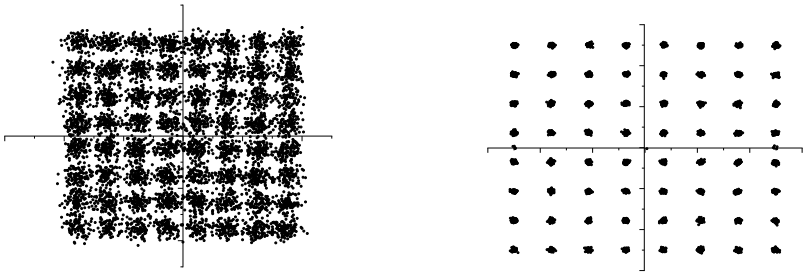

Figure 4-13 (c) Constellation of signal in third band. Left side is the signal without DPD. Right side is the signal with the DPD

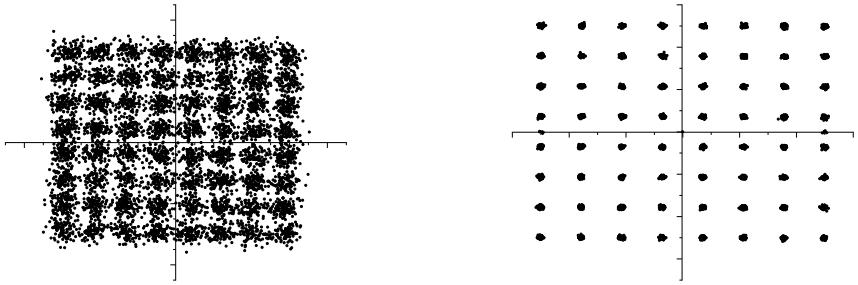

Figure 4-13 (d) Constellation of signal in fourth band. Left side is the signal without DPD. Right side is the signal with the DPD

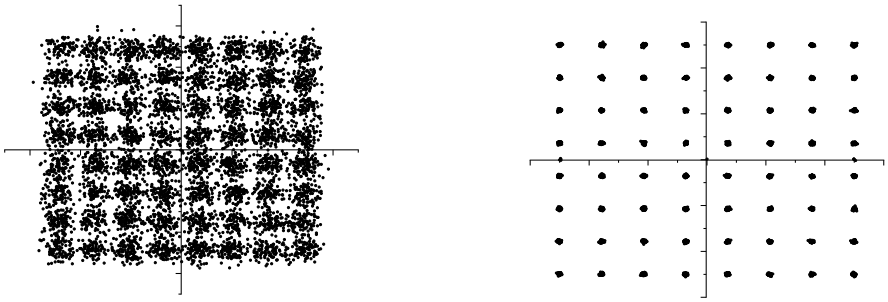

Figure 4-13 (e) Constellation of signal in fifth band. Left side is the signal without DPD. Right side is the signal with the DPD

Figure 4-13 shows the signal constellation of each band with and without the DPD. The left side of Fig. 4-13 is the signal without DPD, and the right side is the signal with the proposed DPD. It is evident that without the proposed DPD, the constellation points of the signal spread, indicating severe distortion. This directly leads to a deterioration in EVM and an increase in the difficulty of signal demodulation and bit error rate. The EVM values for the simulations without the DPD are -20.83 dB, -19.69 dB, -20.20 dB, -19.23 dB, and -19.67 dB for the five bands.

However, with the proposed DPD, it can be observed that the constellation points become concentrated, resulting in an improvement in EVM. The EVM values for the simulations with the proposed DPD are -36.94 dB, -34.97 dB, -35.90 dB, -36.65 dB, and -

39.80 dB for the five bands. The improvement in EVM amounts to 16.11 dB, 15.27 dB, 15.70 dB, 17.42 dB, and 20.12 dB, respectively. On average, an improvement of approximate 16.64 dB across all five bands is obtained.

The simulation results regarding the AM-AM and AM-PM distortions are presented in Fig. 4-14. The result is aligned with conclusion above that the distortions have been mitigated by the proposed DPD, resulting in improved performance.

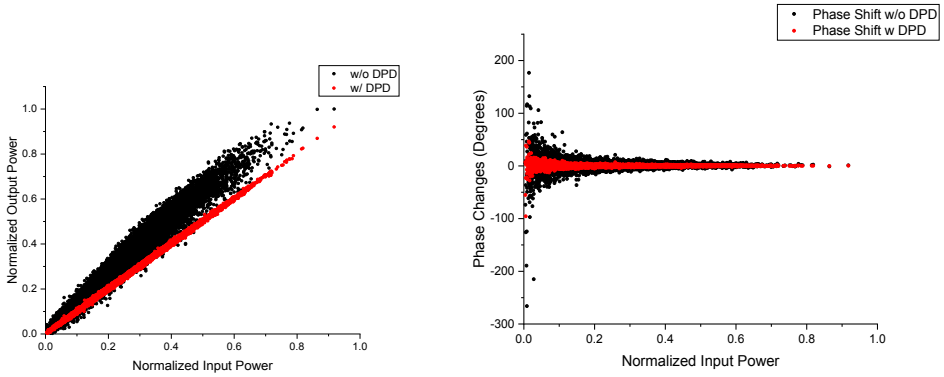

Figure 4-14 (a) AM-AM and AM-PM distortion for the first band with and without the DPD

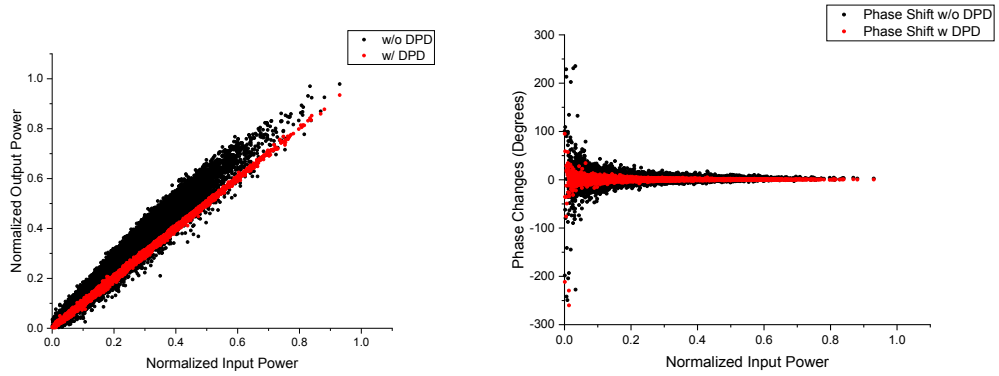

Figure 4-14 (b) AM-AM and AM-PM distortion for the second band with and without the DPD

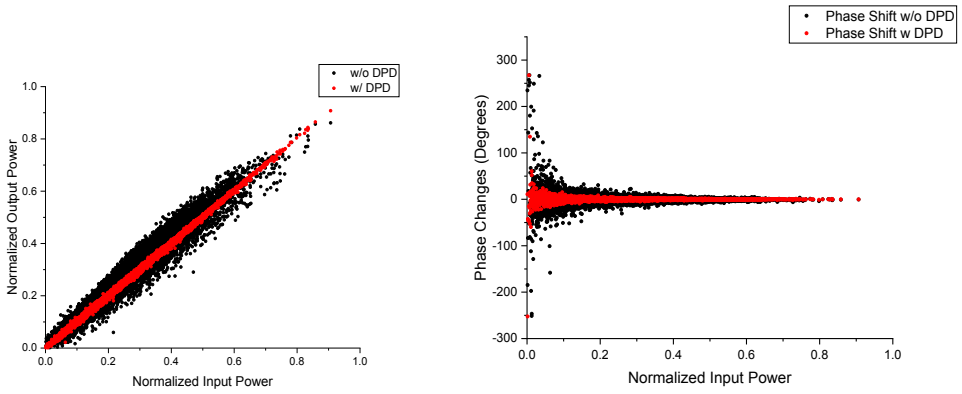

Figure 4-14 (c) AM-AM and AM-PM distortion for the third band with and without the DPD

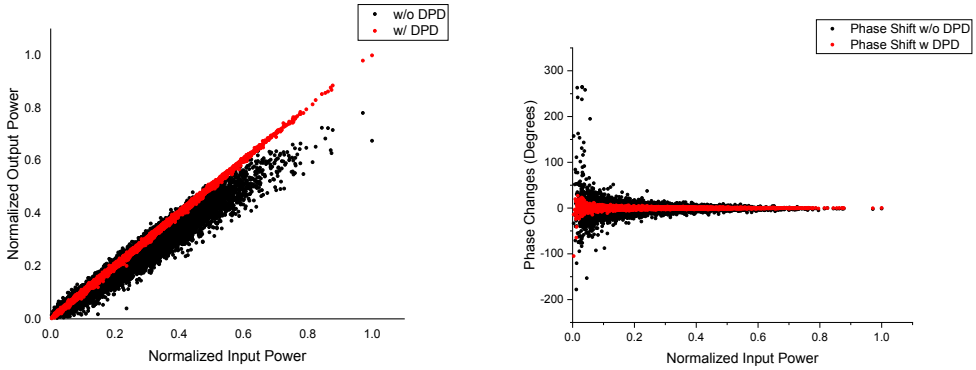

Figure 4-14 (d) AM-AM and AM-PM distortion for the fourth band with and without the DPD

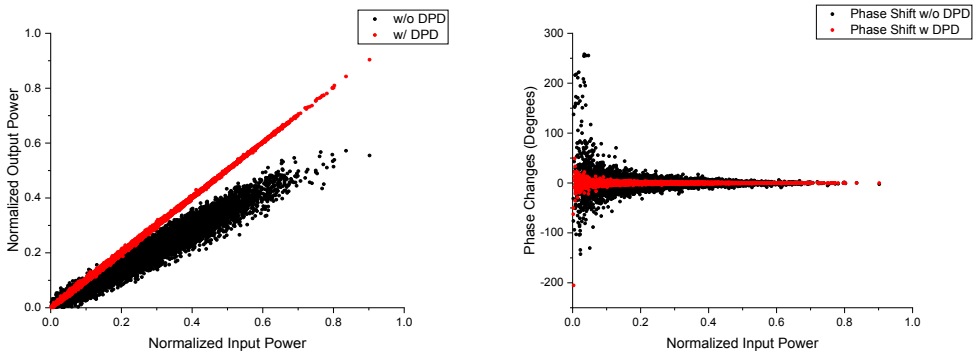

Figure 4-14 (e) AM-AM and AM-PM distortion for the fifth band with and without the DPD

4.6 Simulation for Six-Band DPD

In this section, the simulation focuses on six bands located around 1.05 GHz, 1.53 GHz, 2.1 GHz, 2.83 GHz, 3.52 GHz, and 4.02 GHz, each with a bandwidth of 200 MHz. The DPD function utilizes a memory depth of five and a nonlinearity order of six. The input data is randomly generated and organized into 64-QAM format. The organized signals are then used to construct an OFDM waveform through the Inverse Fast Fourier Transform (IFFT). The following simulation results are presented below.

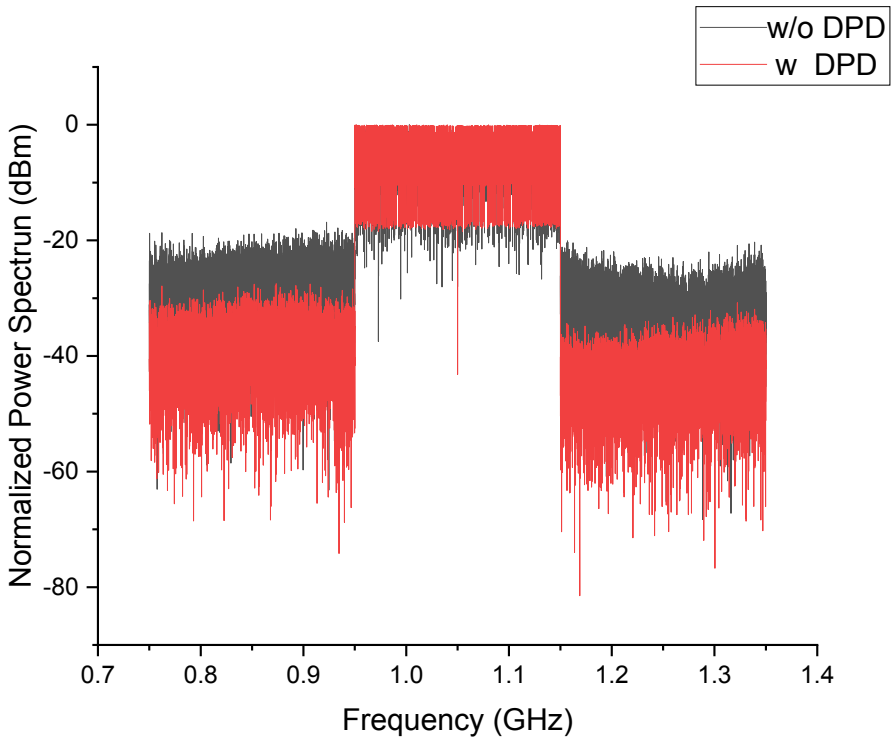

Figure 4-15 (a) Normalized power spectrum for the first band

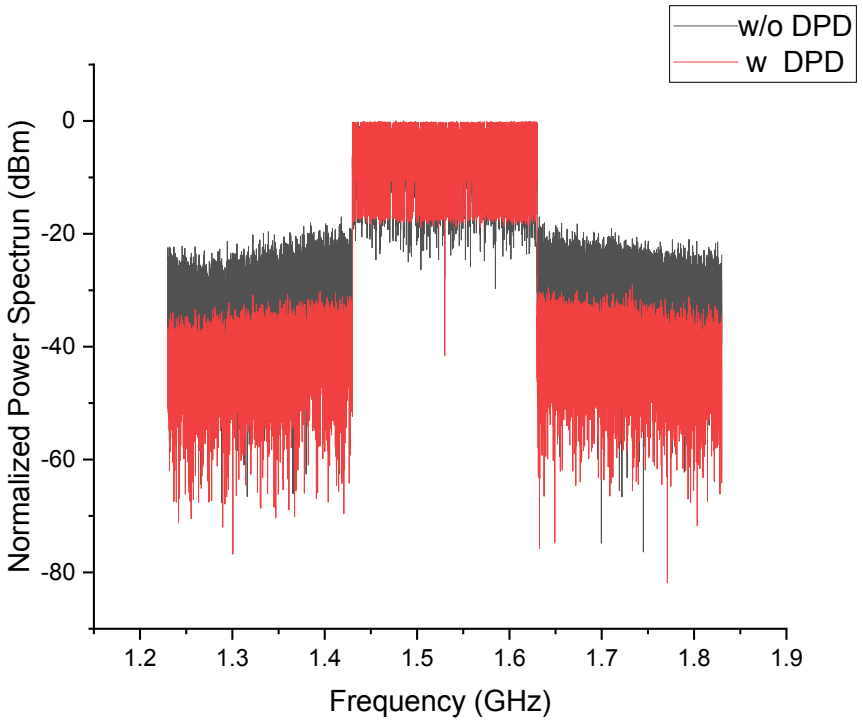

Figure 4-15 (b) Normalized power spectrum for the second band

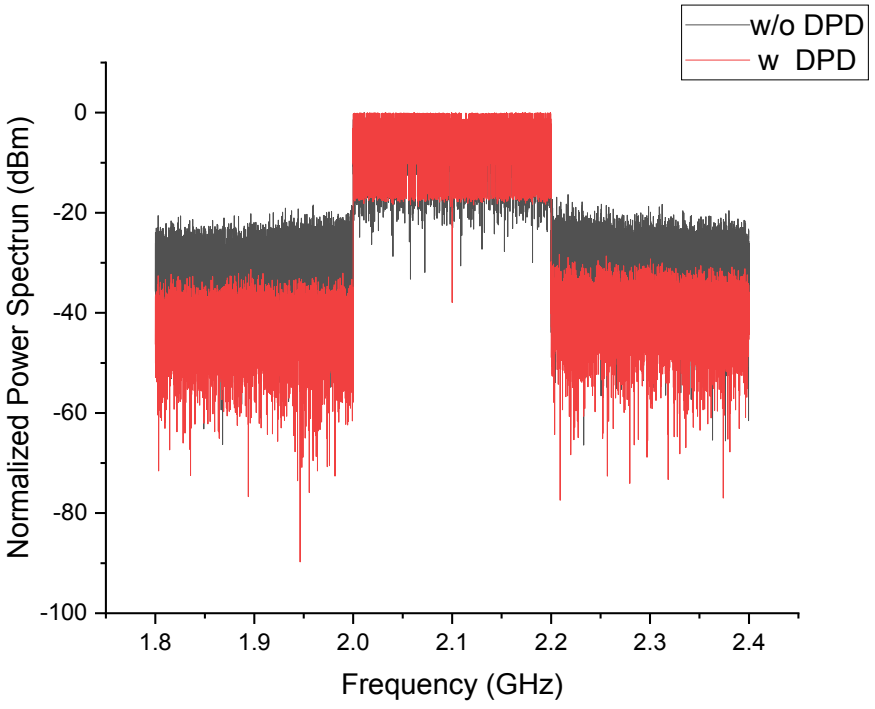

Figure 4-15 (c) Normalized power spectrum for the third band

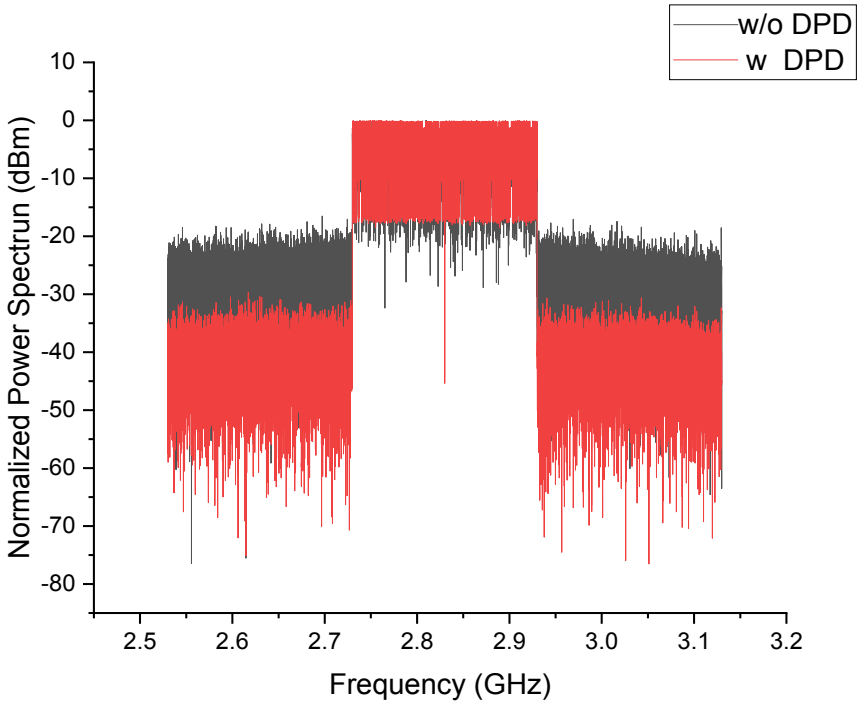

Figure 4-15 (d) Normalized power spectrum for the fourth band

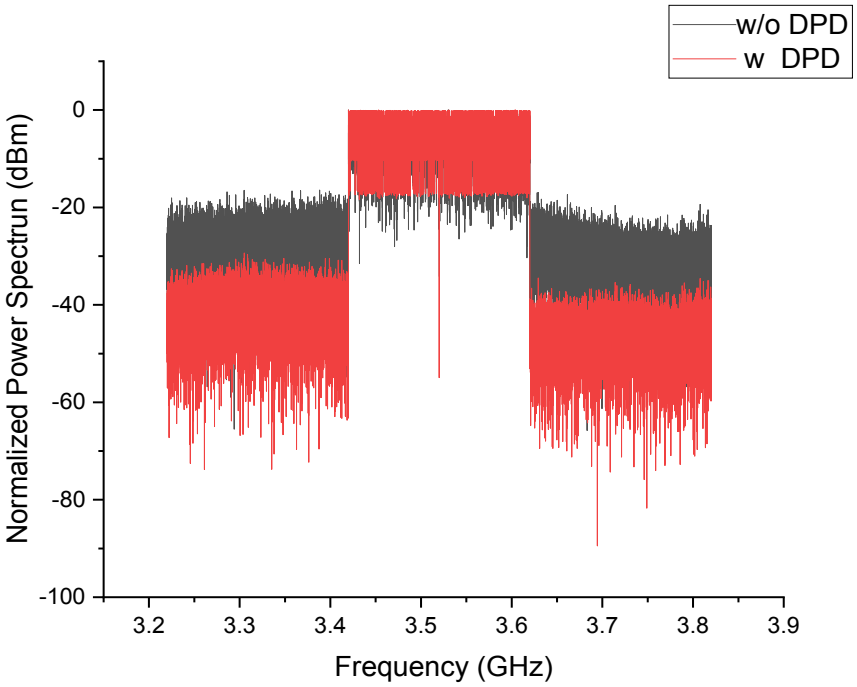

Figure 4-15 (e) Normalized power spectrum for the fifth band

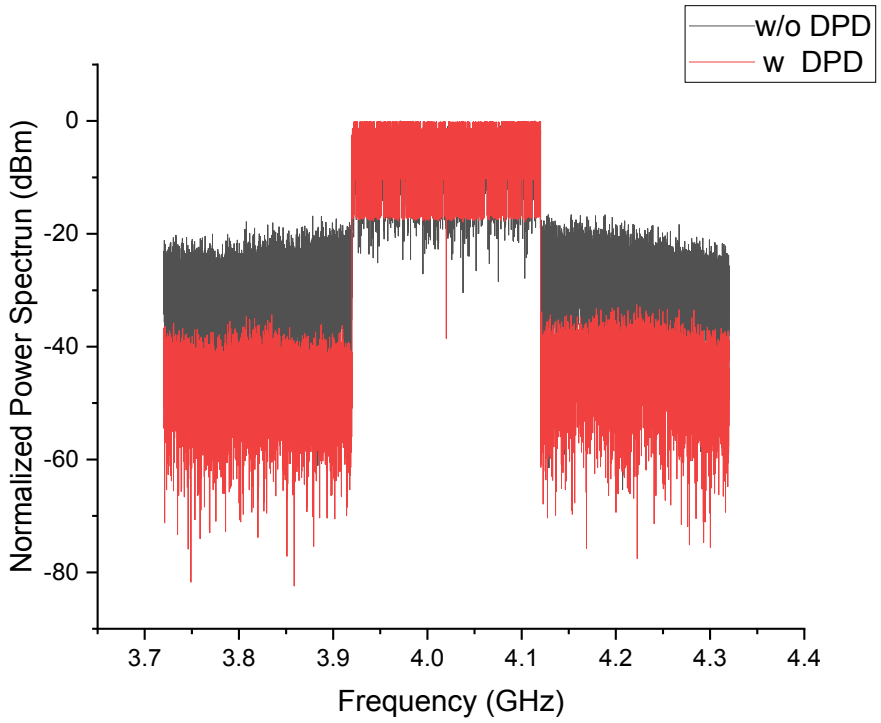

Figure 4-15 (f) Normalized power spectrum for the sixth band

Figure 4-15 shows the power spectrum of each band with and without the DPD. The black line represents the signal without the DPD, and the red line represents the signal with the proposed DPD. The power spectrum analysis reveals that, in the absence of the proposed DPD, the signals centered around 1.05 GHz, 1.53 GHz, 2.1 GHz, 2.83 GHz, 3.52 GHz, and 4.02 GHz show noticeable spectrum expansion distortion caused by nonlinearity without the DPD and has an improved ACPR performance with the proposed DPD. This observation aligns with the previous conclusion. The average ACPR improvement is around 14 dB.

In terms of the constellation map and EVM, the simulation results are shown in Fig. 4-16. The constellation of signal without DPD is adjusted by the phase adjustment.

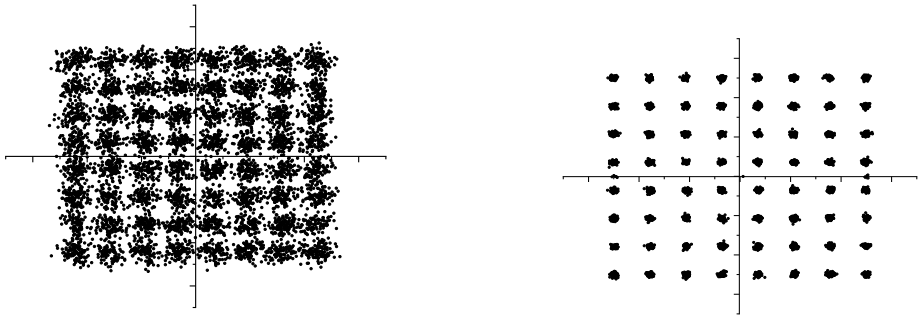

Figure 4-16 (a) Constellation of signal in first band. Left side is the signal without DPD. Right side is the signal with the DPD

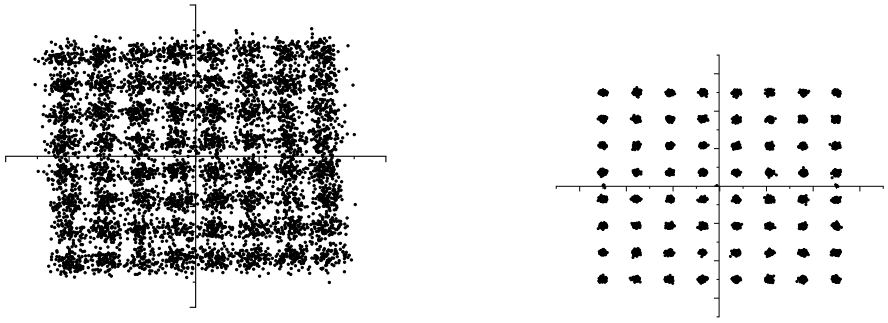

Figure 4-16 (b) Constellation of signal in second band. Left side is the signal without DPD. Right side is the signal with the DPD

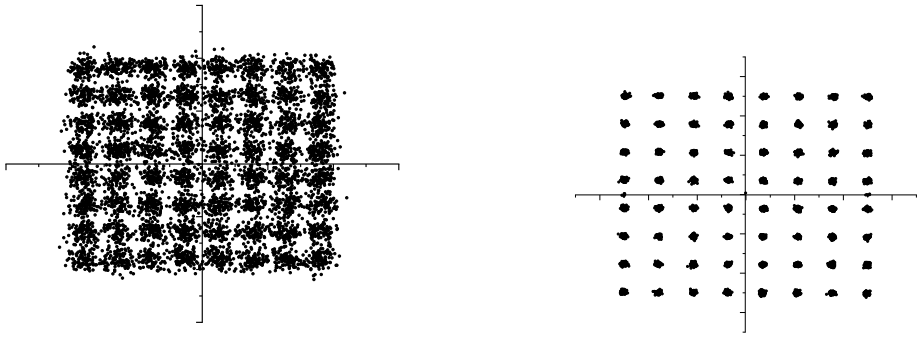

Figure 4-16 (c) Constellation of signal in third band. Left side is the signal without DPD. Right side is the signal with the DPD

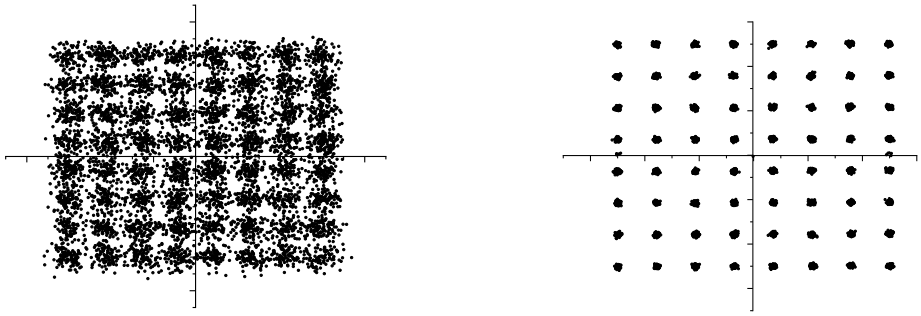

Figure 4-16 (d) Constellation of signal in fourth band. Left side is the signal without DPD. Right side is the signal with the DPD

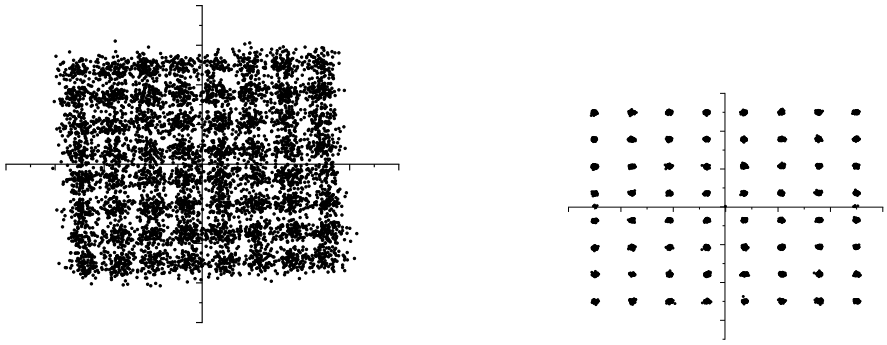

Figure 4-16 (e) Constellation of signal in fifth band. Left side is the signal without DPD. Right side is the signal with the DPD

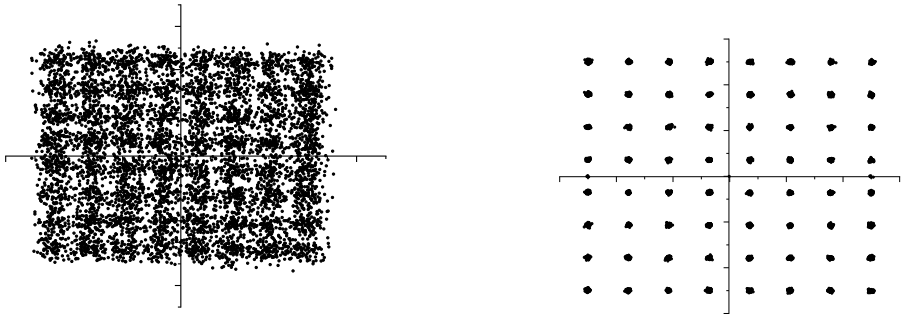

Figure 4-16 (f) Constellation of signal in sixth band. Left side is the signal without DPD. Right side is the signal with the DPD

Figure 4-16 shows the signal constellation of each band with and without the DPD. The left side of Fig. 4-16 is the signal without DPD, and the right side is the signal with the proposed DPD. It is evident that the signal's constellation points spread without the proposed DPD, indicating significant distortion. This distortion directly contributes to the degradation of EVM, resulting in increased difficulty in signal demodulation and higher bit error rate. The EVM values for the simulations without the DPD are -20.33 dB, -19.69 dB, -19.72 dB, 19.83 dB, -19.03 dB, and -18.78 dB.

In contrast, with the implementation of the proposed DPD, the constellation points become concentrated, leading to an improvement in EVM. The EVM values for the simulations with the proposed DPD are -33.65 dB, -32.72 dB, -34.02 dB, -35.31 dB, -36.49 dB, and -37.79 dB. The improvement in EVM is 13.33 dB, 13.05 dB, 14.31 dB, 15.48 dB, 17.46 dB, and 19.02 dB. On average, the improvement in EVM across all six bands is approximately 15.44 dB.

In terms of the AM-AM and AM-PM distortions. The simulation results are shown in Fig. 4-15. It can be observed that both AM and PM have great improvement in terms of linearity.

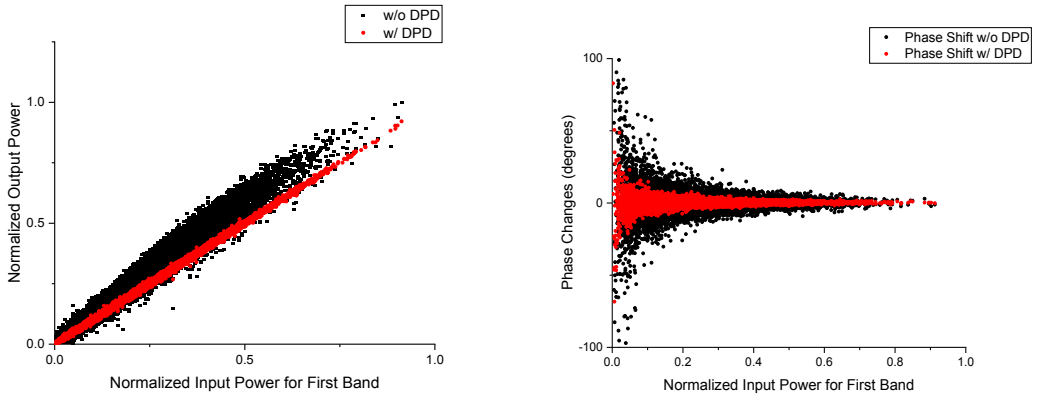

Figure 4-17 (a) AM-AM and AM-PM distortion for the first band with and without the DPD

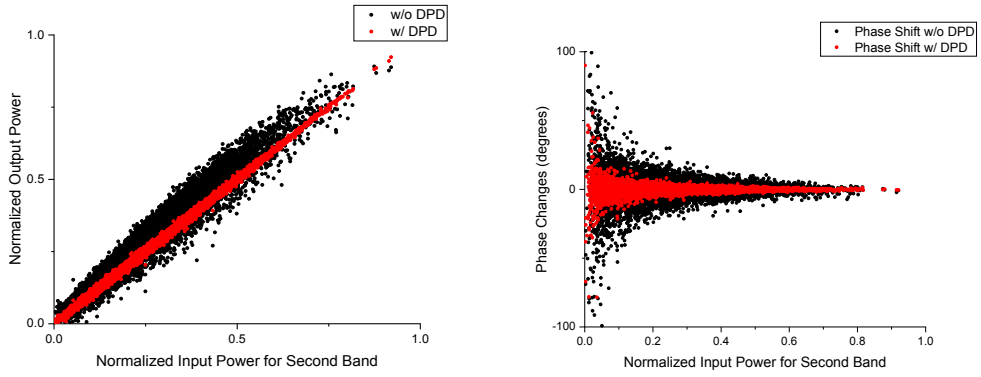

Figure 4-15 (b) AM-AM and AM-PM distortion for the second band with and without the DPD

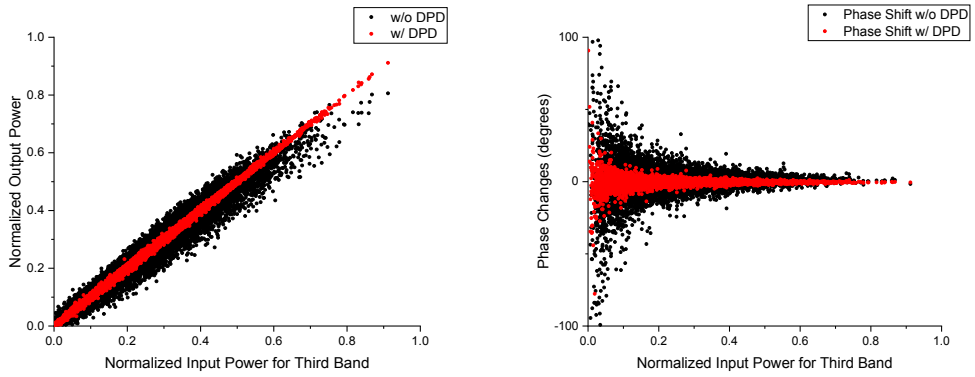

Figure 4-15 (c) AM-AM and AM-PM distortion for the third band with and without the DPD

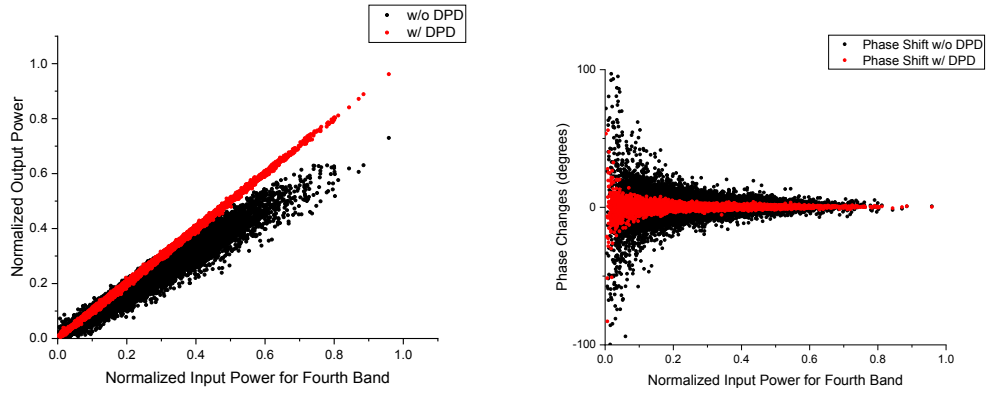

Figure 4-15 (d) AM-AM and AM-PM distortion for the fourth band with and without the DPD

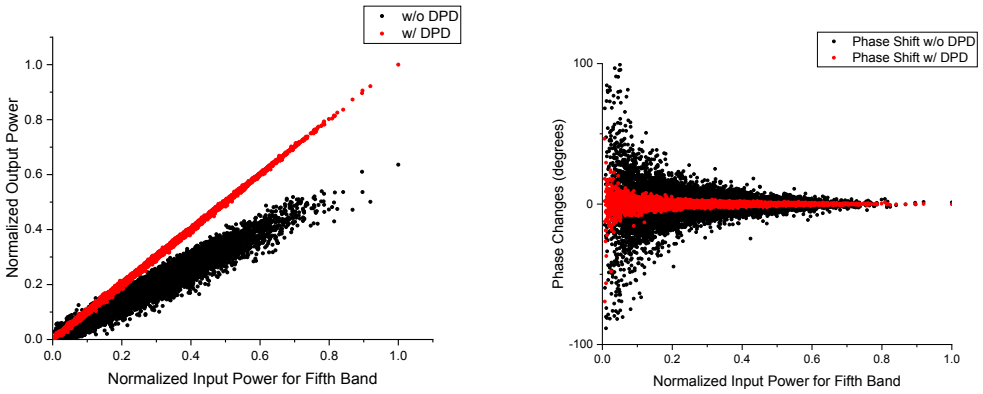

Figure 4-15 (e) AM-AM and AM-PM distortion for the fifth band with and without the DPD

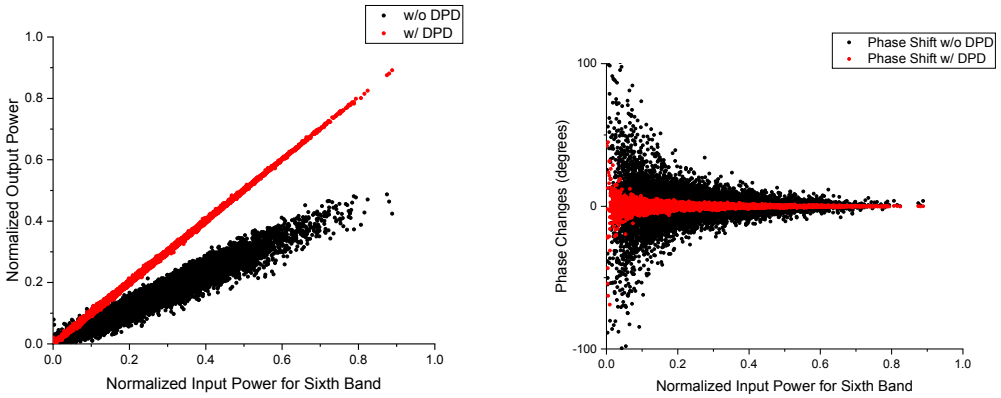

Figure 4-15 (f) AM-AM and AM-PM distortion for the sixth band with and without the DPD

4.7 Simulation Summary

The performances of the proposed DPD are summarized in Tables 4-1 to 4-4. The performance of the proposed DPD is observed to be favorable in all four cases. However, it is worth noting that the overall performance tends to decrease as the number of bands increases. This decrease in performance could be attributed to the increased complexity associated with handling multiple bands.

Band	1	2	3
w/ DPD (dB)	-41.18	-40.47	-45.56
w/o DPD (dB)	-22.84	-22.47	-22.19
Improvement (dB)	18.53	17.99	23.36
Mean (dB)	19.97		

Table 4-1 Three-Band DPD Performance

Band	1	2	3	4
w/ DPD (dB)	-40.71	-38.62	-39.65	-44.08
w/o DPD (dB)	-21.06	-20.27	-19.68	-20.35
Improvement (dB)	19.65	18.35	19.96	23.72
Mean (dB)	18.65			

Table 4-2 Four-Band DPD Performance

Band	1	2	3	4	5
w/ DPD (dB)	-36.94	-34.97	-35.90	-36.65	-39.80
w/o DPD (dB)	-20.83	-19.69	-20.20	-19.23	-19.67
Improvement (dB)	16.11	15.27	15.70	17.42	20.12
Mean (dB)	16.64				

Table 4-3 Five-Band DPD Performance

Band	1	2	3	4	5	6
w/ DPD (dB)	-33.65	-32.72	-34.02	-35.31	-36.49	-37.79
w/o DPD (dB)	-20.33	-19.67	-19.72	-19.83	-19.03	-18.78
Improvement (dB)	13.33	13.05	14.31	15.48	17.46	19.02
Mean (dB)	15.44					

Table 4-4 Six-Band DPD Performance

According to the simulation results, the proposed DPD demonstrates its suitability for application in multi-band signal transmission systems. The performance of the proposed DPD in mitigating nonlinear distortions and improving signal quality across multiple bands is evident. This indicates its potential effectiveness in real-world scenarios where signals are transmitted in multiple frequency bands simultaneously. The successful application of the proposed DPD in multi-band systems opens possibilities for enhanced complexity and efficiency in various communication applications.

Chapter 5 Performance Analysis using Experiments for Low-Complexity Multi-band DPD

5.1 Experiment Overview

Following the successful verification of the proposed DPD through simulation, experiment has been conducted to evaluate its performance in real-world applications. The experiments setup is shown in Figure 5-1. The 64-QAM OFDM signal is generated in Matlab and then loaded into a Tektronix AWG7122B arbitrary waveform generator. The AWG sends the signals to the optical transmitter at a sampling rate of 10.32 Giga samples per second (GS/s). A MITEQ SCM fiber optic link is used to transmit and receive the optical signal. The optical transmitter is a direct modulator, which uses the RF signal to modulate the optical signal. And it contains a pre-amplifier boosting the input signal at bias of 12V and -12V. After the modulated optical signal passing through an 8- kilometer standard single mode optical fiber, which has 0.28 dB/km attenuation and it had been connected with Seikoh-Giken FC/APC SNA-1 fiber adapter which has a total 13 dB attenuation, the optical signal is detected by the optical receiver of the MITEQ SCM fiber optical link and demodulated back into an RF signal. A SHF810 broadband amplifier is connected after the optical receiver to enhance the power level of the RF signal from -15.4 dBm to 13.4 dBm, corresponding to a gain of 28 dB. An Agilent DSO81204B oscilloscope samples the amplified RF signal at a sampling rate of 10.32 GS/s and saves the data into a file, which can be processed by Matlab.

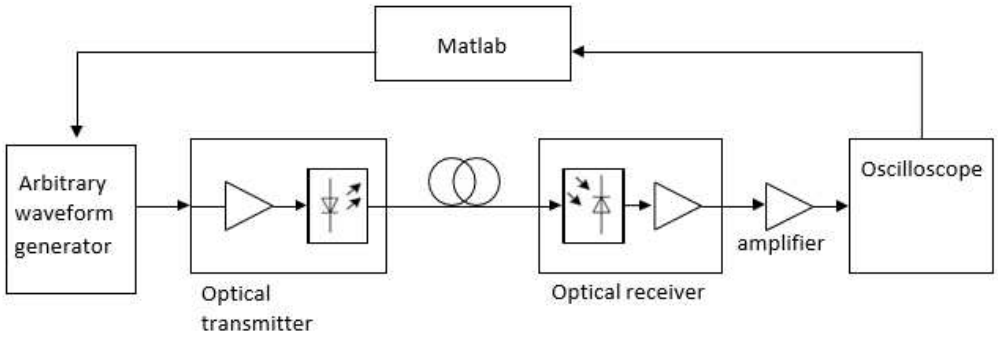

Figure 5-1 Experimental set up

5.2 Experiment of Four-Band DPD

In this section, the experiment focuses on 4-band signal which four bands centered around 720 MHz, 800 MHz, 845 MHz, and 900 MHz. And each band has a bandwidth of 20 MHz and subcarrier bandwidth is 30 kHz. The DPD function utilizes a memory depth of five and a nonlinearity order of six. The input data, generated randomly using Matlab, is organized into 64-QAM. Subsequently, the organized signals are used to construct an OFDM waveform through the IFFT. The generated signal is then loaded onto the AWG to conduct the experiments. The results of the experiments are presented below.

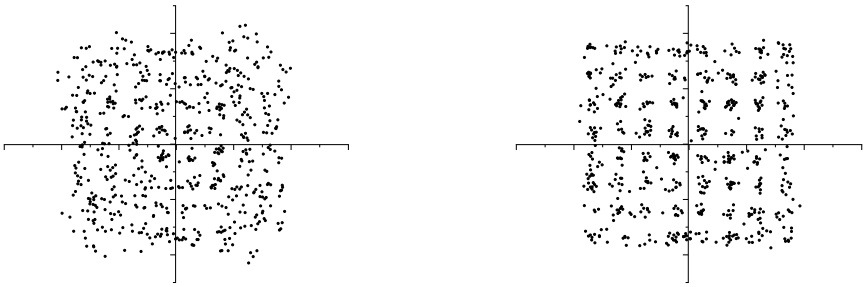

Figure 5-2 (a) Constellation of signal in first band. Left side is the signal without DPD. Right side is the signal with the DPD

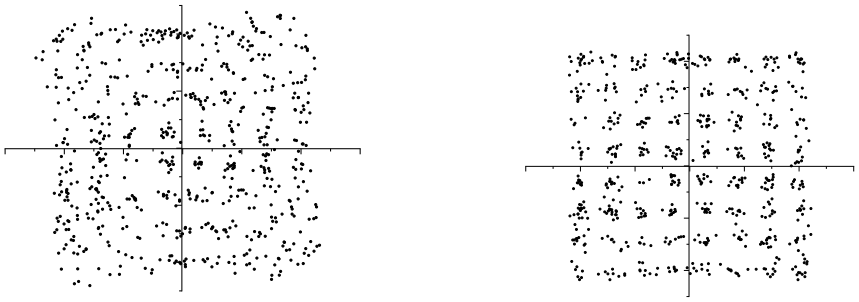

Figure 5-2 (b) Constellation of signal in second band. Left side is the signal without DPD. Right side is the signal with the DPD

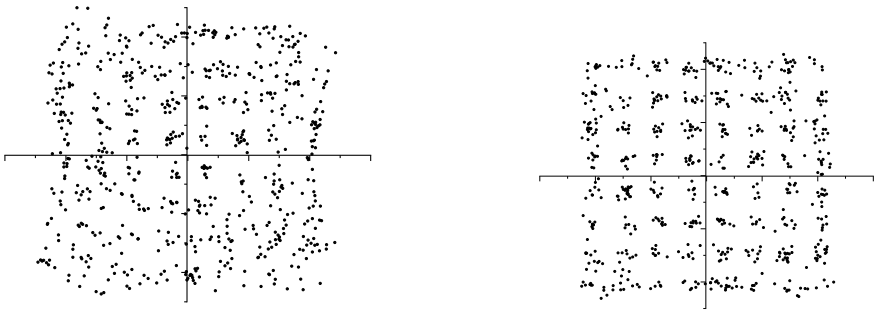

Figure 5-2 (c) Constellation of signal in third band. Left side is the signal without DPD. Right side is the signal with the DPD

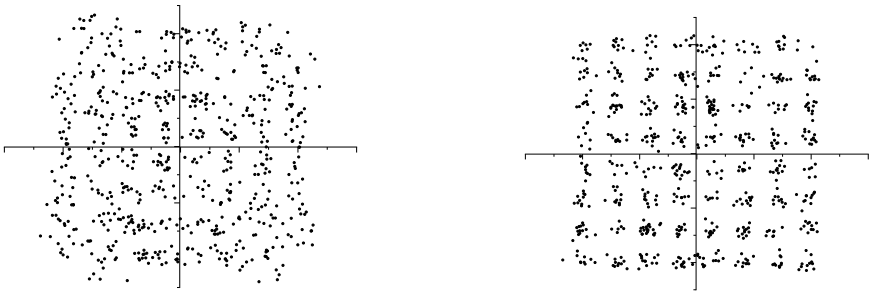

Figure 5-2 (d) Constellation of signal in fourth band. Left side is the signal without DPD. Right side is the signal with the DPD

Band	1	2	3	4
w/ DPD (dB)	-21.53	-22.71	-22.13	-22.37
w/o DPD (dB)	-15.05	-17.46	-17.20	-16.32
Improvement (dB)	6.48	5.24	4.92	6.05
Mean (dB)	5.67			

Table 5-1 Four-band DPD performance

The constellations of the signals are given in Figure 5-2 and the EVM performances are given in Table 5-1. From Figure 5-2 and Table 5-1, it is evident that the absence of the

proposed DPD results in spread-out constellation points, indicating severe distortion. The EVM values obtained from these experiments without DPD are -15.0539 dB, -17.4698 dB, -17.2039 dB, and -16.3208 dB for the four bands.

On the other hand, with the proposed DPD, the constellation points become more concentrated, leading to an improvement in EVM. The EVM values with the proposed DPD are -21.5365 dB, -22.7129 dB, -22.1332 dB, and -22.3739 dB. The average improvement in EVM across all four bands is approximately 5.677 dB.

In terms of power spectrum, the results are shown in Figure 5-3. The black line is the signal without the DPD, and the red line is the signal with the proposed DPD. Without the implementation of DPD, the power spectrum of the transmitted signal suffers from nonlinear distortions. As can be seen from Figure 5-3 (a), there is a nonlinearity distortion presence on the right side of the signal band, which is attributed to the presence of IMD3 or IMD5 coming from other bands. However, by employing the DPD, interference caused by the nonlinear distortion is mitigated. The DPD works by reducing and suppressing the nonlinearity distortion that occurs outside the desired band. As a result, the application of the DPD can enhance the overall signal quality by minimizing distortions and ensuring a more pristine power spectrum.

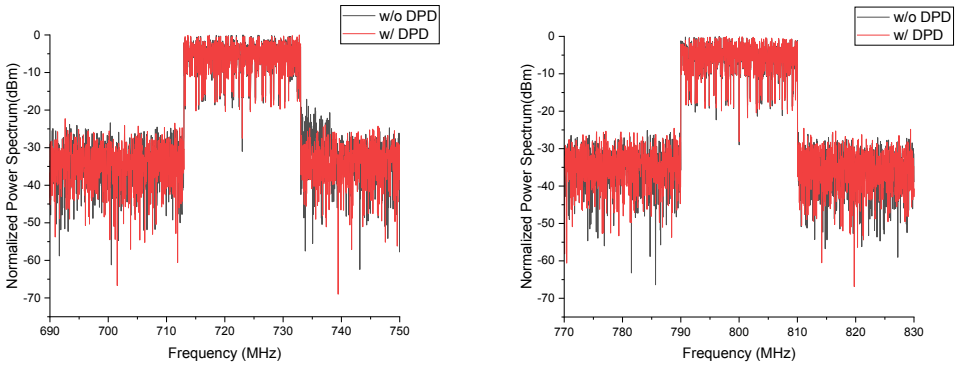

Figure 5-3 (a) and (b) Normalized power spectrum for the first band (left) and for the second band (right)

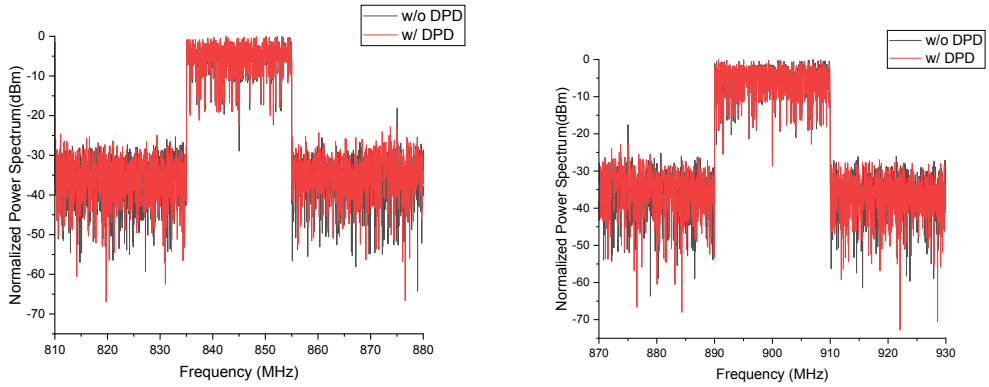

Figure 5-3 (c) and (d) Normalized power spectrum for the third band (left) and for the fourth band (right)

The simulation results regarding AM-AM and AM-PM distortions are presented in Figure 5-4.

The AM-AM graph provides insights into the amplitude distortion characteristics of the RoF system. Figure 5-4 compares its behavior with and without the utilization of the DPD. The black points present the signal without DPD, and red points present the signal with the proposed DPD. It visualizes the relationship between input and output amplitudes and highlights the nonlinear response of the system in the absence of DPD. Without DPD, the output power demonstrates nonlinearity, indicating the presence of gain compression and expansion resulting from system nonlinearities. Conversely, when the DPD is employed, the output power becomes more linear, leading to a significant reduction in gain compression and expansion.

The AM-PM graph, on the other hand, depicts the phase distortion introduced by the system. It illustrates the phase shift or modulation of the output signal relative to the input signal amplitude. In the absence of DPD, substantial phase distortion is observed. However, with the application of the DPD, the phase distortion is effectively mitigated, resulting in a noticeable reduction in the observed phase shift.

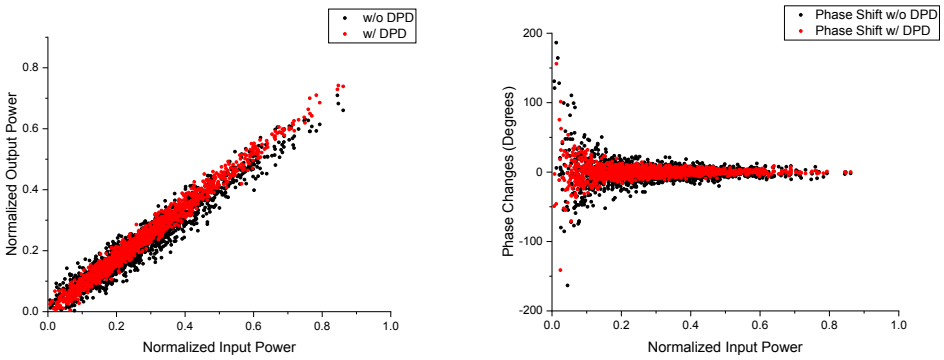

Figure 5-4 (a) AM-AM and AM-PM distortion for the first band with and without the DPD

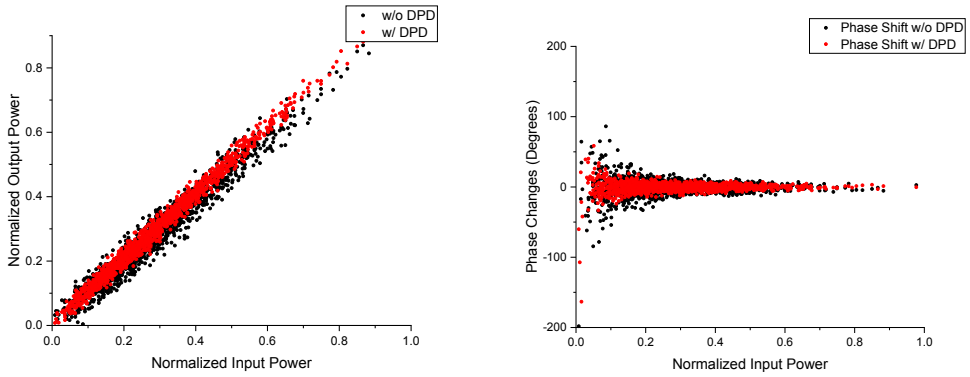

Figure 5-4 (b) AM-AM and AM-PM distortion for the second band with and without the DPD

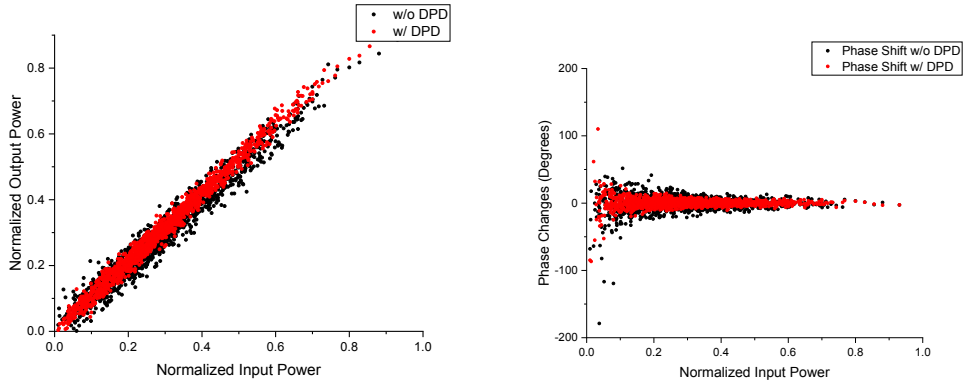

Figure 5-4 (c) AM-AM and AM-PM distortion for the third band with and without the DPD

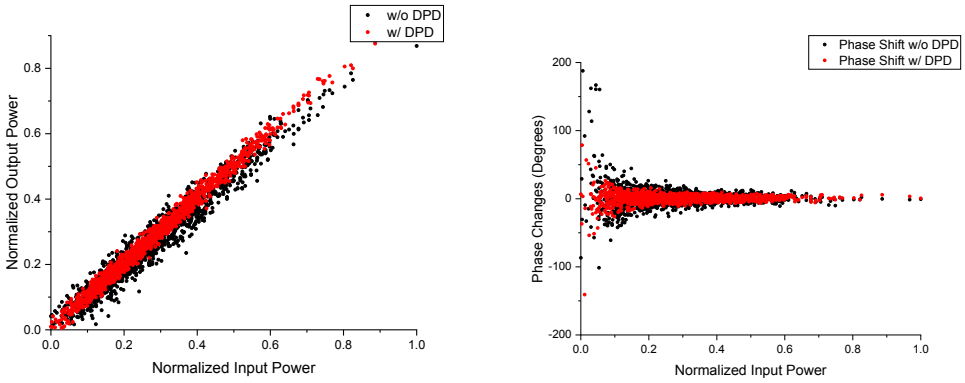

Figure 5-4 (d) AM-AM and AM-PM distortion for the fourth band with and without the DPD

5.3 Experiment of Five-Band DPD

In this section, we focused on 5-band signal, which each band located around 720 MHz, 800 MHz, 845 MHz, 900 MHz, and 960 MHz. Each band possesses a bandwidth of 20 MHz. To perform the required DPD function, we set the memory depth to five and nonlinearity order to six again. The input data was generated using MATLAB and organized into a 64-QAM format. Subsequently, these organized signals were employed to construct an OFDM waveform through the utilization of the IFFT. The resulting signal was then loaded onto the AWG to initiate the experiments. The obtained experimental outcomes are presented below.

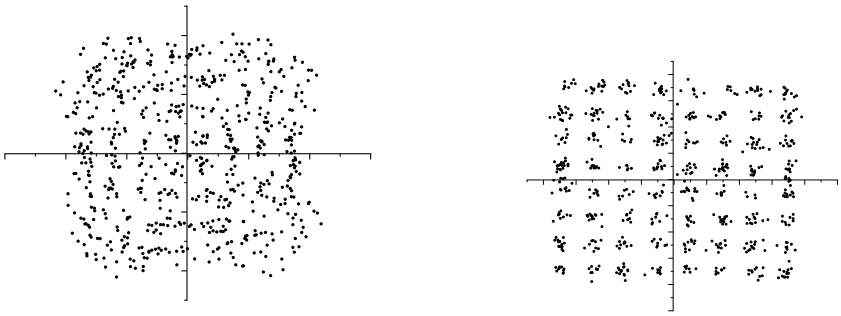

Figure 5-5 (a) Constellation of signal in first band. Left side is the signal without DPD. Right side is the signal with the DPD

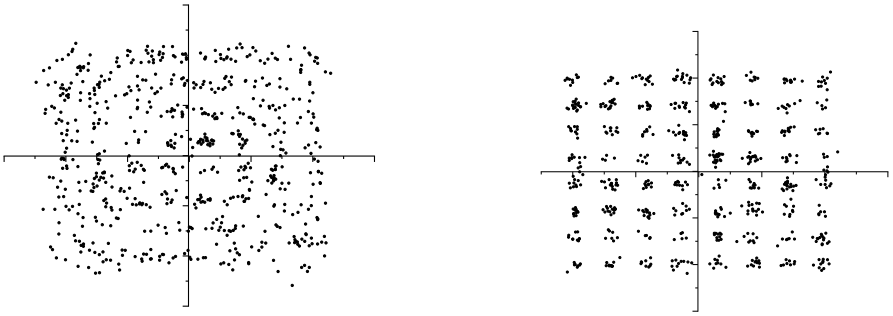

Figure 5-5 (b) Constellation of signal in second band. Left side is the signal without DPD. Right side is the signal with the DPD

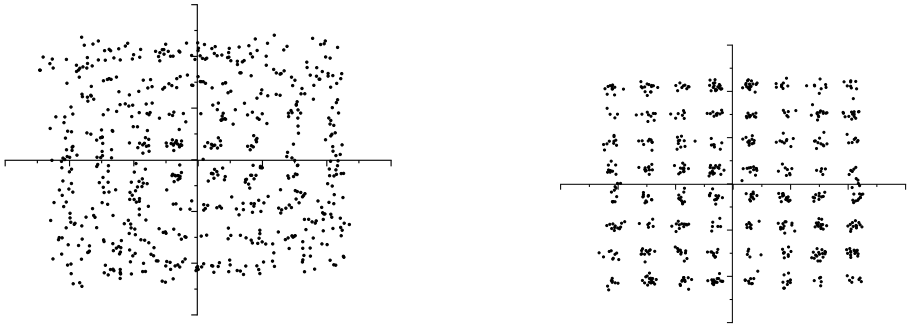

Figure 5-5 (c) Constellation of signal in third band. Left side is the signal without DPD. Right side is the signal with the DPD

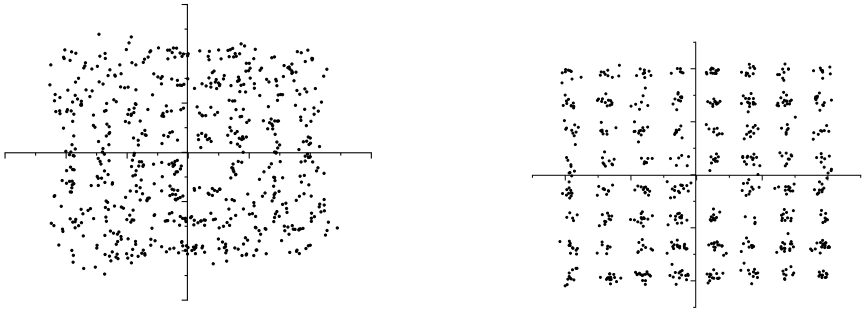

Figure 5-5 (d) Constellation of signal in four band. Left side is the signal without DPD. Right side is the signal with the DPD

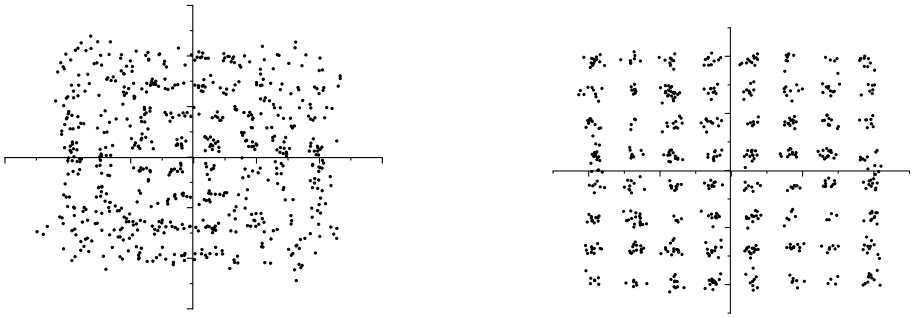

Figure 5-5 (e) Constellation of signal in five band. Left side is the signal without DPD. Right side is the signal with the DPD

Band	1	2	3	4	5
w/ DPD (dB)	-23.5	-25.1	-25.3	-24.1	- 24.6
w/o DPD (dB)	-14.9	-17.0	-17.2	-16.4	-16.7
Improvement (dB)	8.6	8.1	8.1	7.7	7.9
Mean (dB)	8.1				

Table 5-2 Five-band DPD performance

By examining Figure 5-5, it becomes apparent that in the absence of the proposed DPD, the signal's constellation points show spreading, indicating severe distortion. This distortion directly contributes to the deterioration of the EVM. In the experiments conducted without DPD, the EVM values were measured to be approximately -14.9 dB, -17.0 dB, -17.2 dB, -16.4 dB, and -16.7 dB, for the five bands. The summary of EVM performance is shown in Table 5-2.

However, with the implementation of the proposed DPD, improvement can be observed. The constellation points become more concentrated, leading to enhanced EVM values. In the simulations with the proposed DPD, the measured EVM values are approximately -23.5 dB, -25.1 dB, -25.3 dB, -24.1 dB, and -24.6 dB, for the five bands. The

average improvement in EVM across all the five bands is approximately 8.1 dB.

In terms of the power spectrum, the result is aligned with the section of the five-band DPD. The power spectrum is shown in Figure 5-6. The absence of DPD can result in nonlinear distortions that affect the power spectrum of the transmitted signal. As can be seen from Figure 5-6 (c) and (d), there is a nonlinearity distortion presence on the right side of the third band and the left side of the fourth band. This is because the presence of IMD3 or IMD5 coming from other bands. However, the implementation of the proposed DPD effectively mitigates the arising from these nonlinear distortions. Consequently, the application of DPD significantly improves the signal quality by minimizing distortions and maintaining a cleaner power spectrum.

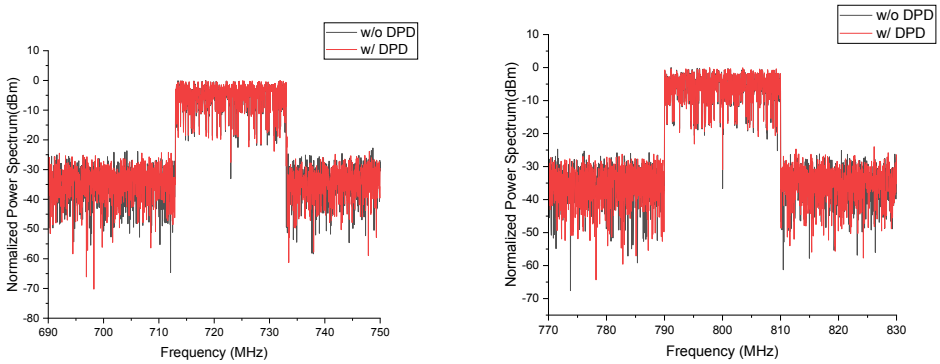

Figure 5-6 (a) and (b) Normalized power spectrum for the first band (left) and for the second band (right)

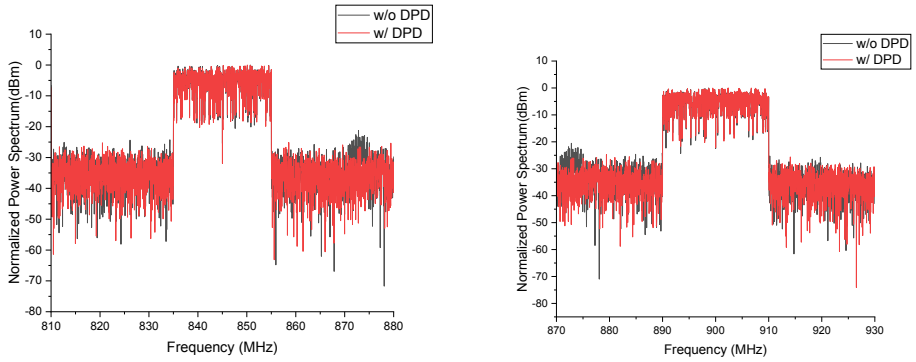

Figure 5-6 (c) and (d) Normalized power spectrum for the third band (left) and for the fourth band (right)

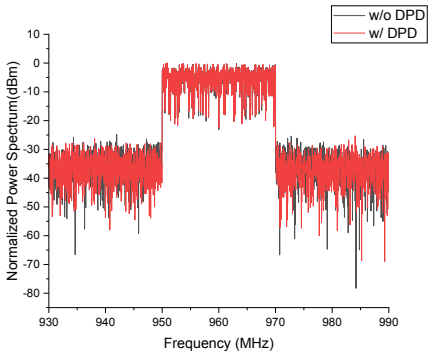

Figure 5-6 (e) Normalized power spectrum for the fifth band

In terms of its AM-AM and AM-PM conversion, the results are aligned with the conclusion in the above section. In Figure 5-7, we can observe that without DPD, the output power shows nonlinearity and the phase distortion introduced by the system. However, when the DPD is utilized, the output power becomes more linear and the phase distortion is reduced.

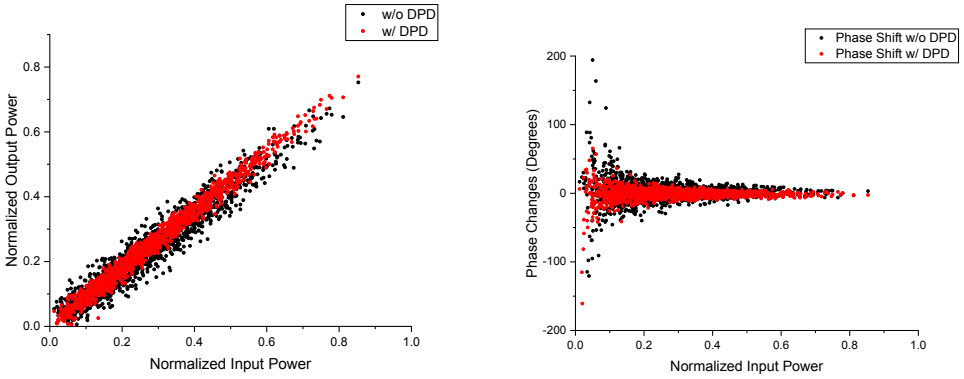

Figure 5-7 (a) AM-AM and AM-PM distortion for the first band with and without the DPD

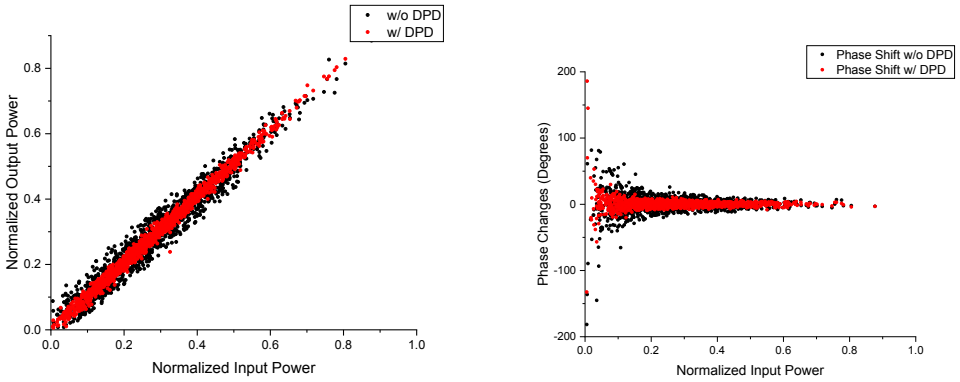

Figure 5-7 (b) AM-AM and AM-PM distortion for the second band with and without the DPD

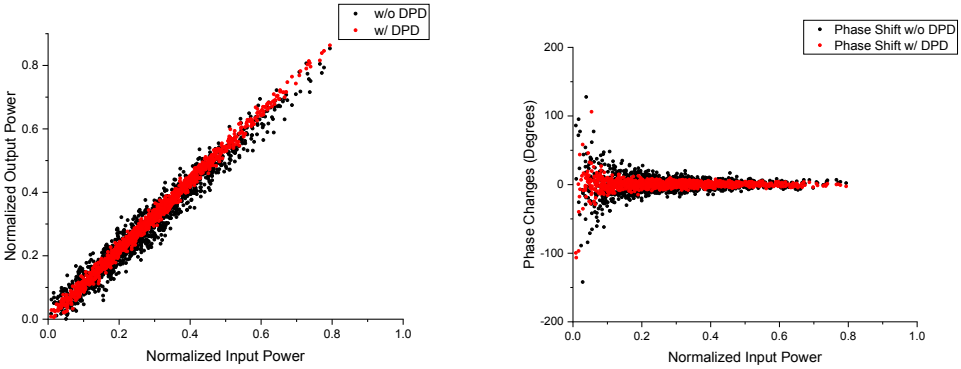

Figure 5-7 (c) AM-AM and AM-PM distortion for the third band with and without the DPD

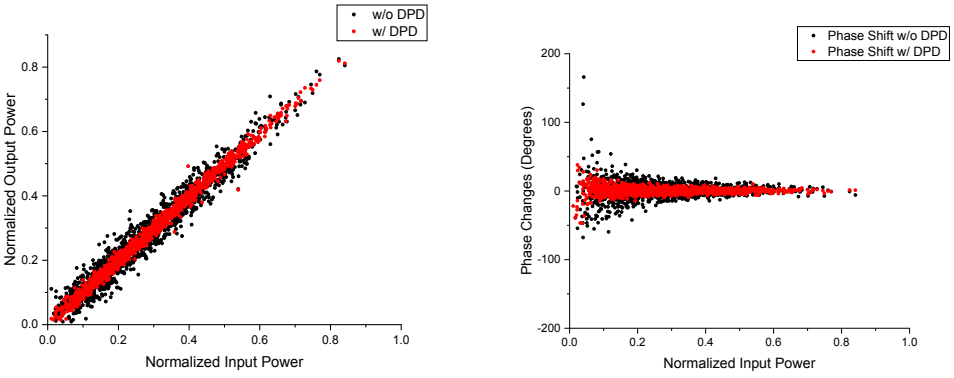

Figure 5-7 (d) AM-AM and AM-PM distortion for the fourth band with and without the DPD

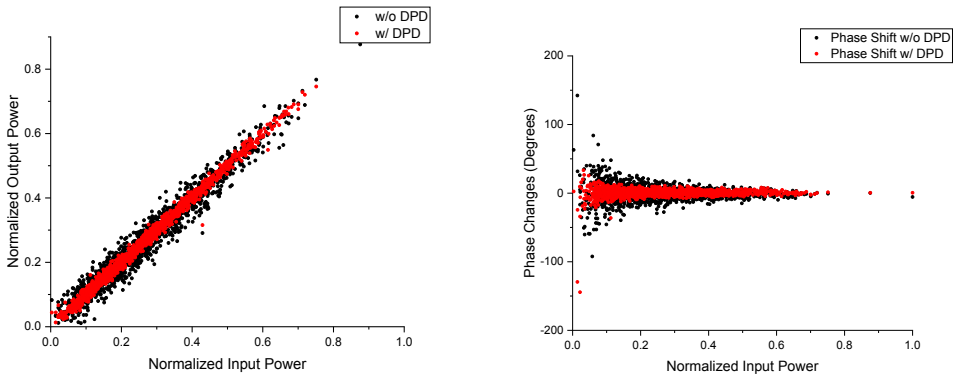

Figure 5-7 (e) AM-AM and AM-PM distortion for the fifth band with and without the DPD

5.4 Experiments Summary

The performance of the proposed DPD is summarized in Table 5-1 for the four-band signals and Table 5-2 for the five-band signals. The experimental results demonstrate the suitability of the proposed DPD for multi-band transmission. Table 5-3 provides a summary of the improvement achieved for four-band and five-band signals.

Bands	4	5
Means Improvement (dB)	5.67	8.1

Table 5-3 Measured mean improvement of EVM

The average improvement of EVM for the four-band DPD is around 5.67 dB. In addition, For the five-band DPD, the mean improvement of EVM is 8.1 dB. Considering the 20 MHz bandwidth of the signal in experiments compared with the 200 MHz bandwidth of the signal in simulation, i.e. a difference of 10 times, the measured improvement agrees to the simulated.

Note that the used nonlinearity order and memory depth in the experiments are not optimal for the considered RoF. Thus, the improvement for the four bands is worse than that for the five bands. With use of optimal nonlinearity order and memory depth it is believed that better performance should be obtained.

Chapter 6 Conclusion

6.1 Thesis Conclusion and advantage of low-complexity DPD

In this study, a new low-complexity multiband DPD approach has been proposed and studied. For this low-complexity DPD, the number of DPD function coefficients is reduced significantly. For example, f a 6-band signal transmitting over a system with nonlinearity order of 10 and memory depth of five, the proposed DPD only needs 640 coefficients rather than 40040 coefficients in the conventional memorial polynomial DPD. To demonstrate the performance of the proposed DPD, both simulation and experiments are conducted. An up to 6-band 64-QAM OFDM signal with each band of 200 MHz is used in simulations and an up to 5-band 20 MHz 64-QAM OFDM signal is used in experiments. The performance is evaluated in EVM of the received signal. The average improvement by simulation is 19.97 dB, 18.65 dB, 16.64 dB and 15.44 dB for 3, 4, 5 and 6 bands of signals, respectively. The average improvement in experiment is 5.67 dB and 8.1 dB for 4 and 5 bands of signals. Both simulation and experimental results confirm the effectiveness of the proposed DPD in multi-band transmission, further highlighting its advantage in simplifying the complexity associated with multidimensional signals.

The comparison of complexity is briefed in Table 3-1. This decreased complexity not only leads to cost savings in the design and implementation of RoF transmission systems but also makes the proposed DPD suitable for linearizing signals across various frequency multi-band signals.

6.2 Future Work

There are many low-complexity linearization models for multi-band signals based on memory polynomials. The new proposed DPD can replace the existing memory polynomials to further simplify the complexity of linearization. For example, the proposed DPD can

integrate with model pruning method to make a real-dynamic multi-band DPD. This could have a huge potential to satisfy the 5G requirements of linearization in the future. By eliminating insignificant terms in the proposed algorithm, it could further reduce the number of terms that need to be estimated and optimized. The integration of DPD with model pruning holds great potential for satisfying the linearization requirements of future 5G systems. It provides reduced computational complexity, efficient handling of multiple frequency bands, improved linearization performance, adaptive processing capabilities, accurate compensation for nonlinear distortion, and compatibility with different communication systems and platforms.

Reference

[1] J. Wood, *Behavioral Modeling and Linearization of RF Power Amplifiers, 1st ed., Norwood, MA: Artech House, 2014.* Artech House.

[2] “3rd Generation Partnership Project; Technical Specification Group Radio Access Network; NR; Base Station (BS) radio transmission and reception,” 3GPP TS 38.104, 2018

[3] X. Zhang, Broadband linearization for 5G fronthaul transmission (invited), Frontiers of Optoelectronics, vol. 11, no.2, pp 107–115, June 2018.

[4] C. Yu, N. Yang, Q. Lu, J. Cai and X. -W. Zhu, "High-precision joint in-band/out-of-band distortion compensation scheme for wideband RF power amplifier linearization," IEEE Microwave and Wireless Components Letters, vol. 28, no. 11, pp. 1044-1046, Nov. 2018.

[5] Y. Li, X. Wang and A. Zhu, "Reducing power consumption of digital predistortion for RF power amplifiers using real-time model switching," IEEE Transactions on Microwave Theory and Techniques, vol. 70, no. 3, pp. 1500-1508, March 2022.

[6] J. Peng, F. You and S. He, "Under-sampling digital predistortion of power amplifier using multi-tone mixing feedback technique," IEEE Transactions on Microwave Theory and Techniques, vol. 70, no. 1, pp. 490-501, Jan. 2022.

[7] A. Borel and V. Barzdenas, “A Review of the Basic Power Amplifier Linearization Methods,” in 2020 IEEE Open Conference of Electrical, Electronic and Information Sciences (eStream), Vilnius, Lithuania, Apr. 2020, pp. 1–4. doi: 10.1109/eStream50540.2020.9108866.

[8] J. L. Dawson and T. H. Lee, “Cartesian feedback for RF power amplifier linearization,” in Proceedings of the 2004 American Control Conference, Boston, MA, USA, 2004, pp. 361–366 vol.1. doi: 10.23919/ACC.2004.1383631.

[9] Q. A. Pham, D. López-Bueno, T. Wang, G. Montoro and P. L. Gilabert, "Partial least squares identification of multi look-up table digital predistorters for concurrent dual-band envelope tracking power amplifiers," IEEE Transactions on Microwave Theory and Techniques, vol. 66, no. 12, pp. 5143-5150, Dec. 2018.

[10] C. Yu, K. Tang and Y. Liu, "Adaptive basis direct learning method for predistortion of RF power amplifier," IEEE Microwave and Wireless Components Letters, vol. 30, no. 1, pp. 98-101, Jan. 2020.

[11] C. Yu et al., "Linear-decomposition digital predistortion of power amplifiers for 5G ultrabroadband applications," IEEE Transactions on Microwave Theory and Techniques, vol. 68, no. 7, pp. 2833-2844, July 2020.

[12] N. Kelly and A. Zhu, "Direct error-searching SPSA-based model extraction for digital predistortion of RF power amplifiers," IEEE Transactions on Microwave Theory and Techniques, vol. 66, no. 3, pp. 1512-1523, March 2018.

[13] Y. Li, X. Wang and A. Zhu, "Sampling rate reduction for digital predistortion of broadband RF power amplifiers," IEEE Transactions on Microwave Theory and Techniques, vol. 68, no. 3, pp. 1054-1064, March 2020.

[14] S. Wang, M. Roger, J. Sarrazin and C. Lelandais-Perrault, "Augmented iterative learning control for neural-network-based joint crest factor reduction and digital predistortion of power amplifiers," IEEE Transactions on Microwave Theory and Techniques, vol. 68, no. 11, pp. 4835-4845, Nov. 2020.

[15] P. Jaraut et al., "Augmented convolutional neural network for behavioral modeling and digital predistortion of concurrent multiband power amplifiers," IEEE Transactions on Microwave Theory and Techniques, vol. 69, no. 9, pp. 4142-4156, Sept. 2021.

[16] Q. Lu, F. Meng, N. Yang and C. Yu, "A uniform digital predistorter for concurrent multiband envelope tracking RF power amplifiers with different envelopes," IEEE Transactions on Microwave Theory and Techniques, vol. 66, no. 9, pp. 3947-3957, Sept. 2018.

[17] J. Zhai et al., "A 2-D simplified memory polynomial model for concurrent dual-band power amplifiers," IEEE Microwave and Wireless Components Letters, vol. 30, no. 8, pp. 761-763, Aug. 2020.

[18] W. Cao, S. Wang, P. N. Landin and T. Eriksson, "Low-complexity digital predistortion of concurrent multiband RF power amplifiers," IEEE Transactions on Microwave Theory and Techniques, vol. 70, no. 9, pp. 4308-4317, Sept. 2022.

[19] Z. Liu, X. Hu, L. Xu, W. Wang and F. M. Ghannouchi, "Low computational complexity digital predistortion based on convolutional neural network for wideband power amplifiers," IEEE Transactions on Circuits and Systems II: Express Briefs, vol. 69, no. 3, pp. 1702-1706, March 2022.

[20] Y. Li, X. Wang and A. Zhu, "Complexity-reduced model adaptation for digital predistortion of RF power amplifiers with pretraining-based feature extraction," IEEE Transactions on Microwave Theory and Techniques, vol. 69, no. 3, pp. 1780-1790, March 2021.

[21] M. Noweir et al., "Digitally linearized radio-over fiber transmitter architecture for cloud radio access network's downlink," IEEE Transactions on Microwave Theory and Techniques, vol. 66, no. 7, pp. 3564-3574, July 2018.

[22] M. Noweir, M. Helaoui, D. Oblak, W. Chen and F. M. Ghannouchi, "Linearization of radio-over-fiber cloud-RAN transmitters using pre- and post-distortion techniques," IEEE Photonics Technology Letters, vol. 33, no. 7, pp. 339-342, 1 April1, 2021.

[23] L. A. M. Pereira, L. L. Mendes, C. J. A. Bastos-Filho and S. Arismar Cerqueira, "Linearization schemes for radio over fiber systems based on machine learning algorithms," IEEE Photonics Technology Letters, vol. 34, no. 5, pp. 279-282, 1 March, 2022.

[24] X. Xie, M. Hui, T. Liu and X. Zhang, "Hybrid linearization of broadband radio-over-fiber transmission," IEEE Photonics Technology Letters, vol. 30, no. 8, pp. 692-695, 15 April15, 2018.

[25] P. Li et al., "Multi-IF-over-fiber based mobile fronthaul with blind linearization and flexible dispersion induced bandwidth penalty mitigation," Journal of Lightwave Technology, vol. 37, no. 4, pp. 1424-1433, 15 Feb.15, 2019.

[26] M. Noweir, M. Helaoui, D. Oblak and F. M. Ghannouchi, "Linearized full duplex radio-over-fiber-over-space mixerless transceiver architecture," IEEE Photonics Technology Letters, vol. 33, no. 2, pp. 113-116, 15 Jan.15, 2021.

[27] M. U. Hadi, P. A. Traverso, G. Tartarini, O. Venard, G. Baudoin and J. -L. Polleux, "Digital predistortion for linearity improvement of VCSEL-SSMF-based radio-over-fiber links," IEEE Microwave and Wireless Components Letters, vol. 29, no. 2, pp. 155-157, Feb. 2019.

[28] L. A. M. Pereira, L. L. Mendes, C. J. A. Bastos-Filho and A. C. S. Jr, "Machine learning-based linearization schemes for radio over fiber systems," IEEE Photonics Journal, vol. 14, no. 6, 8555310, Dec. 2022.

[29] R. Zheng, E. H. W. Chan, X. Wang, X. Feng and B. -O. Guan, "Linearized single sideband modulation link with high SFDR performance," IEEE Photonics Technology Letters, vol. 31, no. 4, pp. 299-302, 15 Feb.15, 2019.

[30] W. Tang, M. Hui, T. Liu, D. Shen and X. Zhang, "A Simple envelope-assisted RF/IF digital predistortion model for broadband RoF fronthaul transmission," Journal of Lightwave Technology, vol. 36, no. 19, pp. 4305-4311, Oct.1, 2018.

[31] P. Li et al., "Fast self-adaptive generic digital linearization for analog microwave photonic systems," Journal of Lightwave Technology, vol. 39, no. 24, pp. 7894-7907, 15 Dec.15, 2021.

[32] Y. Chen and Y. Chen, "Linearization for microwave photonic OFDM transmission systems using an iterative algorithm based on FEC mechanism," Journal of Lightwave Technology, vol. 40, no. 15, pp. 5013-5020, 1 Aug.1, 2022.

[33] Y. Wang et al., "Microwave photonic link with flexible even-order and third-order distortion suppression," IEEE Journal of Quantum Electronics, vol. 55, no. 3, 8000209, June 2019.

[34] F. Wang, S. Shi and D. W. Prather, "LTE signal transmission over a linearized analog photonic link with high fidelity," IEEE Photonics Journal, vol. 11, no. 5, 7204909, Oct. 2019.

[35] L. Zhong et al., "An SNR-improved transmitter of delta-sigma modulation supported ultra-high-order QAM signal for fronthaul/WiFi applications," Journal of Lightwave Technology, vol. 40, no. 9, pp. 2780-2790, 1 May1, 2022.

[36] C. Shen, S. He, X. Zhu, J. Peng and T. Cao, "A 3.3–4.3-GHz high-efficiency broadband Doherty power amplifier," IEEE Microwave and Wireless Components Letters, vol. 30, no. 11, pp. 1081-1084, Nov. 2020.

[37] D. Gan, W. Shi, S. He, Y. Gao and G. Naah, "Broadband Doherty power amplifier with transferable continuous mode," IEEE Access, vol. 8, pp. 99485-99494, 2020.

[38] X. Liu, W. Chen and Z. Feng, "Broadband digital predistortion utilizing parallel quasi- Wiener-Hammerstein model with extended dynamic range," 2021 IEEE MTT-S International Wireless Symposium (IWS), Nanjing, China, May 2021. doi: 10.1109/IWS52775.2021.9499484.

[39] W. Chen, X. Liu, J. Chu, H. Wu, Z. Feng and F. M. Ghannouchi, "A low complexity moving average nested GMP model for digital predistortion of broadband power amplifiers," IEEE Transactions on Circuits and Systems I: Regular Papers, vol. 69, no. 5, pp. 2070-2083, May 2022.

[40] Y. Li and A. Zhu, "On-demand real-time optimizable dynamic model sizing for digital predistortion of broadband RF power amplifiers," IEEE Transactions on Microwave Theory and Techniques, vol. 68, no. 7, pp. 2891-2901, July 2020.

[41] Chao Yu et al., "A reconfigurable in-band digital predistortion technique for mmWave power amplifiers excited by a signal with 640 MHz modulation bandwidth", Proc. 47th European Microwave Conference, pp. 1046-1049, Nuremberg, Germany, Oct. 2017.

[42] T. Abe and Y. Yamao, "Band-split parallel signal processing DPD for nonlinear compensation of broadband RF signal," 15th International Symposium on Wireless Communication Systems (ISWCS), Lisbon, Portugal, August 2018, doi: 10.1109/ISWCS.2018.8491244.

[43] J. Peng, F. You and S. He, "Under-sampling digital predistortion of power amplifier using multi-tone mixing feedback technique," IEEE Transactions on Microwave Theory and Techniques, vol. 70, no. 1, pp. 490-501, Jan. 2022.

[44] M. Younes, A. Kwan, M. Rawat and F. M. Ghannouchi, "Linearization of Concurrent Tri-Band Transmitters Using 3-D Phase-Aligned Pruned Volterra Model," in IEEE Transactions on Microwave Theory and Techniques, vol. 61, no. 12, pp. 4569-4578, Dec. 2013, doi: 10.1109/TMTT.2013.2287176.